وزارة التعليم العالي والبحث العلمي

BADJI MOKHTAR-ANNABA UNIVERSITY
UNIVERSITE BADJI MOKHTAR-ANNABA

جامعة باجي مختار – عنابة

Faculté des Sciences de l'Ingéniorat
Département de Génie des Procédés

Année 2018

Thèse

Présentée en vue de l'obtention du diplôme de **DOCTORAT EN SCIENCES**

Dégradation photocatalytique de colorants présents dans les effluents textiles-Intérêt du couplage photocatalyse/biodégradation

Option : Génie Chimique

Par

Hichem ZEGHIOUD

DIRECTRICE DE THESE : **Nabila KHELLAF, Professeur, Université de Annaba**

DEVANT LE JURY

PRESIDENT :	Nadia FERTIKH, Professeur	Université de Annaba
EXAMINATEURS :	M[ed] BOUHELASSA, Professeur	Université de Constantine 3
	Kamel-Eddine BOUHIDEL, Professeur	Université de Batna 1
	M[ed] Fouzi GHORAB, Professeur	Université de Annaba
	Nadra DEBBACHE, Professeur	Université de Constantine 1
INVITES:	Aymen Amine ASSADI, MC	ENSCR, Rennes

Dédicaces

A mes très chers parents

A mes chers frères et sœurs

Remerciements

Au terme de ce projet, je tiens à remercier **Dieu le Miséricordieux**, qui m'a donné la force et la patience d'achever ce travail.

Je tiens tout d'abord à exprimer ma profonde gratitude à **Mme Nabila KHELLAF**, enseignante chercheure au Département de Génie des Procédés de l'Université de Annaba, pour avoir accepté de diriger ces travaux, pour sa grande disponibilité, sa compréhension et son soutien qui ont été déterminants pour l'aboutissement de ce projet de thèse.

Que **Mr Abdeltif AMRANE** Professeur à l'Université de Rennes 1 (France) et **Mme Hayet DJELAL** Maître de Conférences (HDR) à l'Ecole des Métiers de l'Environnement de Bruz (France) soient assurés de ma profonde reconnaissance pour leur conribution judicieuse dans la réalisation des travaux de cette thèse, pour leurs précieux conseils et surtout pour m'avoir toujours soutenu en m'accordant largement leurs confiances.

Mes remerciments s'adressent également à **Mr Aymen Amine ASSADI**, enseignant chercheur à l'Ecole Nationale Supérieure de Chimie de Rennes (ENSCR, France). Je lui exprime toute ma reconnaissance pour sa contribution, son aide scientifique qui m'a permis de mener à bien ce travail, et de m'avoir accueilli au sein de son laboratoire.

Je veux insister en particulier pour remercier **Mr Sami RTIMI** enseignant chercheur à l'Ecole Polytechnique Fédérale de Lausanne (EPFL, Suisse) pour nous avoir procuré les catalyseurs et aussi pour ses critiques, ses enrichissements et ses conseils judicieux.

Je ne saurai oublier de remercier vivement les responsables de l'Institut Français-Algérie (IF-A) pour avoir contribué au financement de mes séjours scientifiques en France.

Je remercie **Mr Mohammed BOUHELASSA** Professeur à l'université de constantine 3 d'avoir accepté de co-dirigé ce travail et pour ses conseils.

Je remercie **Mme Nadia FERTIKH** pour avoir accepté de présider ce jury ; je remercie également **Mr Kamel-Eddine BOUHIDEL, Mr Mohammed Fouzi GHORAB et Mme Nadra DEBBACHE** d'avoir accepté de juger ce travail et pour leurs conseils et critiques.

Mes remerciements vont au personnel de l'**équipe Chimie et Ingénierie des Procédés** (**CIP**) de l'Ecole Nationale Supérieure de Chimie de Rennes (ENSCR) pour son accueil et aide. Je

remercie énormément : M. KAMAGATE, K. SELLAMI, Tahar, Yasmine, Nouha, Ni Ye, Hanane, Malek, Yasmine, **doctorants du laboratoire**, pour la bonne ambiance dans laquelle nous avons travaillé et pour les fous rires partagés.

Enfin, je rends hommage et j'exprime ma reconnaissance à tous ceux qui ont contribué, de près ou de loin, à la réalisation de ce travail.

Hichem

Avant-Propos

Ce manuscrit de thèse est organisé sous forme de chapitres. La partie synthèse bibliographique sur la photocatalyse et celles comportant les résultats expérimentaux sont présentées sous forme d'articles scientifiques publiés (**Chap. II** et **Chap. III**), en cours de révision (**Chap. IV**) et soumis (**Chap. V**) pour publication.

Un préambule permet de situer chaque article par rapport aux objectifs de l'ensemble du travail présenté dans ce mémoire.

Les articles sont conservés dans leur version anglaise afin de ne pas en modifier le sens.

Les parties « Matériel et Méthodes » sont conservées dans les articles.

Les références bibliographiques sont présentées à la fin de chaque chapitre.

Production Scientifique

- **Articles publiés**

1. **Hichem ZEGHIOUD**, Nabila KHELLAF, Hayet DJELAL, Abdeltif AMRANE & Mohammed BOUHELASSA. Photocatalytic Reactors Dedicated to the Degradation of Hazardous Organic Pollutants: Kinetics, Mechanistic Aspects and Design-A Review, *Chemical Engineering Communications*, 203 (**2016**) 1415–1431.

2. **Hichem ZEGHIOUD**, Nabila KHELLAF, Abdeltif AMRANE, Hayet DJELAL, Walid ELFALLEH, Aymen Amine ASSADI, Sami RTIMI. Photocatalytic performance of TiO_2 impregnated polyester for the degradation of Reactive Green 12: Implications of the surface pretreatment and the microstructure, *Journal of Photochemistry and Photobiology A: Chemistry* 346 (**2017**) 493–501.

- **Article en révision**

Hichem ZEGHIOUD, Aymen Amine ASSADI, Nabila KHELLAF, Hayet DJELAL, Abdeltif AMRANE, Sami RTIMI. Reactive species monitoring and their contribution for removal of textile effluent with photocatalysis. *Journal of Photochemistry and Photobiology A: Chemistry* (janvier **2018**).

- **Article Soumis** (under review)

Hichem ZEGHIOUD, Nabila KHELLAF, Abdeltif AMRANE, Hayet DJELAL, Aymen Amine ASSADI, Sami RTIMI, Mohammed BOUHELASSA. Combining photocatalytic process and biological treatment for enhancing the degradation of a textile pollutant, Reactive Green 12. *Environmental Science and Pollution Research* (mars **2018**).

- **Communication internationale**

Ikram ROUIBAH, **Hichem ZEGHIOUD**, Nabila KHELLAF, Aymen Amine ASSADI, Hayet DJELAL, Abdeltif AMRANE. Photocatalytic degradation of the textile dye Solophenyl Scarlet BNLE- Use of TiO_2 supported on cellulose. *International Conference on Environmental Pollution, Risk Assessment and Remediation* (Mahdia- Tunisie, 18-20 Avril **2018**).

SOMMAIRE

LISTE DES FIGURES

LISTE DES TABLEAUX

LISTE DES ABREVIATIONS

COD:	Carbon Organique Dissous
COT:	Carbon Organique Totale
DCO:	Demande Chimique en Oxygène
ES:	Ecarlate Solophényl BNLE
KHz:	Kilo Hertz
MC:	Marine Cibanone
MHz:	Mega Hertz
nm:	Nanomètre
POA:	Procédé d'Oxydation Avancée
UV:	Ultra-Violet
VC:	Vert Cibacron (RG 12)
GI :	Germination Index
US :	Ultrasons

Résumé

La présence et l'accumulation dans le milieu aquatique de certains composés chimiques dangereux et persistants tels que les colorants synthétiques utilisés par l'industrie textile deviennent une menace sérieuse et néfaste pour la santé de l'homme. Ces composés bloquent l'échange d'oxygène dans l'eau, détériorent la qualité de l'eau de mer et dégradent les équilibres des écosystèmes aquatiques. Ces polluants ne sont pas facilement éliminés dans les stations d'épuration biologique, c'est pourquoi il est nécessaire de développer de nouvelles technologies de décontamination efficaces, propres et sûres.

La première partie de cette thèse traite de l'influence de divers paramètres opératoires sur l'efficacité de la dégradation photocatalytique du colorant Reactive Green 12 (RG 12) choisi comme molécule modèle. Le photocatalyseur supporté utilisé est un polyester imprégné de TiO_2. Les résultats d'optimisation des conditions de la réaction ont montré que pour une concentration initiale de RG 12 égale à 2 mg/L, 5.18 g/L de catalyseur et 2 h d'irradiation UV entraînaient une minéralisation totale du polluant. Un rapport $[H_2O_2]_0/[RG\ 12]_0$ variant dans l'intervalle 20-30 était nécessaire pour avoir un effet positif sur la cinétique de la réaction. Cette cinétique suit le modèle de Langmuir-Hinshelwood (L-H) avec un coefficient de régression de 0,926. Le photocatalyseur synthétique utilisé s'est avéré actif sous lumière UV et visible, et stable pendant plus de cinq cycles de réutilisation.

Afin de choisir le catalyseur le plus rentable, l'activité de deux autres photocatalyseurs synthétiques a été testée et la dispersion des sites actifs a été optimisée dans la seconde partie de cette étude. La minéralisation du colorant RG 12 a également été étudiée et les résultats ont indiqué une diminution de la minéralisation avec une augmentation de la concentration initiale en colorant. Le rôle des espèces oxydantes réactives a également été étudié avec l'aide de scavengers radicalaires sous lumière UV et visible. Les résultats ont montré que les radicaux $O_2^{\bullet -}$ jouaient un rôle crucial en présence de lumière UV ; cependant le $^{\bullet}OH$ était responsable de la dégradation de la molécule sous irradiation visible. Pour s'approcher du cas des effluents réels, certains mélanges binaires ont été étudiés pour différents rapports molaires des deux colorants, Vert Cibacron et Ecarlate Solophényl.

La troisième partie de ce projet concerne l'étude de la possibilité de combiner un traitement biologique avec le procédé photocatalytique dans le but d'améliorer le rendement de dégradation du polluant, diminuer le coût du traitement et réduire la toxicité pour le système aquatique. Les résultats ont montré que des solutions de RG 12 ont été décolorées à 34,50 et 19% après 7 jours de traitement biologique avec des boues activées et ce pour des solutions pré-

photocatalysées pendant 4 et 8 h, respectivement. Une réduction significative de l'indice de permanganate a également été notée. Dans la dernière partie, une amélioration de la phytotoxicité a été enregistrée en mesurant l'indice de germination (IG), où la photocatalyse a contribué à une augmentation de IG (des échantillons photocatalysés pendant 8 h) de 42,49% suivie de 4% pour un traitement biologique ultérieur.

Mots-clés : Colorant textile, Couplage de procédés, Dégradation photocatalytique, TiO_2, Boues activées, Traitement biologique.

Abstract

The presence and the accumulation of some hazardous and persistent chemicals such as synthetic dyes used in the textile industry in the aquatic environment is becoming a serious and adverse threat for the human health. They block the exchange of oxygen in water, deteriorate seawater quality, and degrade aquatic ecosystems equilibria. These pollutants are not easily removed in biological wastewater treatement plants; there is a need to develop effective and new powerful, clean and safe decontamination technology.

The first part of this thesis examined the influence of various operating parameters on the photocatalytic degradation efficiency of reactive Green 12 (RG-12) as model compound with TiO_2 impregnated on UV-C activated polyester as supported photocatalyst. The optimal reaction conditions found in the present study were: 2 mg/L of initial dye concentration, 5.18 g/L of catalyst dose and 2 h of UV irradiation. The ratio $[H_2O_2]_0/[RG\text{-}12]_0$ ranged between 20 and 30 was required to have a positive effect on the reaction kinetic which was found to follow the Langmuir-Hinshelwood (L-H) model with a regression coefficient of 0.926. The synthetic photocatalyst used was found to be active under UV and visible illumination and stable for more than five reuse cycles.

In order to select the most profitable catalyst, the activity of two other synthetic photocatalysts was tested and the dispersion of active sites was optimized for the chosen one, in the second part of this study. The mineralization of RG-12 was also examined and the results indicated a decrease of the mineralization with increasing the initial dye concentration, where 100% of dye abatement was achieved for 2 mg/L within 210 min of UV irradiation. The role of reactive oxygen species was also studied with the help of radical scavengers under UV and visible lights. The results showed that $O_2^{\bullet -}$ played a crucial role under UV light; however, the $^{\bullet}OH$ was responsible for the dye degradation under visible light irradiation. To approach a real case, some

binary mixtures were investigated for various molar ratios of the two dyes; Reactive Green 12 and Direct Red 89.

The third part of this project concerned the study of the possibility of combining a biological treatment with photocatalytic process in the aim to improve the mineralization yield, decrease the cost of treatment and reduce the toxicity for aquatic systems. The results showed that 34.50 and 19% of RG-12 was discolored after 7 days of biological treatment with activated sludge for pre-photocatalyzed solution during 4 and 8 h, respectively. A significant reduction of Permanganate Index was also noticed. In the last part, an enhancement in phytotoxicity was recorded by measuring the Germination Index (GI), where photocatalysis contributed by an increase of GI (of photocatalyzed samples for 8 h of irradiation) by 42.49% followed by 4% for further biological treatment.

Keywords: Textile dye, Process combination, Photocatalytic degradation, TiO_2, Activated sludge, Biological treatment.

INTRODUCTION GENERALE

1. Contexte de l'étude

Les effluents industriels liquides sont des rejets issus de procédés d'extraction ou de transformation de matières premières en vue de fabriquer des produits industriels ou des biens de consommation. Ces effluents étant extrêmement hétérogènes, leur quantité et leur qualité varient en fonction du procédé mis en œuvre et du domaine industriel. Ils présentent souvent un large spectre de polluants chimiques : composés à l'état solide ou dissous, matières organiques et minérales, métaux, hydrocarbures, solvants, polymères, huiles, graisses, sels, … à divers niveaux de toxicité. Cette grande diversité requiert une approche spécifique de traitement pour chaque type d'effluent et type d'industrie.

Les technologies industrielles de traitement des eaux usées doivent être capables de fournir pour chaque type d'effluent le procédé remplissant les critères de performance et de fiabilité qui permettent de répondre aux exigences réglementaires de rejet et de sécurité environnementale, aux contraintes économiques, et parfois également aux contraintes plus spécifiques de l'industriel, telles que les espaces disponibles.

Le défi posé par les polluants est une question que la majorité des stations de traitement des eaux usées ne sont pas en mesure de les gérer. Les micropolluants sont invulnérables au traitement biologique ; le transfert de la source vers l'environnement est donc facilité, ce qui entraîne une accumulation supplémentaire dans l'environnement. Leur présence est associée à des risques mineurs et majeurs pour la santé et à la toxicité (Fent et Weston, 2006 ; Luo et al., 2014).

Les différents travaux de recherche sur le recyclage et le traitement des eaux usées sont souvent menés selon deux principaux axes : « comment mieux caractériser les effluents et comment mieux les traiter ensuite ».

Certains procédés de dégradation ou d'élimination de polluants organiques ne peuvent pas être appliqués seuls ; c'est le cas de la biodégradation. L'utilisation d'un procédé biologique nécessite une caractérisation de l'effluent d'un point de vue physico-chimique et microbiologique, ainsi qu'un prétraitement (Crini et al., 2007). En effet, ces procédés qui utilisent le pouvoir oxydant des microorganismes, conviennent au traitement d'eaux contenant des polluants oxydables, biodégradables et surtout non-toxiques.

2. Problématique

Les colorants sont largement utilisés dans les imprimeries, les produits alimentaires, cosmétiques et cliniques, mais en particulier dans les industries textiles pour leur stabilité chimique, la facilité de leur synthèse et leur variété de couleurs. Cependant, ces colorants sont à l'origine d'une grande pollution une fois évacués dans l'environnement. La production mondiale des colorants est estimée à plus de 800 ktonnes/an (kta) et les colorants azoïques sont majoritaires et représentent 60-70 %. Compte tenu de la composition très hétérogène de ces derniers, leur dégradation conduit souvent à la conception d'une chaîne de traitement physico-chimique et biologique assurant l'élimination des différents polluants par étapes successives. Des études ont montré que plusieurs colorants azoïques sont toxiques et mutagènes et le traitement biologique de ces colorants semble présenter un intérêt scientifique majeur. Les traitements physico-chimiques communs (adsorption, coagulation/floculation, précipitation etc.) sont couramment utilisés pour les effluents industriels. Malgré leur rapidité, ces méthodes se sont avérées peu efficaces compte tenu des normes exigées sur ces rejets (Ben Mansour et al., 2011).

Un effluent peut contenir des molécules toxiques qui peuvent inhiber l'action des microorganismes ou les détruire (Henze et al., 2002 ; Robinson et al., 2001 ; Fu et Viraraghavan, 2001). Il doit donc subir un prétraitement antérieur à la biodégradation, afin d'oxyder les polluants en sous-produits facilement biodégradables et moins toxiques, évitant ainsi la lyse des microorganismes présents dans le traitement biologique ultérieur (Tekin et al., 2006).

Au cours des dernières décennies, les processus d'oxydation avancée (POA) sont apparus comme des technologies innovantes pour oxyder, dégrader et minéraliser les polluants organiques toxiques et biorecalcitrants (Zhu et al., 2004). Ces procédés sont basés sur la production et l'exploitation *in-situ* d'un oxydant puissant, très réactif et non sélectif, tel que les radicaux hydroxyles (•OH) (Lee et al., 2003 ; Taborda et al., 2001). Ces radicaux ont un pouvoir oxydant supérieur à celui des oxydants traditionnels tels que H_2O_2, Cl_2, ClO_2 ou O_3.

3. Objectifs de la thèse

L'objectif principal de ce travail de thèse peut être divisé en trois voies essentielles.

La première voie réside dans l'examen de differents paramètres mis en jeu durant la préparation du catalyseur tel que le dopage, le support, le type de traitement du support et le degré de dispersion du semiconducteur (TiO_2), sur l'activité photocatalytique (dans l'UV et le Visible). Le choix de la molécule à dégrader, le colorant permet de faire ressortir le bon catalyseur selectionné alors pour la suite de l'étude (**Figure 1**).

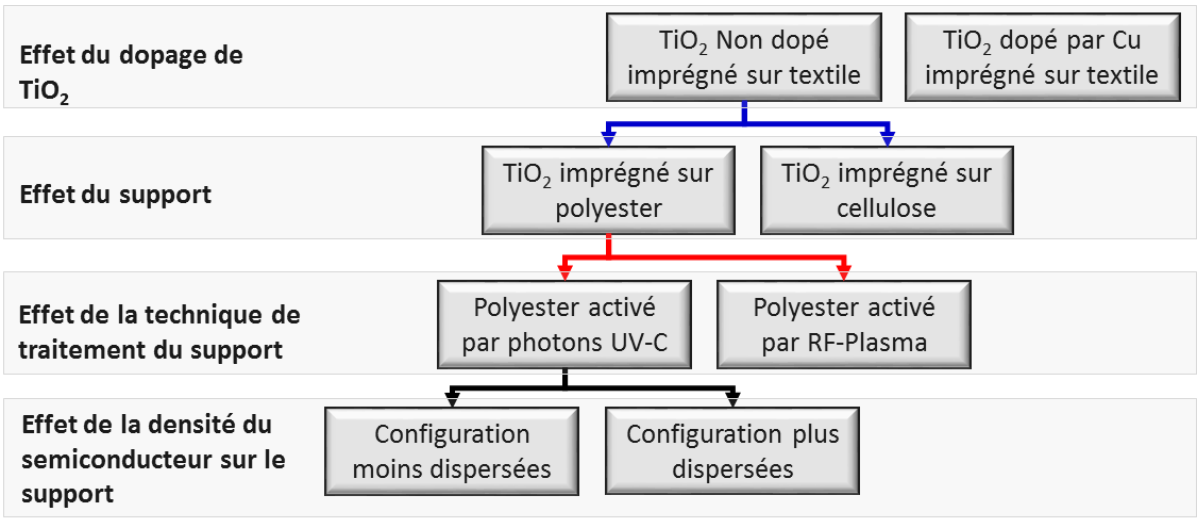

Figure 1 : Première voie de l'objectif de l'étude

La deuxième voie consiste à voir l'intérêt du procédé d'oxydation avancée, la photocatalyse hétérogène dans la dégradation et la minéralisation des colorants selectionnés dans la présente étude : le Reactive Green 12 (RG 12), l'Ecarlate Solophényl BNLE (ES) et le Marine Cibanone (MC). En vue de s'approcher des cas réels des rejets industriels, des mélanges binaires des deux premiers colorants ont été étudiés. De plus, une étude a été réalisée afin de comprendre le mécanisme de dégradation des polluants et les paramètres d'influence (**Figure 2**).

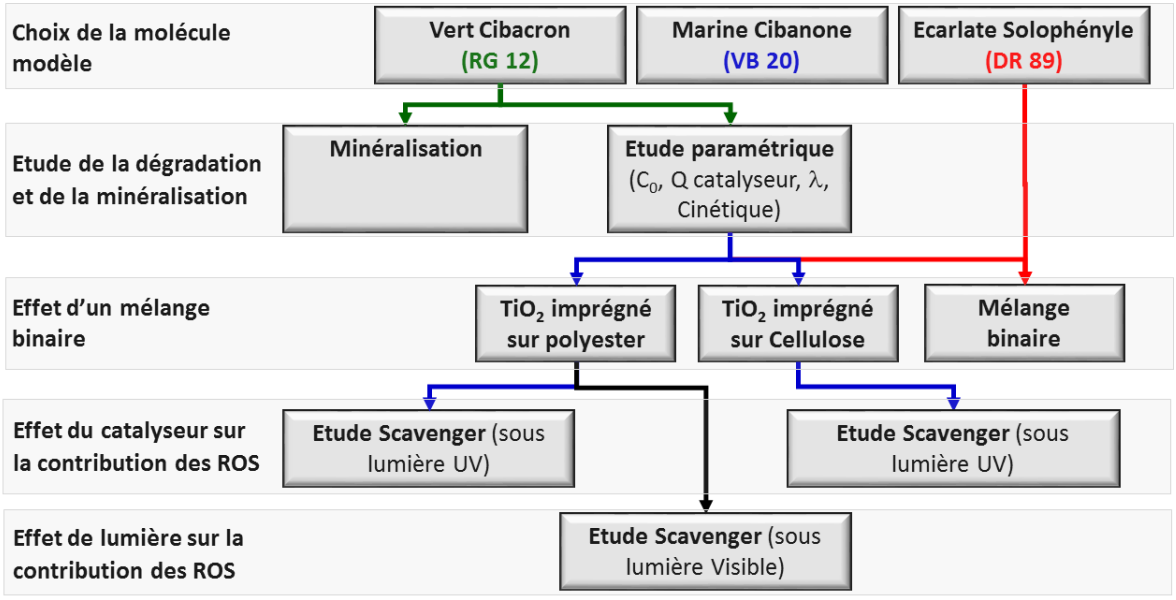

Figure 2 : Deuxième voie de l'objectif de l'étude

La troisième voie consiste à l'examen de la faisabilité du couplage de la photocatalyse (TiO_2-Polyester/UV) avec un traitement biologique par les boues activées en vue d'améliorer le

procédé global de dégradation du polluant et optimiser le temps de traitement par photocatalyse. L'impact sur le rendement de la dégradation et la réduction de la toxicité a aussi été visé (**Figure 3**).

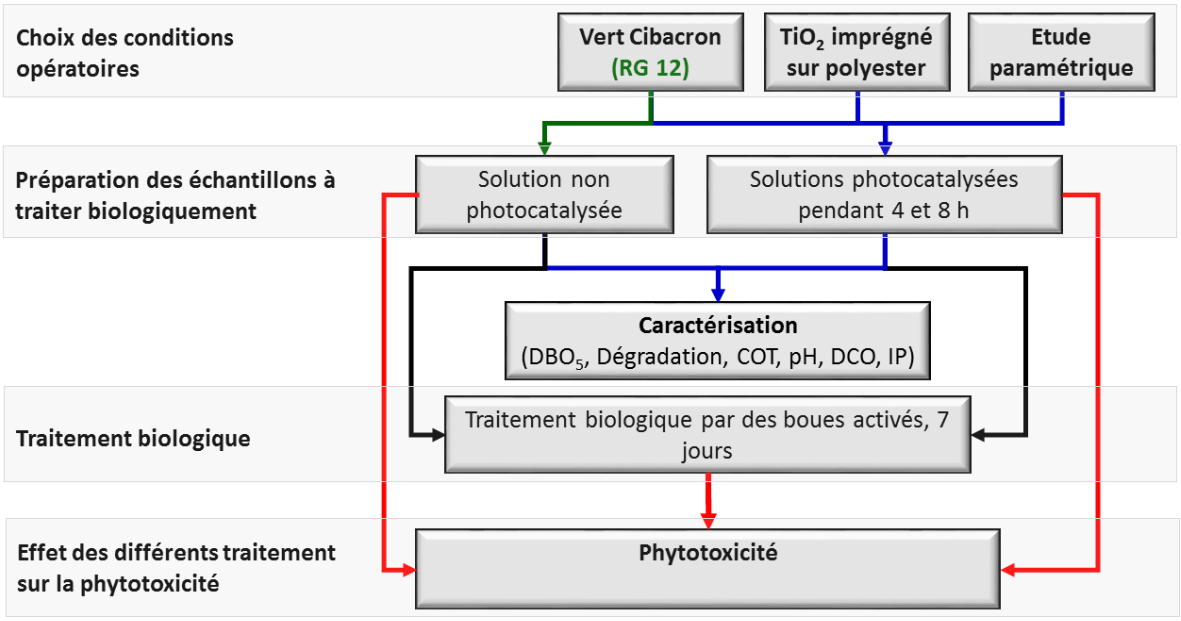

Figure 3 : Troisième voie de l'objectif de l'étude

4. Organisation du Manuscrit

La présente thèse est structurée en cinq chapitres.

Le premier chapitre est consacré à une synthèse bibliographique sur les procédés physico-chimiques de traitement de polluants organiques, les principaux procédés d'oxydation avancée (généralités, principe et mécanisme) et le couplage entre ces derniers et le traitement biologique.

Dans le deuxième chapitre, nous présentons une recherche bibliographique très poussée sur les photoréacteurs dédiés à la dégradation de polluants organiques dans le milieu liquide et dans l'air. L'effet des caractéristiques structurales et morphologique du semi-conducteur (structure cristalline, taille des particules et surface spécifique) ainsi que les paramètres opératoires réactionnels tel que la concentration initiale du polluant, la quantité de catalyseur, le pH, la longueur d'onde et l'intensité de la lumière, la température, l'humidité relative…etc., sur le processus photocatalytic ont été abordés en détail.

Le troisième chapitre est réservé à la présentation de la méthode de synthèse du photocatalyseur utilisé ainsi que sa caractérisation structurale et spectrale dans un premier temps. Dans un deuxième temps, une optimisation des principaux paramètres opératoires a été réalisée pour la dégradation photocatalytique du colorant Vert Cibacron (RG-12).

Le quatrième chapitre présente les résultats de l'activité photocatalytique de différents catalyseurs, de l'étude de dégradation des mélanges binaires de deux colorants (Vert Cibacron et Ecarlate Solophényl), de la minéralisation et de l'identification des espèces oxydantes réactives responsable de la dégradation (sous d'irradiation UV et visible) avec des mécanismes proposés.

Le contenu du cinquième chapitre tourne autour de la possibilité du couplage du procédé de photocatalyse (TiO_2-Polyester/UV) comme étape de prétraitement et un traitement biologique avec les boues activées. Les performances de cette combinaison ont été évaluées par l'étude de différents paramètres à savoir, le rendement de dégradation, le taux de minéralisation, la pollution chimique totale et la réduction de la phytotoxicité.

Une conclusion générale permet de faire la synthèse des principaux résultats et de donner des perspectives de recherche, à la fois par rapport à la problématique scientifique de départ mais aussi en termes d'application environnementale à grande échelle.

Références bibliographiques

Ben Mansour H., Boughzalaa O., Dridi D., Barillier D., Chekir-Ghedirab L., Mosrati R., 2011. Les colorants textiles sources de contamination de l'eau : Criblage de la toxicité et des méthodes de traitement, Revue des Sciences de L'eau, 24(3), 209-238.

Crini G., Badot P.M., 2007. Traitement et épuration des eaux industrielles polluées : Procédés membranaires, bioadsorption et oxydation chimique, Presses universitaires de Franche-Comté, http://books.google.tn/books?id=stqpsN7Ld7oC.

Fent, K., Weston, A.A., Caminada, D., 2006. Ecotoxicology of human pharmaceuticals. Aquat. Toxicol. 76,122–159.

Fu Y., Viraraghavan T., 2001. Fungal decolorization of dye wastewaters: a review, Bioresour. Technol. 79, 251–262.

Henze M., Harremoës P., Jansen J.l.C., Arvin E., 2002. Wastewater treatment. Biological and chemical processes. 3rd ed. Springer, Berlin.

Lee H.-S., Hur T., Kim S., Kim J.-H., Lee H.-I., 2003. Effects of pH and surface modification of TiO_2 with SiOx on the photocatalytic degradation of a pyrimidine derivative, Catal. Today 84, 173-180.

Luo Y., Guo W., Ngo H.H., Nghiem L.D., Hai F.I., Zhang J., Liang S., Wang X.C., 2014. A review on the occurrence of micropollutants in the aquatic environment and their fate and removal during wastewater treatment. Sci. Total Environ. 473–474, 619–641.

Robinson T., McMullan G., Marchant R., Nigam P., 2001. Remediation of dyes in textile effluent: a critical review on current treatment technologies with a proposed alternative, Bioresour. Technol. 77, 247–255.

Taborda A.V., Brusa M.A., Grela M.A., 2001, Photocatalytic degradation of phthalic acid on TiO_2 nanoparticles, Appl. Catal. A: Gener. 208, 419-426.

Tekin H., Bilkay O., Ataberk S., Balta T., Ceribasi I., Sanin F., 2006. Use of Fenton oxidation to improve the biodegradability of a pharmaceutical wastewater, J. Hazard. Mater. 136, 258–265.

Zhu X., Feng X., Yuan C., Cao X., Li J., 2004. Photocatalytic degradation of pesticide pyridaben in suspension of TiO_2: identification of intermediates and degradation pathways, J. Mol. Catal. A : Chem. 214, 293-300.

CHAPITRE I: Synthèse Bibliographique sur Les Procédés de Dégradation de Polluants Organiques

I.1. Introduction

Un grand nombre de procédés physiques, chimiques, photochimiques et électrochimiques sont utilisés pour le traitement des eaux polluées par des composés organiques réfractaires, toxiques et non biodégradables. Ces polluants sont issus d'activités industrielles qui génèrent des effluents continus ou discontinus d'une extrême diversité. Certains polluants organiques sont plus ou moins biodégradables ; ils sont alors éliminés par des procédés biologiques dans lesquels les mico-organismes utilisent la pollution comme substrat et/ou énergie. Dans certains cas, le recours au couplage d'un procédé physico-chimique et d'un traitement biologique pourrait conduire à une épuration optimale en garantissant une solution économique et durable aux problèmes de pollution.

I.2. Procédés d'Oxydation Avancée (POAs)

Les procédés d'oxydation avancée (POAs) font l'objet d'un nombre considérable de travaux de recherche et de publications depuis le début des années 1980. Par définition, les procédés d'oxydation avancée sont des procédés qui conduisent à la génération *in-situ* de radicaux libres tel que ; les radicaux hydroxyle ($^{\bullet}OH$) (Zsilák et al., 2014), les radicaux super oxyde ($O_2^{\bullet-}$) (Zhao et al., 2017) et les lacunes électroniques (h^+) (Wang et al., 2016). Ces intermédiaires radicalaires sont extrêmement réactifs vis-à-vis de la plupart des composés organiques et sont capables de minéraliser partiellement ou en totalité la plupart des polluants organiques.

Il existe de nombreux procédés d'oxydation avancée comme le montre la **Figure I.1** qui classe les POAs en différentes catégories. Certains ne peuvent pas être utilisés couramment pour le traitement des eaux à cause d'une grande consommation d'énergie ou de conditions opératoires contraignantes (oxydation électrochimique, oxydation à l'air humide, etc.).

Le **Tableau I.1** présente les principaux POAs étudiés dans la littérature. Ces procédés sont basés sur l'utilisation d'un oxydant comme l'ozone, le peroxyde d'hydrogène ou l'oxygène en association avec un agent d'activation comme le rayonnement UV ou un sel de fer (Andreozzi et al., 1999 ; Pera-Titus et al., 2004). Ces procédés peuvent également utiliser des méthodes physiques pour générer des espèces radicalaires comme les faisceaux d'électrons, la radiolyse, les ultrasons, etc.

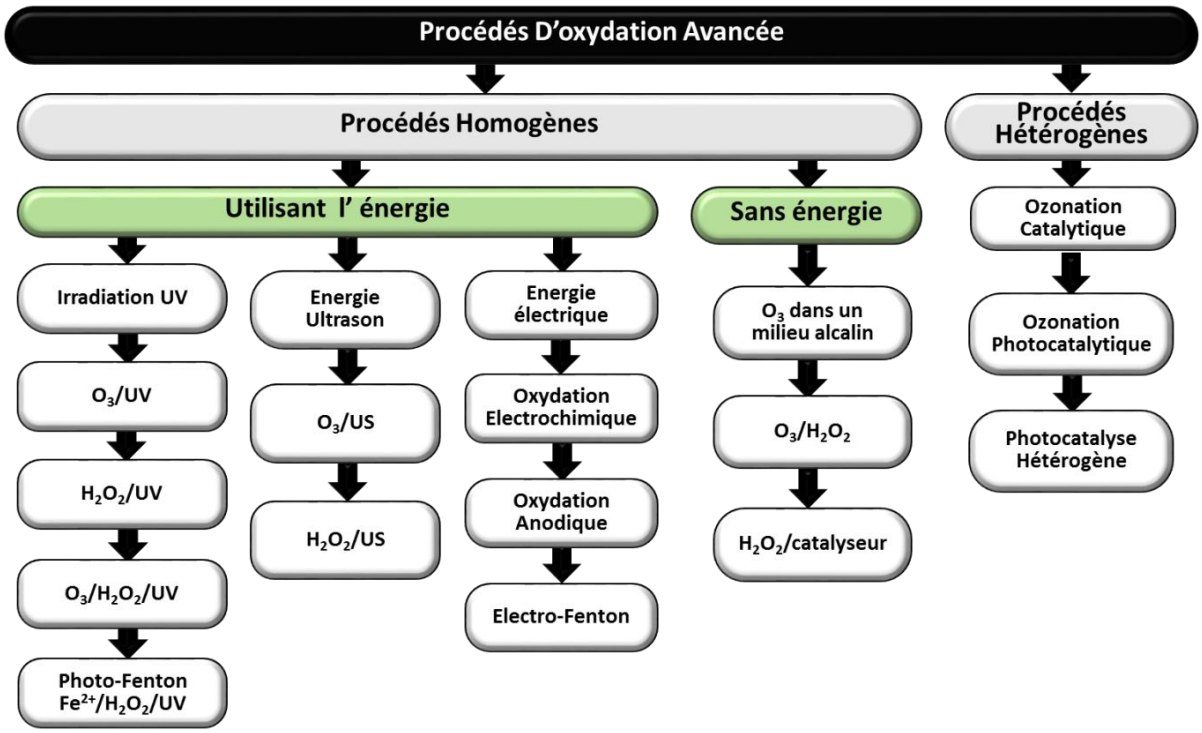

Figure I.1: Classification des Procédés d'Oxydation Avancée (Poyatos et al., 2010)

Tableau I.1: Classification des procédés d'oxydation avancée (Edelahi, 2004)

H_2O_2/ Fe^{2+}	Fenton
H_2O_2/ Fe^{2+}(Fe^{3+}) UV	Photo-Fenton (Photocatalyse homogène)
TiO_2 / UV	Photocatalyse hétérogène
O_3 / UV	Oxydation UV
H_2O_2/ UV	Photochimie assistée
Nouvelles technologies	Electrochimie, irradiation sous vide et Sonochimie (Ultrasons)

I.2.1. Oxydation

L'efficacité de l'ozonation dans la destruction des bactéries, virus et certaines algues justifie sa principale application en désinfection des eaux de consommation. Néanmoins, cette technique peut également être employée en traitement des eaux industrielles. L'ozone est l'un des oxydants les plus puissants mais son instabilité impose qu'il soit produit *in situ*, ce qui engendre des coûts de fonctionnement élevés. La décomposition de l'ozone en phase aqueuse passe par la formation de radicaux $^{\bullet}OH$ et est accélérée en milieu basique (Kasprzyk-Hordern et al., 2003). L'ozone attaque facilement les sites nucléophiles et les liaisons insaturées mais oxyde plus difficilement les liaisons simples, ce qui conduit à une élimination incomplète des polluants en solution (Gogate et Pandit, 2004).

L'efficacité du procédé peut être augmentée par l'ajout de H_2O_2, par activation au moyen d'un rayonnement ultraviolet (UV) ou par l'emploi d'un catalyseur. Ce procédé est basé sur la formation de radicaux $^{\bullet}OH$ par photolyse directe de la molécule de H_2O_2 (**Eq. I.1**) et des réactions de propagation (**Eq. I.2-I.6**) qui sont engendrées par la suite. Cette photolyse est possible à condition que la longueur d'onde de la radiation soit inférieure à 400 nm (Legrini et al., 1993).

$$H_2O_2 + h\nu \rightarrow 2HO^{\bullet} \quad (I.1)$$

Le coefficient d'absorption molaire du peroxyde d'hydrogène (ε) à 253,7 nm est faible, environ 20 $(mol/L)^{-1}$ cm^{-1} et les radicaux hydroxyles sont formés par les photons incidents absorbés. A cette longueur d'onde, la vitesse de la réaction de photolyse de la molécule de H_2O_2 est 50 fois plus faible que celle de la molécule d'ozone. Ce procédé (H_2O_2 couplé à UV) nécessite donc une forte concentration en peroxyde d'hydrogène ou un temps d'exposition au rayonnement plus important que dans le cas, par exemple, d'un procédé O_3/UV. D'après Glaze et al. (1987) la vitesse de cette réaction augmente quand le pH est de plus en plus basique ; en effet dans ces conditions l'anion peroxyde HO_2^- doit se former et ce dernier présente un coefficient d'absorption molaire bien supérieur à celui de H_2O_2 (240 contre 18,6 $(mol/L)^{-1}$ cm^{-1} à 253,7 nm) ; la réaction suivante se produit :

$$HO_2^- + h\nu \rightarrow HO^{\bullet} + O^{\bullet -} \quad (I.2)$$

Les réactions du procédé H_2O_2/UV mises en jeu sont les suivantes :

- Initiation :

$$H_2O_2 + h\nu \rightarrow HO^{\bullet} + HO^{\bullet} / O^{\bullet -} \quad (I.3)$$

$$H_2O_2 / HO_2^- \rightarrow H_2O / HO^- + 1/2\ O_2 \quad (I.4)$$

- Propagation :

$$HO^{\bullet} + H_2O_2 / HO_2^- \rightarrow HO_2^{\bullet} + H_2O / HO^- \quad (I.5)$$

$$HO_2^{\bullet} + H_2O_2 / HO_2^- \rightarrow HO^{\bullet} + H_2O / HO^- + O_2 \quad (I.6)$$

- Terminaison :

$$HO^{\bullet} / O^{\bullet -} + HO_2^{\bullet} \rightarrow H_2O / HO^- + O_2 \quad (I.7)$$

$$HO^{\bullet} / O^{\bullet -} + HO^{\bullet} \rightarrow H_2O_2 / HO_2^- \quad (I.8)$$

$$2HO_2^{\bullet} \rightarrow H_2O_2 + O_2 \quad (I.9)$$

- Dégradation du polluant :

$$Polluant + HO^{\bullet} \rightarrow Intermediaires \quad (I.10)$$

$$Polluant + H_2O_2 \rightarrow Intermediaires + H_2O \quad (I.11)$$

$$Polluant + h\nu \rightarrow Intermediaires \quad (I.12)$$

$$Polluant + H_2O_2 \rightarrow CO_2 + H_2O \quad (I.13)$$

$$Polluant + HO^{\bullet} \rightarrow CO_2 + H_2O \quad (I.14)$$

$$Polluant + h\nu \rightarrow CO_2 + H_2O \quad (I.15)$$

Le procédé H_2O_2/UV présente tout de même quelques inconvénients. En effet, la vitesse d'oxydation des composés organiques est limitée par la vitesse de formation des radicaux hydroxyles. De plus, le faible coefficient d'absorption de la molécule de H_2O_2 à 254 nm est un désavantage, en particulier lorsque les molécules organiques à traiter agissent comme des filtres. Les vitesses de formation de ces radicaux s'avèrent plus élevées lorsque la radiation est plus énergétique c'est-à-dire pour des longueurs d'onde plus faibles. C'est le cas d'utilisation des lampes à vapeur de mercure dopées au xénon où l'émission est comprise entre 210 et 240 nm. Certains auteurs comme De et al. (1999) et Alnaizy et al. (2000) ont montré que la concentration en peroxyde d'hydrogène était un facteur important dans ce type de procédé. Certes, l'augmentation de cette concentration est favorable à une augmentation du taux ou de la vitesse de destruction du polluant mais au-delà d'une certaine limite, le peroxyde d'hydrogène a un effet inhibiteur sur l'oxydation du polluant. Le ratio optimal phénol/H_2O_2 varie suivant les auteurs ; il est compris entre 0,004 et 0,02 (De et al., 1999 ; Alnaizy et al., 2000).

I.2.2. Photolyse

Les polluants organiques peuvent être dissociés par excitation UV directe ($\lambda < 250$ nm). Pour ce faire, les polluants doivent avoir une forte absorption pour la lumière d'excitation et un rendement quantique suffisant. Le rayonnement UV permet tout d'abord d'exciter la molécule organique à traiter (**Eq. I.16**). Une fois excitée, cette molécule peut subir une rupture homolytique d'une liaison pour former des radicaux (**Eq. I.17**) qui réagissent par la suite avec l'oxygène (**Eq I.18**), ou initier un processus de transfert d'électrons sur la molécule d'oxygène (**Eq I.19**). Il peut y avoir ensuite hydrolyse du cation radicalaire résultant de l'équation (**Eq. I.20**) pour former des sous-produits à poids moléculaires plus faibles. L'ion radicalaire $O_2^{\bullet -}$ est connu pour être capable de dégrader les composés aromatiques.

Le traitement des polluants organiques par photolyse directe a rapidement été abandonné pour de nombreuses raisons incluant les coûts très élevés de fonctionnement, la faible fiabilité du matériel et les problèmes de maintenance.

$$R + h\nu \longrightarrow R^* \quad \text{(I.16)}$$

$$R^* \longrightarrow R_1^\bullet + R_2^\bullet \quad \text{(I.17)}$$

$$R_1^\bullet + R_2^\bullet \longrightarrow produit \quad \text{(I.18)}$$

$$R^* + O_2 \longrightarrow R^{\bullet+} + O_2^{\bullet-} \quad \text{(I.19)}$$

$$R^{\bullet+} \longrightarrow produits \quad \text{(I.20)}$$

Les lampes les plus couramment utilisées pour la génération de radiations UV sont les lampes à vapeur de mercure à haute, moyenne (émission entre 254 et 400 nm) ou basse (émission à 253,7 nm) pression (Zissis, 2007 ; Bauer et al., 1999 ; Benitez et al., 2001 ; Benitez et al., 2000). La photolyse UV est utilisée pour dégrader des composés aromatiques chlorés, des phénols, des aliphatiques halogénés, des effluents issus des industries pétrolières, de la fabrication d'acier et d'autres déchets toxiques présents dans l'eau.

Espuglas et al. (2002) ont mis en évidence l'effet du pH sur le rendement du procédé UV pour la dégradation du phénol. Lorsque le pH n'était pas fixé (3,9-4,3) ils ont observé les taux de dégradation les plus importants (25%), en revanche lorsque le pH augmentait, le taux de dégradation diminuait (5% pour un pH de 11,5). En fixant le pH à l'aide de solutions tampons, des espèces supplémentaires sont introduites dans le réacteur (phosphates, ammoniaque, etc.) et sont susceptibles d'absorber une partie du rayonnement UV et par conséquent de réduire son efficacité vis à vis des molécules à traiter. Ces espèces sont appelées espèces à effet filtre.

I.2.3. Fenton

Ce procédé a été découvert à la fin du 19ème siècle par Henry John Horstman Fenton (Fenton et al., 1894) mais fait encore l'objet d'un grand nombre de recherches dans le domaine du traitement de l'eau. C'est un procédé d'oxydation très simple produisant des radicaux hydroxyles à partir de H_2O_2 et des ions Fe^{2+} (**Eq. I.21**). Le peroxyde d'hydrogène peut réagir avec les ions Fe^{3+} (**Eq. I.22**) (Pignatello et al., 1992) ou les radicaux $HO^\bullet$ (**Eq. I.23**) ainsi formés, aboutissant à la production de radicaux hydroperoxyle $HO_2^\bullet$, qui bien que très réactifs, possèdent un potentiel oxydant inférieur à celui des radicaux hydroxyle.

$$Fe^{2+} + H_2O_2 \rightarrow Fe^{3+} + HO^- + HO^\bullet \quad \text{(I. 21)}$$

$$Fe^{3+} + H_2O_2 \rightarrow Fe^{2+} + H^+ + HO_2^\bullet \quad \text{(I. 22)}$$

$$HO^\bullet + H_2O_2 \rightarrow H_2O + HO_2^\bullet \quad \text{(I. 23)}$$

Les radicaux •OH et HO_2•peuvent oxyder le substrat organique RH en radical alkyl par abstraction d'un proton (**Eq. I.24-I.25**) (Walling et al., 1975 ; Sadanaand Katzer, 1974).

$$RH + HO^{\bullet} \rightarrow R^{\bullet} + H_2O \quad (I.24)$$

$$RH + HO_2^{\bullet} \rightarrow R^{\bullet} + H_2O_2 \quad (I.25)$$

Le radical hydroperoxyle conduit, par diverses réactions, à la formation d'oxygène moléculaire (**Eq. I.26-I.27**) (Pignatello et al., 1992).

$$HO_2^{\bullet} + H_2O_2 \rightarrow H_2O + HO^{\bullet} + O_2 \quad (I.26)$$

$$HO_2^{\bullet} + Fe^{3+} \rightarrow Fe^{2+} + H^{+} + O_2 \quad (I.27)$$

Cet oxygène peut participer aux réactions de propagation, par formation de radicaux alkylperoxyle (**Eq. I.28**) (Rivas et al., 1998 ; Pintar and Levec, 1992).

$$R^{\bullet} + O_2 \rightarrow ROO^{\bullet} \quad (I.28)$$

$$ROO^{\bullet} + RH \rightarrow \ ROOH + R^{\bullet} \quad (I.29)$$

Enfin, la décarboxylation des alkylhydroperoxydes ROOH formés selon l'équation **I.29** (Rivas et al., 1998 ; Pintar et Levec, 1992) provoque l'abattement du Carbone Organique Total (**Eq. I.30**) où R' est un fragment organique possédant un carbone de moins que R).

$$ROOH \rightarrow CO_2 + R'H \quad (I.30)$$

I.2.4. Électro-Fenton

Le procédé Electro-Fenton regroupe les techniques électrochimiques qui permettent de régénérer un constituant ou les deux des réactifs de la réaction de Fenton. Selon le système électrochimique mis en place, différentes voies catalytiques sont possibles. A la cathode, H_2O_2 peut être électro-générée par la réduction de l'oxygène dissous ou le Fe(III) réduit en Fe(II) (**Eq. I.31**). A l'anode, le Fe^{2+} peut être produit par l'oxydation d'une anode constituée de fer métallique (**Eq. I.32**) (Qiang et al., 2003 ; Chou et al., 1999).

$$Cathode \quad \begin{cases} O_2 + 2\,H^{+} + 2\,e^{-} \rightarrow H_2O_2 \\ Fe^{3+} + e^{-} \rightarrow Fe^{2+} \end{cases} \quad (I.31)$$

$$Anode \quad \{Fe_0 \rightarrow Fe^{2+} + 2\,e^{-} \quad (I.32)$$

Ces méthodes peuvent présenter l'avantage de produire *in-situ* des réactifs. Cependant, elles dépendent fortement des conditions de pH, de l'intensité du courant et de la concentration en électrolyte si la conductivité du système est faible (Yavuz et al., 2007). De plus, l'anode est consommée.

I.2.5. Photo-Fenton

La réaction de Fenton est un processus thermique qui est efficace en présence de Fe(II). Cependant, la réaction de Fenton ralentit au fur et à mesure que le Fe(III) se forme et le degré de minéralisation reste limité (Pignatello et al., 2006 ; Bauer et Fallmann, 1997). Il a été montré que l'irradiation dans le domaine spectral de l'UV et/ou du visible dans ce système permet une augmentation de la vitesse des réactions et des taux de minéralisation par rapport à la réaction de Fenton. Ceci est dû à un recyclage de Fe(II) et à une production de radicaux plus efficace grâce à la photoréduction de Fe(III) (Nogueira et al., 2007 ; Pignatello et al., 2006).

Les vitesses de réaction de Fenton sont fortement augmentées par l'irradiation de la lumière UV (Ruppert et al., 1993 ; Sun et al., 1993). Au cours du mécanisme de Fenton, les ions Fe^{3+} s'accumulent et les ions Fe^{2+} se consomment, la réaction de Fenton est par conséquent pratiquement stoppée.

Comme l'illustre la **Figure I.2**, cet effet s'explique principalement par i) la photoréduction du Fe(III), ii) l'existence de plusieurs voies réactionnelles conduisant à une production plus importante de radicaux.

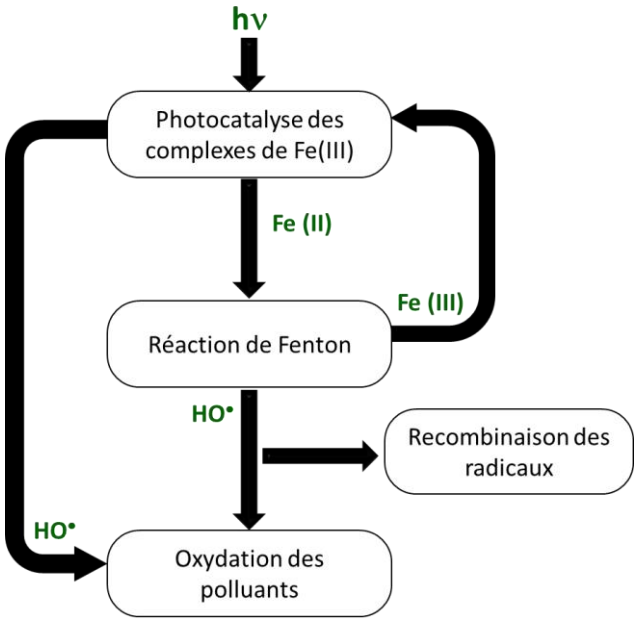

Figure I.2: Principe du photo-Fenton (Haddou, 2010).

Faust et Hoigne (1990) ont montré que les ions Fe^{2+} pouvaient être régénérés photochimiquement par photoréduction des ions Fe^{3+} (**Eq. I.33**). Les nouveaux ions Fe^{2+} générés réagissent avec H_2O_2 pour former à nouveau des radicaux $^{\bullet}OH$ et des ions ferriques et ainsi de suite.

$$Fe^{3+} + H_2O \rightarrow Fe^{2+} + HO^{\bullet} \qquad (I.33)$$

Chamarro et Espuglas (2001) ont utilisé le procédé Fenton pour la dégradation du phénol, du4-chlorophénol et du 2,4-dichlorophénol. Le coefficient stœchiométrique utilisé pour la réaction de Fenton était de 0,5 mole de composé organique par mole de H_2O_2. Ce procédé s'est avéré efficace pour éliminer les substances toxiques et pour augmenter la biodégradabilité de l'eau traitée.

I.2.6. Sono-Fenton

Dans le cas des ultrasons couplés au processus Fenton, la dégradation des polluants est accélérée. La décomposition du H_2O_2 sous l'irradiation ultrasonore produit une concentration plus élevée de $^{\bullet}OH$ selon la réaction (**Eq. I.34**). Sans compter que dans les réactions de Fenton décrites précédemment, le complexe $Fe(OOH)^{2+}$ peut être efficacement dissocié en Fe^{2+}et $HO_2^{\bullet}$ sous irradiation ultrasonore (**Eq. I.35-I.36**), qui rend plus disponible Fe^{2+} dans la solution provoquant un taux plus élevé de la réaction de Fenton (**Eq. I.37**).

$$H_2O_2 \rightarrow 2\,HO^{\bullet} \qquad (I.34)$$

$$Fe^{3+} + H_2O_2 \leftrightarrow Fe(OOH)^{2+} + H^{+} \qquad k = 3{,}1 \times 10^{-3} M^{-1} s^{-1} \qquad (I.35)$$

$$Fe(OOH)^{2+} \rightarrow Fe^{2+} + HO_2^{\bullet} \qquad k = 2{,}7 \times 10^{-3} M^{-1} s^{-1} \qquad (I.36)$$

$$Fe^{2+} + H_2O_2 \rightarrow Fe^{3+} + HO^{\bullet} + OH^{-} \qquad k = 63\ M^{-1} s^{-1} \qquad (I.37)$$

I.2.7. Sonochimie

La propagation des ultrasons dans un solvant conduit, pour des fréquences comprises entre 20 kHz et 1 MHz, à l'apparition de bulles de gaz qui contiennent les gaz dissous dans le solvant ou la vapeur même du solvant. La pulsation induite par la fréquence sur la bulle conduit à sa croissance (pendant la phase de dépression) puis à son effondrement (pendant la phase de compression). Un point chaud (hot spot) se forme, les conditions de température et de pression (T ~ 5000 °C et P > 1200 bars) sont propices à la formation de radicaux (**Figure I.3**).

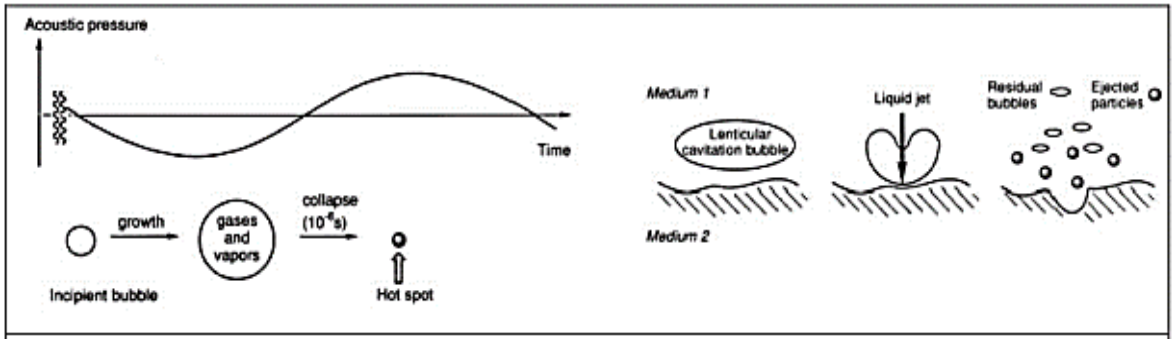

Figure I.3: Phénomène induit par les ultrasons et effet sur les particules solides (Mason, 1997).

La sonochimie peut être utilisée pour effectuer des réactions de chimie radicalaire (Mason, 1997) dans des solvants organiques. Dans le cas de l'eau comme solvant, Jiang et al. (2002) ont étudié l'oxydation de composés organohalogénés (chlorobenzène et chloronaphtalène). L'utilisation d'un transducteur de 500 kHz avec une puissance efficace de 25 W conduit à un abattement de plus de 90 % des molécules aromatiques (4.10^{-5} mol/L $<C_0<$ 4.10^{-4} mol/L pour un volume de 250 mL). Le chlore des molécules initiales est libéré sous forme d'ions chlorure. La concentration en H_2O_2 qui prouve la formation de radicaux $^{\bullet}OH$ atteint $0{,}5.10^{-3}$ mol/L en 4 h. L'utilisation des ultrasons avec des fréquences de 20-100 kHz permet également de préparer les boues de stations d'épuration en désagrégeant les flocs et en perçant les membranes cellulaires. Pour ces fréquences, aucune réaction chimique n'a lieu, seuls des phénomènes physiques sont mis en jeu. Les travaux de Gonze et al. (2003) ont montré que les agrégats de plus de 55 µm étaient rompus. La réduction du volume des boues d'un facteur 6 est effectuée en injectant une puissance de 60 kJ/L sous forme d'ultrasons. Cependant, les auteurs mettent en avant la difficulté de filtrer ces boues après traitement. Des applications industrielles d'une puissance de plusieurs dizaines de kW pour le pré-traitement de boues existent en Allemagne (IWE, 2007). Les boues prétraitées digérées de façon anaérobie produiraient plus de biogaz et la production de boues se limiterait à 40% de la quantité produite sans pré-traitement pour un temps de séjour plus court.

I.2.8. Oxydation électrochimique

L'élimination du polluant peut être réalisée par voie électrochimique, soit directement par activation de l'oxygène au niveau de l'anode (Pacheco et al., 2007), soit indirectement par génération *in-situ* d'espèces oxydantes telles que Cl_2, ClO^- (à l'anode) ou H_2O_2 (à la cathode) (Panizza et Cerisola, 2007).

I.2.9. Photocatalyse

Les procédés photocatalytiques font appel aux propriétés de semi-conducteurs, en présence de dioxygène. Relativement efficaces, ils sont peu onéreux car réalisés à température ambiante et à pression atmosphérique. Plusieurs catalyseurs ont été testés mais le plus prometteur reste l'oxyde de titane TiO_2, qui est à la fois, stable, peu coûteux et performant. L'absorption d'une radiation UV par le semi-conducteur conduit à l'excitation d'un électron, qui passe de la bande de valence à la bande de conduction du matériau. Il se forme ainsi une paire électron/trou (e^-/h^+)

(**Eq. I.38**). Sur la surface activée du catalyseur, les électrons excités peuvent réduire le dioxygène en ions radicalaires superoxyde (**Eq. I.39**) tandis que les trous sont capables d'oxyder l'eau et les ions hydroxydes adsorbés en radicaux hydroxyle (**Eq. I.40-I.41**) (Chong et al., 2010). Certains substrats adsorbés peuvent également être directement oxydés (**Eq. I.42**). Les deux principaux inconvénients de cette technique sont ; (i) la séparation délicate de l'effluent traité et du dioxyde de titane, ce dernier, très pulvérulent, a tendance à s'agglomérer au cours de cette opération, et (ii) le faible recouvrement entre le spectre solaire et le spectre d'absorption de TiO_2 qui limite l'efficacité du procédé.

$$TiO_2 + h\nu \rightarrow e^- + h^+ \quad (I.38)$$

$$(O_2)_{Ads} + e^- \rightarrow O_2^{\bullet -} \quad (I.39)$$

$$(H_2O)_{Ads} + h^+ \rightarrow HO^\bullet + H^+ \quad (I.40)$$

$$(OH^-)_{Ads} + h^+ \rightarrow HO^\bullet \quad (I.41)$$

$$(RH)_{Ads} + h^+ \rightarrow RH^{\bullet +} \quad (I.42)$$

Ce procédé, constitutuant l'un des objectifs de cette thèse, sera traité exaustivement dans les chapitres II, III et IV.

I.3. Procédés biologiques

Le traitement biologique est incontestablement, la technique de dépollution de référence. Basée sur les propriétés digestives de certains micro-organismes, elle peut être opérée en la présence de dioxygène (voie de dégradation aérobie) ou en son absence (voie de dégradation anaérobie), chacune des deux alternatives présentant des avantages et des inconvénients (Chan et al., 2009). Les micro-organismes dégradent les polluants organiques en composés moins toxiques ou les minéralisent en dioxyde de carbone, eau et sels inorganiques. Ces techniques peuvent être utilisées *in-situ* ou *ex-situ* (à travers des bioréacteurs) sous des conditions aérobies ou anaérobies (Farhadian et al., 2008).

Le traitement *in-situ* présente de nombreux avantages en termes de simplicité, de coût et d'efficacité (Dott et al., 1995). Au sein d'une station d'épuration, il est souvent utilisé en aval des procédés physiques. Un bioréacteur est un système dans lequel la dégradation biologique des contaminants est effectuée *ex-situ* selon des paramètres (température, pH, aération, agitation) bien définis et contrôlés. Par ce procédé, il a été rapporté dans la littérature de nombreux cas de traitement d'eau contaminée par divers polluants chimiques (perchlorates (Min et al., 2004), bromates (Butler et al., 2006), hydrocarbones chlorés (Ohlen et al., 2005) ou encore des hydrocarbones aromatiques polycycliques (Guieysse et al., 2000). Les principaux

inconvénients des bioréacteurs sont l'apport d'énergie nécessaire et le pompage de l'eau à traiter.

La popularité de ce procédé tient, essentiellement, à son faible coût, sa facilité de mise en œuvre et son applicabilité à presque tous les types d'effluents. Néanmoins, la durée du traitement et la surface de l'installation sont considérables et le procédé génère des boues qu'il est nécessaire d'extraire puis d'éliminer, par enfouissement ou par incinération. D'autre part, les bactéries sont sensibles aux variations brutales de température et de concentration. Enfin, le recours à des micro-organismes rend cette technique inadaptée aux effluents trop concentrés ou bien contenant des substances toxiques ou non-biodégradables.

Le procédé de traitement à boues activées, faisant partie des objectifs de ce projet, sera revu dans le chapitre V.

I.4. Couplage de procédés

La souplesse d'utilisation des POAs est liée à la possibilité de produire les radicaux libres par différentes techniques. Les potentialités offertes par les POAs peuvent être combinées avec les traitements biologiques en procédant à une dégradation oxydante des substances toxiques réfractaires entrant ou sortant d'une étape biologique (Andreozzi et al., 1999).

Un autre aspect concernant les opportunités d'applications des POAs : seuls des rejets avec des valeurs de la DCO inférieures à 5,0 g/L peuvent être traités par ces techniques, car de grandes valeurs de DCO nécessitent la consommation d'importantes quantités des réactifs. C'est pourquoi les eaux usées avec de grandes masses polluantes peuvent être plus efficacement traitées par oxydation humide ou incinération comme le montre la **Figure I.4**.

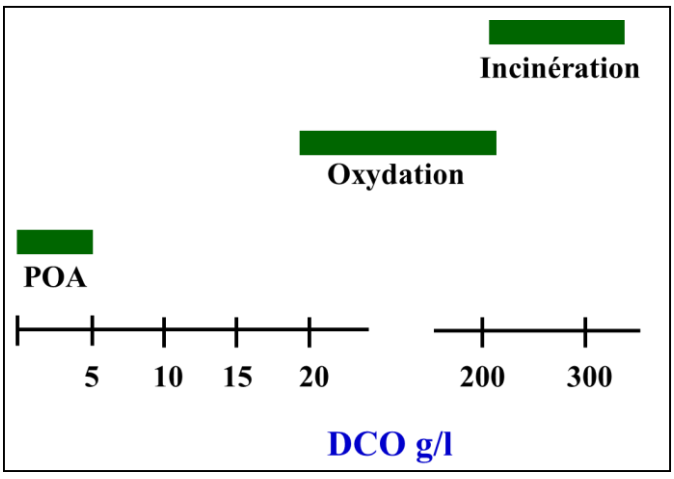

Figure I.4 : Choix des technologies de traitement des eaux usées selon leurs teneurs en DCO (Andreozzi et al., 1999)

Des couplages avec les traitements biologiques ont été testés (Malato et al., 2007). Récemment, Sirtori et al. (2009) ont couplé le photo-Fenton solaire et un réacteur de biomasse pour le traitement d'un rejet d'eau industrielle contaminée par le nalidixique, un antibiotique biorécalicitrant. Sa présence rendait le traitement de l'effluent par le traitement biologique classique long et inefficace. Grâce au procédé hybride, après 190 minutes d'irradiation, la totalité du nalidixique a été dégradée et la valeur du TOC initial (775 mg/L) a été réduite de 95%.

Yahiat et al. (2011) ont étudié la minéralisation de deux antibiotiques, à savoir la tylosine (TYL) et la tétracycline (TC) par procédé combiné : un prétraitement photocatalytique TiO_2/UV suivi d'un traitement biologique à boues activées. Les résultats obtenus ont montré qu'après 2h de prétraitement, les deux molécules cibles étaient dégradées à 98,3% et 80,6% pour la TC et la TYL, respectivement ; les taux d'abattement de la DCO étaient de 60,8 et 39,1% pour la TC et la TYL, respectivement. Cette diminution de la DCO implique une oxydation des molécules cibles et par conséquent une modification de leur structure chimique, qui pourrait mener à une diminution de la toxicité des deux solutions. Afin de compléter la minéralisation, les auteurs ont effectué un traitement biologique à boues activées des solutions irradiées de TC et TYL. Les résultats obtenus ont révélé que le couplage était intéressant dans le cas de la TYL. En effet une diminution de 56% de la DCO a été observée après 22 jours de culture, ce qui prouve la biodégradation de la solution irradiée par les boues activées, contrairement à la TC ou le couplage est inopérant. La photocatalyse s'est avérée inadaptée dans le cas de la TC puisqu'aucune augmentation de la biodégradabilité n'a été constatée. Les auteurs ont conclu que les sous-produits issus de la dégradation photocatalytique de la TC ne sont pas biodégradables contrairement à ceux issus de la photocatalyse de la tylosine qui présentaient une biodégradabilité significative. Ils ont expliqué que cette différence était probablement due à la différence de structure chimique des deux antibiotiques étudiés.

L'élimination de l'hydrochlorure de tétracycline (TC) par oxydation électrochimique sur une électrode de Pb/PbO_2 (50mm×40mm×1mm) et la faisabilité de coupler l'oxydation anodique à un traitement par boues activées ont été examinées par Yahiaoui et al. (2013). Un prétraitement de 100 mg/L de TC a été réalisé durant 5h. La densité de courant appliqué a été maintenue à 13,75 mA cm^{-2}. Les résultats obtenus ont montré une diminution de 36,7% du Carbone Organique Dissous (COD) et une amélioration significative de la biodégradabilité de la solution prétraitée, ce qui a été confirmé par un traitement biologique ultérieur. En effet, 76% du COD initial a été éliminé par couplage du prétraitement électrochimique et d'un traitement biologique. Dans le même cadre, Fontmorin et al. (2013) ont étudié la minéralisation de l'acide 2,4-dichlorophenoxyacétique (2,4-D) par procédé combiné : un prétraitement électrochimique

suivi d'un traitement biologique à boues activées. L'oxydation électrochimique du 2,4-D a été effectuée en utilisant un feutre de graphite comme électrode de travail. Les résultats obtenus ont montré que le prétraitement électrochimique a diminué le COD de 29% et que le traitement biologique de la solution électrolysée a réduit 49% du COD restant, soit donc un taux de minéralisation totale de 78%. Zapata et al. (2010) ont étudié la faisabilité du couplage du procédé photo-Fenton et d'un traitement biologique pour la décontamination d'un effluent industriel pollué par des pesticides commerciaux ; ils ont démontré que le procédé photo-Fenton est capable d'améliorer la biodégradabilité de l'effluent considéré, et que le système combiné peut éliminer les pesticides et réduire le COD et la DCO de l'effluent de 80%. Dans le même contexte Ballesteros Martin et al. (2009) ont combiné le procédé photo-Fenton et un traitement biologique à boues activées pour le traitement d'un mélange de quatre pesticides commerciaux ; cette méthode a conduit à un taux d'abattement du COD de 90%. Sirtori et al. (2009) ont étudié la dégradation des quinolones par procédé photo-Fenton combiné à un traitement biologique. Ils ont obtenu un taux d'abattement global du COD de 95% dont 33% par photo-Fenton et 62% par traitement biologique.

La pertinence de la combinaison de deux procédés : électro-Fenton et biologique, pour la minéralisation de la tylosine (TYL), a été examinée par Ferrag-Siagh et al. (2014). Le prétraitement par électro-Fenton a été effectué en utilisant une cathode en feutre de carbone et une anode en platine. L'intensité du courant appliqué a été maintenue à 300 mA. Les résultats obtenus ont révélé qu'une durée d'électrolyse de 15 min était nécessaire pour la dégradation totale de la tylosine tandis que 4 h d'électrolyse permettaient de réduire seulement 21% du COT initial. Une amélioration de la biodégradabilité a été également observée, ce qui laissait suggérer que les sous-produits issus de la dégradation de la TYL peuvent être assimilable par les micro-organismes lors du traitement biologique. La solution électrolysée durant 4h a été traitée par boues activées durant 25 jours, le taux de minéralisation obtenu à la fin du traitement était de 67%.

Moussavi et al. (2012) ont combiné le procédé électro-Fenton et le traitement biologique afin de dégrader le formaldéhyde à une concentration élevée (7500 mg/L). La cathode et l'anode utilisées lors de l'électrolyse sont deux plaques en fer de même dimension (2cm×10cm×0,1cm). La densité de courant appliqué a été maintenue à 8,5 mA cm^{-2}. Les résultats obtenus ont montré que le prétraitement par procédé électro-Fenton a permis la dégradation totale du formaldéhyde ainsi que la réduction de 51% du COD initial au bout de 6 min. Le traitement biologique de la solution électrolysée a éliminé le COD restant au bout de 16 jours alors qu'un traitement

biologique réalisé sur une solution non traitée a besoin de 26 jours pour dégrader le formaldéhyde et de 31 jours pour éliminer la totalité du COD.

La minéralisation de la tétracycline (TC) par couplage du procédé électro-Fenton et du traitement biologique a été également étudiée (Ferrag-Siagh et al., 2013). L'électrolyse de 100 mg/L de TC a été effectuée en présence de de 0,1 mM d'ion ferreux à pH 3, en utilisant une cathode en feutre de carbone et une anode en platine. L'intensité du courant a été fixée à 300 mA. L'évolution du COT au cours du temps a été suivie, les taux de minéralisation atteints après 2 et 4 h de traitement étaient respectivement de 46 et 72%. L'évolution de la biodégradabilité de la TC a été également suivie au cours du traitement. Les résultats ont pu démontrer que le rapport DBO_5/DCO augmentait de 0,02 à 0,33 et 0,44 après 2 et 4 h d'électrolyse, respectivement prouvant ainsi l'efficacité du prétraitement par procédé électro-Fenton. En raison de l'amélioration de la biodégradabilité, un traitement par boues activées pendant 25 jours a été élaboré ; les taux d'abattement du COT obtenus en fin de traitement étaient de 68 et 86% pour les solutions de TC électrolysées pendant 2 et 4h, respectivement. Bien que le traitement biologique soit un procédé économiquement rentable, son efficacité est limitée par les composés organiques récalcitrants et par le temps requis lorsqu'une longue période d'acclimatation est nécessaire. D'autre part, lors de la minéralisation des composés organiques récalcitrants par procédé électro-Fenton, la consommation en énergie électrique et relativement le coût de traitement sont d'autant plus élevés que la durée d'électrolyse est assez longue. Par conséquent, le couplage de ces deux procédés permet un traitement efficace et moins onéreux.

En outre, l'ensemble des travaux réalisés sur le couplage du procédé électro-Fenton et d'un traitement biologique montre que le prétraitement permet d'améliorer la biodégradabilité des effluents contenant des composés organiques récalcitrants et de générer des sous-produits assimilables par les micro-organismes présents dans le traitement biologique ultérieur. Ainsi, afin d'assurer leur croissance et leurs besoins énergétiques, les micro-organismes qui possèdent à la fois des capacités digestives et oxydantes, vont minéraliser ces composés (Crini et al., 2007).

Des procédés de traitement combinés ont été proposés pour traiter les eaux usées contenant des colorants, y compris UV/H_2O_2 ou UV/O_3, suivi d'un traitement biologique. Plusieurs chercheurs ont également étudié l'application de l'ozonation partielle ou POA comme étape de prétraitement, suivi par des traitements biologiques ultérieurs pour traiter des solutions colorées (Lu et al., 2009).

I.5. Conclusion

Les procédés d'oxydation avancée sont des techniques de traitement de l'eau ou bien de l'air qui permettent la production d'un oxydant puissant à partir d'un réactif oxydant primaire. Ces technologies agissent et réagissent en général suivant deux modes d'action, soit par action directe (O_3/UV, H_2O_2/UV, O_3/H_2O_2) ou par action indirecte sur le polluant cible. L'efficacité des POA vis-à-vis de la dégradation des polluants résulte de la génération *in-situ* d'espèces radicalaires très réactives, principalement les radicaux hydroxyles. Ils ont une durée de vie extrêmement courte qui n'excède pas le dixième de microseconde. Ils peuvent instantanément oxyder la plupart des composés organiques par des réactions d'addition et des réactions d'abstraction d'hydrogène. Les POA sont souvent employés pour la dégradation des polluants organiques réputés non oxydables ou difficilement oxydables par des procédés chimiques ou biologiques conventionnels. Ces techniques sont susceptibles d'améliorer la biodégradabilité de la molécule récalcitarante en la transformant en sous produits facilement assimilables par les micro-organismes. C'est ainsi que le traitement biologique peut être appliqué afin de tenter une minéralisation du polluant organique.

Références bibliographiques

Alanizy R., Akgerman A., 2000. Advanced oxidation of phenolic compounds, Advances in Environ. Res., 4, 233-244.

Andreozzi R., Caprio V., Insola A., Marotta R., 1999. Advanced Oxidation Process (AOP) for Water Purification and Recovery, Catal. Today 53, 51-59.

Ballesteros Martín M.M., Sánchez Pérez J.A., Casas López J.L., Oller I., Malato Rodríguez S., 2009. Degradation of a four-pesticide mixture by combined photo-Fenton and biological oxidation, Water Res. 43, 653-660.

Bauer R., Fallmann H., 1997. The Photo-Fenton oxidation - A cheap and efficient wastewater treatment method, Res. Chem. intermediates, 23, 341-354.

Benitez F.J., Beltran Heredia F.J., Acero J.L. Et Rubio F.J., 2001. Oxidation of several chlorophenolic derivatives by UV irradiation and hydroxyl radicals, J. Chem. Technol. Biotechnol., 76, 312-320.

Benitez F.J., Beltran Heredia F.J., Acero J.L. Rubio F.J., 2000. Rate constants for the reactions of ozone with chlorophenols in aqueous solutions, J. Hazard. Mater., B 79, 271-285.

Butler R., Ehrenberg S., Godley A.R., Lake R., Lytton L., Cartmell E., 2006. Remediation of bromate-contaminated groundwater in an ex situ fixed-film bioreactor, Sci. Total Environ., 366, 12–20.

Chamarro E., Espuglas S., 2001. Use of Fenton reagent to improve organic chemical biodegradability, Water Res., 35, 1047-1051.

Chan Y.J., Chong M.F., Law C.L., Hassell D.G., 2009. A review on anaerobic-aerobic treatment of industrial and municipal wastewater, Chem. Eng. J., 155, 1-18.

Chong M.N., Jin B., Chow C.W.K., Saint C., 2010. Recent developments in photocatalytic water treatment technology: A review, Water Res., 44, 2997-3027.

Chou S.S., Huang Y.H., Lee S.N., Huang G.H., Huang C.P., 1999. Treatment of high strenght hexamine-containing wastewater by electro-Fenton method, Water Res., 33, 751-759.

Crini G., Badot P.M., 2007. Traitement et épuration des eaux industrielles polluées : Procédés membranaires, bioadsorption et oxydation chimique, Presses universitaires de Franche-Comté. http://books.google.tn/books?id=stqpsN7Ld7oC.

De A.K., Chaudury B., Bhattacharjee S. et Dutta B.K., 1999. Estimation of $HO^{\bullet}$ radical reaction rate constants for phenol and chlorinated phenols using UV/H_2O_2 photo-oxidation, J. Hazard. Mater. B 64: 91-104.

Dott W., Feidieker D., Steiof M., Becker P.M., Kampfer P., 1995. Comparison of *ex-situ* and *in-situ* techniques for bioremediation of hydrocarbon-polluted soils. Int. Biodeterior. Biodegrad. 35, 301-316.

Edelahi M., 2004. Contribution à l'Etude de Dégradation *in-situ* des Pesticides par Procédés d'Oxydation Avancés Faisant Intervenir le Fer. Application aux Herbicides Phénylurées', Thèse de Doctorat, Université de Marne-La-Vallée, France.

Esparza P., Borges M.E., Díaz L., Alvarez-Galván M.C., Fierro J.L.G., 2010. Photodegradation of dye pollutants using new nanostructured titania supported on volcanic ashes. Appl. Catal. A : General 388, 7-14.

Espuglas S., Gimenez J., Contreras S., Pascual E., Rodriguez M., 2002. Comparison of different advanced oxidation processes for phenol degradation, Water Res., 36, 1034-1042.

Farhadian M., Duchez D., Vachelard C., Larroche C., 2008. Monoaromatics removal from polluted water through bioreactors-A review, Water Res., 42, 1325-1341.

Faust B. et Hoigne J., 1990. Photolysis of Fe(III) – hydroxy complexes as sources of OH radicals in clouds, fog and rain, Atmosph. Environ., 24A,79-89.

Fenton H.J.H., 1894. Oxidation of tartaric acid in the presence of iron, J. Chem. Soc., 65, 899.

Ferrag-Siagh F., Fourcade F., Soutrel I., Aït-Amar H., Djelal H., Amrane A., 2014. Electro-Fenton pretreatment for the improvement of tylosin biodegradability, Environ. Sci. Pollut. Res. 21, 8534-8542.

Ferrag-Siagh F., Fourcade F., Soutrel I., Aït-Amar H., Djelal H., Amrane A., 2013. Tetracycline degradation and mineralization by the coupling of an electro-Fenton pretreatment and a biological process: Tetracycline degradation and mineralization, J. Chem. Technol. Biotechnol. 88, 1380–1386.

Fontmorin J.-M., Fourcade F., Geneste F., Floner D., Huguet S., Amrane A., 2013. Combined process for 2,4-Dichlorophenoxyacetic acid treatment-Coupling of an electrochemical system with a biological treatment, Biochem. Eng. J. 70, 17–22.

Glaze W.H., Kang J.W., Chapin D.H., 1987. the chemistry of water treatment processes involving ozone, hydrogen peroxide and ultraviolet radiation, Ozone Sci. Eng., 9 (4), 335-342.

Gogate P.R., Pandit A.B., 2004. A review of imperative technologies for wastewater treatment I: oxidation technologies at ambient conditions, Adv. Environ. Res., 8, 501-551.

Gonze E., Pillot S., Valette E., Gonthier Y., Bernis A., 2003. Ultrasonic treatment of an aerobic activated sludge in a batch reactor, Chem. Eng. Process., 42, 965-975.

Guieysse B., Bernhoft I., Andersson B.E., Henrysson T., Olsson S., Mattiasson B., 2000. Degradation of acenaphthene, phenanthrene and pyrene in a packed-bed biofilm reactor, Appl. Microbiol Biotechnol., 54, 826–831.

Haddou M., 2010. Dégradation de dérivés de l'acide benzoïque par les procédés d'oxydation avancée en phase homogène et hétérogène : Procédés Fenton, photo-Fenton et photocatalyse, Thèse de Doctorat Université Toulouse III - Paul Sabatier, France, 44 pages.

IWE, (2007), http://www.iwe-radebeul.de/.

Jiang Y., Petrier C., Waite T., 2002. Kinetics and mechanisms of ultrasonic degradation of volatile chlorinated aromatics in aqueous solutions, Ultrason. Sonochem., 9, 317-323.

Kasprzyk-Hordern B., Ziółek M., Nawrocki J., 2003. Catalytic ozonation and methods for enhancing molecular ozone reactions in water treatment, Appl. Catal. B : Environ., 46, 639-669.

Legrini O., Oliveros E. Et Braun A.M., 1993. Photochemical processes for water treatment, Chem. Rev. 93, 671-698.

Li D., Zheng H., Wang Q., Wang X., Jiang W., Zhang Z., Yang Y., 2014. A novel double-cylindrical-shell photoreactor immobilized with monolayer TiO_2-coated silica gel beads for photocatalytic degradation of Rhodamine B and Methyl Orange in aqueous solution. Separ. Purif. Technol. 123, 130-138.

Lu X, Yang B, Chen J, Sun R. 2009. Treatment of wastewater containing azo dye reactive brilliant red X-3B using sequential ozonation and upflow biological aerated filter process. J. Hazard. Mater.161, 241-245.

Malato S., Blanco J., Maldonado M.I., Oller I., Gernjak W., Perez-Estrada L., 2007. Coupling solar photo-Fenton and biotreatment at industrial scale: Main results of a demonstration plant, J. Hazard. Mater., 146, 440–446.

Mason T. J., 1997. Ultrasound in synthetic organic chemistry, Chem. Soc. Rev., 26, 443-451.

Min B., Evans P.J., Chu A.K., Logan B.E., 2004. Perchlorate removal in sand and plastic media bioreactors. Water Res., 38, 47–60.

Mohammadi-Aghdam S., Marandi R., Olya M.E., Mehrdad Sharif A.A., 2014. Kinetic modeling of BB41 photocatalytic treatment in a semibatch flow photoreactor using a nanocomposite film. J. Saudi Chem. Soc. 18, 317-326.

Moussavi G., Bagheri A., Khavanin A., 2012. The investigation of degradation and mineralization of high concentrations of formaldehyde in an electro-Fenton process combined with the biodegradation, J. Hazard. Mater. 237-238, 147–152.

Nogueira R.F.P., Trovo A.G., da Silva M.R.A., Villa R.D., de Oliveira M.C., 2007. Fundaments and environmental applications of Fenton and photo-Fenton processes, Quimica Nova, 30, 400-408.

Ohlen K., Chang Y.K., Hegemann W., Yin C.R., Lee S.T., 2005. Enhanced degradation of chlorinated ethylenes in groundwater from a paint contaminated site by two-stage fluidized bed reactor, Chemosphere, 58, 373–377.

Pacheco M.J., Morão A., Lopes A., Ciríaco L., Gonçalves I., 2007. Degradation of phenols using boron-doped diamond electrodes: A method for quantifying the extent of combustion, Electrochim. Acta, 53, 629-636.

Panizza M., Cerisola G., 2001. Removal of organic pollutants from industrial wastewater by electrogenerated Fenton's reagent, Water Res., 35, 3987-3992.

Panthi G., Barakat N. A.M., Park M., Kim H.-Y., Park S.-J., 2015. Fabrication of PdS/ZnS NPs doped PVAc hybrid electrospun nanofibers: Effective and reusable catalyst for dye photodegradation. J. Industr. Eng. Chem. 21, 298-302.

Pera-Titus M., García-Molina V., Baños M. A., Giménez J., Esplugas S., 2004. Applied Catalysis B: Environmental, 47 (4), 219.

Pignatello J.J., 1992. Dark and Photoassisted $Fe3^{+}$-Catalyzed Degradation of Chlorophenoxy Herbicides by Hydrogen Peroxide, Environ. Sci. Technol., 26, 944-951.

Pignatello J.J., Oliveros E., MacKay A., 2007. Advanced oxidation processes for organic contaminant destruction based on the Fenton reaction and related chemistry, Crit. Rev. Envi. Sci. Technol. 36, 2006, 1-84; Erratum, 37, 273-275.

Pinho L.X., Azevedo J., Miranda S. M., Ângelo J., Mendes A., Vilar V.J.P., Vasconcelos V., Boaventura R.A.R., 2015. Oxidation of microcystin-LR and cylindrospermopsin by heterogeneous photocatalysis using a tubular photoreactor packed with different TiO_2 coated supports. Chem. Eng. J. 266, 100-111.

Pintar A., Levec J., 1992. Catalytic oxidation of organics in aqueous solutions-i. Kinetics of phenol oxidation, J. Catal., 135, 345-357.

Poyatos J. M., Muñio M. M., Almecija M. C., Torres J. C., Hontoria E., Osorio F., 2010. Advanced oxidation processes for wastewater treatment: state of the art. Water Air Soil Pollution, 205,187–204.

Qiang Z., Chang J., Huang C., 2003. Electrochemical regeneration of Fe^{2+} in Fenton oxidation processes, Water Res., 37, 1308–1319.

Rajeshwar K., Osugi M.E., Chanmanee W., Chenthamarakshan C.R., Zanoni M.V.B., Kajitvichyanukul P., Krishnan-Ayer R., 2008. Heterogeneous photocatalytic treatment of organic dyes in air and aqueous media. J. Photochem. Photobiol. C: Photochem. Rev. 9, 171-192.

Rasoulifard M., Fazli M., Eskandarian M., 2014. Kinetic study for photocatalytic degradation of Direct Red 23 in UV–LED/nano-TiO_2/S_2O82- process: Dependence of degradation kinetic on operational parameters. J. Indust. Eng. Chem. 20, 3695-3702.

Rasoulifard M.H., Fazli M., Eskandarian M. R., 2015. Performance of the light-emitting-diodes in a continuous photoreactor for degradation of Direct Red 23 using UV-LED/S_2O82- process. J. Indust. Eng. Chem. 24, 121-126.

Rivas F.J., Kolaczkowski S.T., Beltrán F.J., Mc-Lurgh D.B., 1998. Development of a model for the wet air oxidation of phenol based on a free radical mechanism, Chem. Eng. Sci., 53, 2575-2586.

Ruppert G., Bauer R. et Heisler G., 1993. The photo-Fenton reaction–an effective photochemical wastewater treatment process, J. Photochem. Photobiol. A., 73, 75-78.

Sadana A., Katzer J.R., 1974. Involvement of Free Radicals in the Aqueous-Phase Catalytic Oxidation of Phenol Over Copper Oxide, J. Catal., 35, 140-152.

Sirtori C., Zapata A., Oller I., Gernjak W., Agüera A., Malato S., 2009. Decontamination industrial pharmaceutical wastewater by combining solar photo-Fenton and biological treatment, Water Res. 43, 661–668.

Sun Y. Et Pignatello J., 1993. Photochemical-reactions involved in the total mineralization of 2,4-D by Fe^{3+}/H_2O_2 /UV, Environ. Sci. Technol. 27, 304-310.

Tahir B., Tahir M., Amin N.S., 2015a. Gold–indium modified TiO_2 nanocatalysts for photocatalytic CO_2 reduction with H_2 as reductant in a monolith photoreactor. Appl. Surf. Sci. 338, 1-14.

Tahir B., Tahir M., Amin N.S., 2015b. Performance analysis of monolith photoreactor for CO_2 reduction with H_2. Energy Conver. Manage. 90, 272-281.

Walling C., 1975. Fenton's Reagent Revisited, Acc. Chem. Res., 8, 125-131.

Wang J., Sun Y., Feng J., Xin L., Ma J., 2016. Degradation of triclocarban in water by dielectric barrier discharge plasma combined with TiO_2/activated carbon fibers: Effect of operating parameters and byproducts identification, Chem. Eng. J., 300, 36-46.

Wurtele M.A., Kolbe T., Lipsz M., Kulberg A., Weyers M., Kneissl M., Jekel M., 2011. Application of GaN-based ultraviolet-C light emitting diodes – UV LEDs – for water disinfection. Water Res. 45, 1481-1489.

Yahiaoui I., Aissani-Benissad F., Fourcade F., Amrane A., 2013. Removal of tetracycline hydrochloride from water based on direct anodic oxidation (Pb/PbO_2 electrode) coupled to activated sludge culture, Chem. Eng. J. 221, 418–425.

Yahiat S., Fourcade F., Brosillon S., Amrane A., 2011. Removal of antibiotics by an integrated process coupling photocatalysis and biological treatment-Case of tetracycline and tylosin, Int. Biodeterior. Biodegrad. 65, 997–1003.

Yavuz Y., 2007. EC and EF processes for the treatment of alcohol distillery wastewater, Sep. Purif. Technol., 53, 135–140.

Zapata A., Oller I., Sirtori C., Rodríguez A., Sánchez-Pérez J.A., López A., 2010. Decontamination of industrial wastewater containing pesticides by combining large-scale homogeneous solar photocatalysis and biological treatment, Chem. Eng. J. 160, 447–456.

Zhao Y., Lin C., Bi H., Liu Y., Yan Q., 2017. Magnetically Separable $CuFe_2O_4$/AgBr Composite photocatalysts: Preparation, characterization, photocatalytic activity and photocatalytic mechanism under visible light, Appl. Surf. Sci., 392,701–707.

Zissis G. et Damelincourt J-J., 2007. Sources de lumière du XXIe siècle, Techniques de l'Ingénieur.

Zsilák Z., Fónagy O., Szabó-Bárdos E., Horváth O., Horváth K., Hajós P., 2014. Degradation of industrial surfactants by photocatalysis combined with ozonation, Environ. Sci. Pollut. Res., 21, 11126–11134.

CHAPITRE II: Réacteurs Photocatalytiques Dédiés à la Dégradation de Polluants Organiques Dangeureux : Cinétique, Aspects Mécanistiques et Conception - Revue

---

Photocatalytic Reactors Dedicated to the Degradation of Hazardous Organic Pollutants: Kinetics, Mechanistic Aspects, and Design – A Review

Hichem ZEGHIOUD [1,2], Nabila KHELLAF [1,2], Hayet DJELAL [3,6], Abdeltif AMRANE [4,6], Mohammed BOUHELASSA [5]

Chemical Engineering Communications, 203 (2016) 1415–1431

[1] Department of Process Engineering, Faculty of Engineering, Badji Mokhtar University, P.O. Box 12, 23000 Annaba, Algeria.
[2] Laboratory of Organic Synthesis-Modeling and Optimization of Chemical Processes, Badji Mokhtar University, P.O. Box 12, 23000 Annaba, Algeria.
[3] Ecole des Métiers de l'Environnement, Campus de Ker Lann, 35170 Bruz, France.
[4] Université de Rennes 1, ENSCR, CNRS, UMR 6226, Allée de Beaulieu, CS 50837, 35708 Rennes Cedex 7, France.
[5] LIPE, Faculty of Process Engineering, Constantine 3 University, 25000 Algeria
[6] Université Européenne de Bretagne, 5 Boulevard Laennec, Rennes, France.

Préambule

Ces dernières années, la photocatalyse hétérogène est apparue comme une nouvelle technologie de décontamination efficace, puissante, propre et sûre pour le traitement de polluants organiques et la transformation de produits chimiques dangereux en différentes formes. Son principe est basé sur la photo-génération des paires séparées d'électrons (e^-)/trous positifs (h^+) dans les particules des semi-conducteurs sous l'effet de l'éclairement de ce dernier (par exemple TiO_2) par une source UV ou visible.

Le mécanisme d'un processus de photocatalyse hétérogène classique peut être divisé en cinq étapes distinctes :

1) Diffusion des réactifs de la phase fluide à la surface du photocatalyseur ;
2) Adsorption d'au moins un des réactifs ;
3) Réaction photocatalytique pour la phase adsorbée sur la surface du semi-conducteur ;
4) Désorption du (des) produit (s) de la surface du semiconducteur ;
5) Retrait du (des) produit (s) de la région d'interface à la phase fluide.

Cet article de synthèse se concentre sur le développement récent de diverses technologies conventionnelles de réacteurs destinés à la photodégradation de polluants organiques dangereux avec leurs avantages et inconvénients. Le phénomène est fortement influencé par les conditions d'opération de la réaction photocatalytique telles que la température, le pH, l'intensité lumineuse et la longueur d'onde, la concentration de polluants, la quantité de photocatalyseur, l'humidité relative et d'autres paramètres. L'activité photo-catalytique dépend des caractéristiques structurelles du semi-conducteur, de sa morphologie et de la taille de ses particules.

L'article présente la progression des réacteurs photocatalytiques pour la dégradation des colorants synthétiques en accordant une attention particulière à l'utilisation du photocatalyseur synthétique supporté, en raison de l'avantage majeur d'une séparation facile du catalyseur par rapport au système homogène et/ou en suspension. En outre, une attention particulière a été accordée à la littérature traitant de la promotion de l'efficacité lumineuse en testant diverses sources lumineuses.

Nomenclature

AOPs:	Advanced Oxidation Processes
CMCPR:	Cylindrical Multi-Column Photocatalytic Reactor

DCS:	Double-Cylindrical-Shell
EPA:	Environmental Protection Agency
GFT:	TiO_2 deposited on a fiber glass support
G-L:	Gaz-Liquid
LED:	Light Emitting Diode
M:	Montmorillonite
MO:	Methyl orange
MPA:	Mercaptopropionic
PAH:	Polycyclic aromatic hydrocarbon
PMR:	Photocatalytic Membrane Reactor
PVDF:	Polyvinyldene fluoride
RDPFC:	Rotating Disk Photocatalytic Fuel Cell
RH:	Relative Humidity
TCE:	Trichlorethylene
UV:	Ultraviolet
VOC:	Volatile Organic Compound
WHO:	World Health Organization
ZPC:	Zero Point Charge

Abstract

In recent years, heterogeneous photocatalysis has emerged as a new effective, powerful, clean and safe decontamination technology for the treatment of organic pollutants and the transformation of hazardous chemicals into different forms. This review focuses on the recent development of various conventional technologies of reactors designated for the photodegradation of hazardous organic pollutants with their limitations. The phenomenon is strongly influenced by reaction conditions such as temperature of reaction, pH, light intensity and wavelength, pollutant concentration, photocatalyst quantity, relative humidity and other parameters. The catalyst photo activity depends on the structural characteristics of the semiconductor, its morphology and its particles size.

This paper presents the progression of photocatalytic reactors for synthetic dye degradation with special consideration to the use of supported photocatalyst and nanostructured titanium supported over volcanic ashes, owing to the major advantage of an easy separation of the catalyst if compared to homogenous system, namely suspended catalyst. In addition, a special

attention was paid to the literature dealing with the promotion of light efficiency by testing various light sources.

Keywords: Organic pollutants, Photocatalysis, Photoreactors, Synthetic dyes, Water treatment.

II.1. Introduction

Since the onset of the industrial revolution, there has been a steady change in the composition of the atmosphere, water and soils. In fact, in the developing world, the highest air and water pollution exposures occur in the environment mainly due to a wide variety of organic pollutants (pesticides, polynuclear aromatic hydrocarbons, detergents, solvents, dyes, pharmaceuticals, petroleum hydrocarbons, etc.). These pollutants are present in the environment as a result of anthropogenic activities (domestic, agricultural and industrial activities) and most of them have some characteristics, namely persistence, bioaccumulation, bioconcentration or long half-lives in the environment. Yearly, there are 3 million critical pesticide-poisoning with about 220,000 deaths (Ojanperä, 2000). Detergents, when concentrated in water surface, produce foam and emulsification. They block the exchange of oxygen in water, deteriorate seawater quality and degrade aquatic ecosystems. Some synthetic benzene compounds are very poisonous, resistant to biodegradation, and toxic to microorganisms (Liu et al., 2010). During deactivation, pharmaceutical compound residues have the tendency to cause the development of antibiotic resistant microbes and to increase the resistance of the pathogenic bacteria in the aquatic environment (Dalrymple et al., 2007). Aromatic hydrocarbons, widely used in printing, painting, synthetic resin and synthetic rubber industries, are toxic and often classified as carcinogens for humans (Ning et al., 2015). Dye and pigment pollution originating from several industries is considered as a significant source of aquatic ecosystem disequilibria. The discharge of colored effluents into the environment is aesthetically displeasuring, impedes light penetration, retards photosynthesis, inhibits the growth of aquatic life and damages the quality of the receiving streams (Garg et al., 2004; Padmesh et al., 2006).

The different hazardous chemicals can be transported in our atmosphere, oceans and introduced into the water systems, food chains and accumulate in places far away from their original source; they are originated from various sources such as industrial effluents, power generation, transport, agricultural sectors and domestic. The exposure to the contaminated environment by these chemicals pose a seriously and adversely threat for the community's health and can cause numerous diseases such as allergies, digestive problems, cancer, asthma, respiratory and cardio-pulmonary diseases. There is therefore an urgent need for effective and environmentally friendly technologies for wastewater and gas effluent treatment.

II.2. Environmental protection

Several lists of dangerous chemical substances have been drawn up by various national and international organisms such as WHO (World Health Organization) and EPA (Environmental Protection Agency). The WHO has estimated that billions of people worldwide cannot be supplied with clean drinking water. In addition, millions of people die every year due to waterborne diseases transmission (Chong et al., 2010).

The majority of organic pollutants initiated from industrial processes are highly recalcitrant to traditional wastewater treatments because of their synthetic origin and complex aromatic structure (Silva and Faria, 2003). During the various manufacturing operations, thousands of tons of these compounds are lost in effluents causing a high threat to human health owing to the toxicity and potential carcinogenicity of these synthetic compounds (Karkmaz et al., 2004). Environmental standards and requirements related to industrial effluents should be adopted restricting the discharge of these effluents without efficient and sufficient treatment.

II.3. The need to treat contaminated waters

Water pollution caused by harmful substances has become a global concern and the control of organic toxins in water is an important measure in natural ecosystems and public health protection. There is an increasing volume of wastewaters discharged into the aquatic environment that contains persistent pollutants, which are not only toxic but also only partly biodegradable, and hence they are not easily removed in biological wastewater plants. That is why there is a need to develop effective and new powerful, clean and safe decontamination technologies for the degradation of organic pollutants, either to less harmful compounds or to their complete mineralization.

Photocatalysis is among the recent detoxification techniques developed in order to destroy and/or eliminate these substances from wastewaters. It belongs to the advanced oxidation processes (AOPs) and associates the use of UV light and TiO_2; it has received a careful attention because it leads to the degradation of organic pollutants until the conversion to carbon dioxide, water, nitrogen and other minerals as final by-products in the case of a complete mineralization (**Eq. II.1**).

$$^{\bullet}OH + Pollutant \rightarrow CO_2 + H_2O + inorganic\ acids \qquad (II.1)$$

However, during photocatalysis, total mineralization was not always achieved and the obtained by-products can be even more toxic and harmful to the environment than the target pollutants.

II.4. Photocatalysis

II.4.1. Principle and definitions

According to the conventional chemical terminology, photocatalysis is defined as a natural phenomenon, namely thermodynamically favoured, in which a substance, the photocatalyst, accelerates the rate of a chemical photoreaction, induced by the absorption of light by a catalyst or a coexisting molecule. This may be the most commonly known definition of photocatalysis as it encompasses all aspects of the field including photosensitization (Serpone and Salinaro, 1999; Braslavsky, 2007).

The heterogeneous photocatalysis principle is based on the photogeneration of separated pairs electrons (e^-)/positive holes (h^+) in the semiconductor particles under the effect of the illumination of this latter (e.g. TiO_2) by an UV source (**Eq. II.2**).Photon absorption by TiO_2 results in the promotion of an electron from the valence band to the conduction band of the titania, leaving behind a ‘‘hole’’ (electron vacancy) in the valence band and an excess of negative charges in the conduction band. These charge carriers either recombine inside the particle or move to its surface, where they initiate a wide range of chemical redox reactions with adsorbed organic molecules (Hoffmann et al., 1995) of an acceptor and of a donor if their redox potentials lie within the band gap.

$$TiO_2 \xrightarrow{h\nu} h^+ + e^- \qquad (\lambda \leq 380\ nm) \qquad \text{(II.2)}$$

II.4.2. Implementation of the photocatalyst (in suspension, immobilized on a support)

The development of the UV/TiO_2 process in order to achieve complete mineralization of organic pollutants has been widely tested for a large variety of chemicals. Photocatalysts are often applied in the form of suspension or slurry. In 2014, Djellabi et al. (2014) developed a new photocatalyst based on anatase TiO_2, which was prepared by impregnation with $TiCl_4$, a photoactive TiO_2–montmorillonite composite. The photoactivity tests showed that the activity of TiO_2–M in suspension is more important for cationic dyes where the removal rates can reach 97.1% for crystal violet. The comparison of the activity of this composite with that of the commercial P25 demonstrates that synthesized TiO_2–M exhibits a higher adsorptive behaviour and can be used as low-cost alternative to the commercial TiO_2 for wastewater treatment. Several studies have been reported on the degradation of a herbicide derivative (isoproturon) and pesticide derivatives (dichlorvos, phosphamidon, triclopyr and daminozid) in whichthe degradation kinetics was studied under different conditions namely pH, catalyst concentration,

substrate concentration andthe presence of electron acceptors (H_2O_2, $KBrO_3$, $(NH_4)_2S_2O_8$. Degradation rates of these compounds were found to be strongly influenced by all the above parameters (Haque et al., 2003; Atiqur Rahman et al., 2005; Qamar et al., 2006). In slurry systems, the catalyst must be removed with a solid–liquid separation stage, which adds to the overall capital and running costs of the plant (Byrne et al., 1998; Thiruvenkatachari et al., 2008). In order to make environmental applications of TiO_2 photocatalysis more practical, immobilization of TiO_2 or fixed to various rigid supports is required. In this regards, TiO_2-P25 (Degussa) can be immobilized onto a solid substrate such as sand, polymer films and glass (Dhananjeyan et al., 2000; Sakthivel et al., 2002). However, although immobilized systems are less photoactive than slurry systems, they can lead to comparable irradiation time to obtain the required efficiency (Colmenares and Xu, 2016).

Li et al. (2014) developed a double-cylindrical-shell (DCS) photoreactor immobilized with monolayer TiO_2-coated silica gel beads; they used UV–VIS–NIR spectroscopy analysis and kinetic studies to confirm the degradation of some pollutants. They found that the developed photocatalytic reactor, in comparison with reported slurry-suspension and thin-film photoreactors, showed higher efficiency, lower energy consumption and better repetitive operation performance for the degradation of Rhodamine B (RhB) and Methyl Orange (MO). Moreover, the development of a novel cylindrical multi-column photocatalytic reactor (CMCPR) (Li et al., 2015a) showed high photodegradation (100%) and mineralization (78.1%) for amoxicillin (AMX). On the other hand, the electrical energy consumption for photocatalytic degradation of methyl orange (MO), amoxicillin (AMX) and 3-chlorophenol (3-CP) were one thousand time less than those reported for slurry and thin-film photoreactors.

II.4.3. Mechanism of photodegradation of chemicals

The mechanism of a conventional heterogeneous photocatalysis process can be divided into five distinct stages (Herrmann, 1999):

1. Diffusion of the reactants from the bulk phase to the surface of the photocatalyst;
2. Adsorption of at least one of the reactants;
3. Photocatalytic reaction for the adsorbed phase on the TiO_2 surface;
4. Desorption of the product(s) from the TiO_2 surface;
5. Removal of the product(s) from the interface region to the bulk fluid.

Lichtfouse et al. (2013) reported a series of oxidation-reduction reactions that might occur during TiO_2 photocatalysis (**Eq. II.3-II.11**).

A typical characteristic of semiconducting metallic oxides (TiO_2, ZnO, MoO_3, CeO_2, ZrO_2, WO_3, α-Fe_2O_3, SnO_2, $SrTiO_3$) is the extremely high oxidative potential of the holes. In the hole (*h*+) pathway, hydroxyl radical is formed via direct hole transfer to water which is an essential process in TiO_2 photocatalysis, or to hydroxyl ion (OH^-) to form powerful $^{\bullet}OH$ radicals (**Eq. II.3-II.4**).

$$h^+_{vB} + H_2O_{ads} \rightarrow {}^{\bullet}OH_{ads} + H^+ \quad \text{(II.3)}$$

$$h^+_{vB} + OH^-_{ad} \rightarrow {}^{\bullet}OH_{ads} \quad \text{(II.4)}$$

The $^{\bullet}OH$ radicals are able to oxidize and react with almost all water pollutants (organic molecules) P to consequently initiate the oxidative degradation which can lead then to complete mineralization (**Eq. II.5**). When molecular oxygen is available, it is adsorbed onto the surface of TiO_2 and can scavenge an electron to form the superoxide anion radical ($O_2^{\bullet -}$) (**Eq. II.6**).

$${}^{\bullet}OH_{ads} + P \rightarrow\rightarrow H_2O + CO_2 \quad \text{(II.5)}$$

$$(O_2)_{ads} + e^- \rightarrow O_2^{\bullet -} \quad \text{(II.6)}$$

Holes can also directly oxidize pollutants P by electron transfer (**Eq II.7-II.8**).

$$h^+_{vB} + P_{ads} \rightarrow P^{\bullet}_{ads} \quad \text{(II.7)}$$

$${}^{\bullet}OH_{ads} + P_{ads} \rightarrow \text{intermediates/degradation products} \quad \text{(II.8)}$$

The photogenerated e^-/h^+ pairs can undergo rapid recombination within nanoseconds in the absence of electron scavengers, such as oxygen, releasing heat without favouring any reactions. The e^-_{TR} and h^+_{TR} (**Eqs. II.9-II.11**) represent the surface trap valence band electron and conduction band hole, respectively.

$$\text{charge carrier trapping: } e^-_{cB} \rightarrow e^-_{TR} \quad \text{(II.9)}$$

$$\text{charge carrier trapping: } h^+_{vB} \rightarrow h^+_{TR} \quad \text{(II.10)}$$

$$e^-/h^+ \text{ recombination : } e^-_{TR} + h^+_{vB}(h^+_{TR}) \rightarrow e^-_{cB} + \text{heat} \quad \text{(II.11)}$$

II.4.4. Factors influencing the photocatalysis phenomenon

It is known that the optical properties of TiO_2 and, as a consequence, its photoactivity, are strongly influenced by its characteristics like structure, morphology and particles size. For this purpose, many researchers have developed several methods for the preparation of the

photocatalyst. Moreover, the photoactivity performances are strongly dependant on the adsorption capacity of the photocatalyst, the temperature of reaction, pH, wavelength and intensity of the light source, catalyst loading, pollutant concentration, presence of anions and oxidizing agents (Das and Bhattacharyya, 2015).

II.4.5. Effect of reaction conditions

a) Temperature

Temperature is an important environmental factor; the light variation in temperature does not affect the rate of photocatalytic transformation in an important way. But, for huge variations of temperature an impact can be observed leading to an increase in radical ions attraction as a result to the presence of a variety of different ions. It may result in unusual reactivity of $^{\bullet}OH$ or $SO_4^{-\bullet}$ for example. Rasoulifard et al. (2015) studied the effect of temperature on the photo-degradation of Direct Red 23 using UV-LED/$S_2O_8^{2-}$ in the temperature range 10–80 °C. They found that increasing the temperature involved an increase in degradation rates and decolourization efficiency, the increase in temperature furthermore helped the reaction to compete more efficiently with electron–hole recombination (Karimi et al., 2014). Similar result has been reported in the study of Tolvaj et al. (2013) and Shamsipur et al. (2015). Additionally, at high temperatures ($T \geq 70$–80 °C), the activity decreases and the apparent activation energy becomes negative. When temperature increases above 80 °C, nearing the boiling point of water, the exothermic adsorption of reactants becomes disfavoured and tends to become the rate limiting step of the whole reaction. The decrease in temperature favours adsorption (which is a spontaneous exothermic phenomenon), and especialy that of the final product, which becomes the inhibitor of the reaction (Herrmann, 2010). Therefore, the optimum temperature is generally between 10 and 80 °C.

b) pH

In heterogeneous photocatalysis, pH is one of the operating factors that influence the rate of the photocatalytic process (Franco et al., 2009; Gmurek et al., 2015). Depending on the surface charge of the photocatalyst and the nature of the organic compound, the pH is considered as a very complex parameter. Habib et al. (2012) reported in their study that the maximum decolorization of dye pollutants occurred at pH value equal to the zero-point charge (ZPC) of the semiconductors. This is because the photocatalyst surface becomes positively charged at pH < ZPC making the electrostatic interactions between the dye and the catalyst surfaces the predominant adsorption process. Hence, the standardization of the pH conditions for the

degradation of organic compounds is very difficult to operate (Zhang et al., 2014). Chen et al. (2013) reported a relatively low degradation efficiency under acidic and neutral conditions which was attributed to: (1) it is difficult for cationic dye molecules to be adsorbed on a TiO_2 surface; and (2) lower pH conditions produce less active •OH radicals. Conversely, an alkaline environment favours the formation of active •OH species, thus increasing the removal efficiency (Chen et al., 2013; Chen et al., 2014). For example, TiO_2 in acidic conditions tends to agglomerate, reducing the surface area available for dye adsorption (Wang et al., 2006). Otherwise, the decrease in pH could lead to an increase of percent degradation (Feng et al., 2014; Karimi et al., 2014). Li et al (2015a) found that the decrease in pH of the reaction medium when the photocatalyst surface was positively charged involves an increase of the degradation efficiency because the adsorption of pollutant on the catalyst surface was facilitated by electrostatic attraction between the positively charged photocatalyst surface and organic compound anions.

c) Wavelength and intensity of the light source

The threshold value of the wavelength corresponds to the band gap energy for the photocatalyst; e.g. for the TiO_2 catalyst having a band gap energy of 3.02 eV, the ideal wavelength is 400 nm (Herrmann, 1999). As discussed earlier, in some cases, sunlight may also be used for the excitation of the catalyst, leading to considerable economic savings (Velmurugan et al., 2014). The radiation source is a very important ingredient of the photocatalytic process and photon flux is a key factor in photochemical reactions. The light intensity plays an important role in the degradation of pollutants because of its effective role in the formation of high amounts of •OH (Behnajady et al., 2007). Therefore, an increase in light intensity is expected to lead to an increase in reaction rates (Guo et al., 2015); however, as the light intensity increases, its effects on reaction kinetics decrease so that its impact becomes negligible at high intensity (Faramarzpour et al., 2009).Terzian and Serpone (1995) in their studies indicated that at low light intensities (0–20 mW cm^{-2}), the reaction rate would increase linearly with increasing light intensity (first order); at intermediate light intensities (approximately 25 mW cm^{-2}), the reaction rate would depend on the square root of the light intensity (half order); and at high light intensities, the reaction rate is independent of the light intensity. Such an observation may be interpreted as follows: at low light intensity, reactions involving electron-hole formation predominate, while the electron-hole recombination is negligible. Nevertheless, as the light intensity is increased, electron-hole pair separation competes with electron-hole recombination, decreasing the reaction rate (Ollis et al., 1991). It is also in agreement with the findings of Assadi et al. (2013). They worked on volatile organic compounds (VOCs) and observed no

significant effect on the removal efficiency at high initial concentration, which was attributed to the fact that the degradation rate is not limited by the number of active sites; while, the effect of the UV intensity was significant at low initial concentration.

d) Photocatalyst loading

The amount of photocatalyst is an important parameter; it can affect the degradation rate of organic compounds (pesticide, dye, HAP, etc.). An increase in photocatalyst dosage contributes to increase the number of active sites but may reduce the degradation efficiency of the organic pollutant MO dye, by blocking UV irradiation (Huang et al., 2008). Nguyen et al. (2015) reported that the increase in TiO_2 dose increased the degradation efficiency of p-chlorophenol because TiO_2 exhibits a high capacity for promoting the interactions between hydroxyl radicals and organic compounds. However, when the concentration of catalyst is increased beyond an optimal value, no significant improvement of efficiency can be obtained. This effect indicates that excess photocatalyst would cause the aggregation of free catalyst and also increased opacity leading to a decrease in UV light penetration via the shielding effect of the suspended particles (Dixit et al., 2010; Esparza et al., 2010); the consequence is a lower photon transmission and low degradation rate (Xiao-gang et al., 2009). For Hu et al. (2014) a catalyst overdose in slurry system could pose a steric effect; the particle-particle interaction would block the light penetration and decreases the number of active reaction sites. In slurry and immobilized photocatalytic processes for the degradation of atrazine, the optimal photocatalyst concentrations reported in the literature for TiO_2 Degussa P-25 varied from 100 to 5000 mg L^{-1}, depending on the nature of the compounds, the contaminant level and the photoreactor geometry (Parra et al., 2004).

e) Pollutant concentration

It is essential from an application point of view to study the dependence of removal efficiency on the initial concentration of organic compounds. The rate of the degradation reactions is proportional to the initial concentration of the pollutants (Saikia et al., 2015). However, for some classes of pollutants, such as organic dyes, the decolourization efficiency decreases as the initial dye concentration is increased because the solution becomes more and more impermeable to UV radiation, leading to a slower production of hydroxyl radicals ($^{\bullet}OH$) according to **Eq. II.12**. In combination with this, fewer $^{\bullet}OH$ available are required to oxidize more dye molecules (Tang et al., 2004). Some researchers have proposed that solution decolourization occurs through direct electron (e^-) transfer from the catalyst surface to the dye molecule (**Eq. II.13**) (Tang and An, 1995), or/and direct oxidation by reaction with holes (h^+) (Houas et al., 2001).

Thus, with increasing dye concentration, less photocatalyst activation will result in fewer electrons available for direct reduction and fewer holes (h^+), which further inhibits degradation (**Eq. II.14**).

$$Dye + {}^{\bullet}OH \rightarrow Dye^{\bullet -} + H_2O \xrightarrow{{}^{\bullet}OH} \text{Degradation products} \quad \text{(II.12)}$$

$$Dye + e^- \rightarrow Dye^{\bullet -} \rightarrow \text{Degradation products} \quad \text{(II.13)}$$

$$Dye + h^+ \rightarrow Dye^{\bullet +} \rightarrow \text{Degradation products} \quad \text{(II.14)}$$

Baeissa (2014) found that increasing the initial concentration of methylene blue (MB) dye increases the photocatalytic efficiency in the first time; but above an optimal value, further increase causes an increase of the time needed for a total decolourization of the MB dye.

f) Presence of anions and oxidizing agents

For practical application of photocatalysis in water and wastewater treatment, it is imperative to investigate the influence of common matrix species on the degradation efficiency of organic pollutants. In general, the presence of sulfate, nitrate, and chloride only causes marginal reduction in pollutant removal efficiencies (Wang and Mil, 2010; Ma et al., 2014). The inhibitory effect at high anion concentrations might be generally due to two phenomena. First, anions could compete with pollutants for active sites of adsorption on the surface of photocatalyst, since their concentrations are far beyond that of pollutant. In addition, anions such as chloride, nitrate, sulfate, and bicarbonate have been reported to scavenge •OH and form ionic radicals, such as $Cl^{\bullet}$, $NO_3^{\bullet}$, $SO_4^{\bullet -}$ and $HCO_3^{\bullet}/CO_3^{\bullet -}$ (**Eqs. II.15–II.17**) which are less reactive than •OH (Burns, 1999; Rincoin et al., 2004). Kamble et al. (2006) indicated that the effect of carbonate and bicarbonate is relatively important; because these anions are alkaline in nature, it may change the surface charge of the photocatalyst.

$${}^{\bullet}OH + (Cl^- + NO_3^- + SO_4^{2-} \text{ and } HCO_3^-) \rightarrow OH^- + (Cl^{\bullet} + NO_3^{\bullet} + SO_4^{\bullet -} \text{ and } HCO_3^{\bullet}) \quad \text{(II.15)}$$

$$h^+ + (Cl^- + NO_3^- + SO_4^{2-} \text{ and } HCO_3^-) \rightarrow (Cl^{\bullet} + NO_3^{\bullet} + SO_4^{\bullet -} \text{ and } HCO_3^{\bullet}) \quad \text{(II.16)}$$

$${}^{\bullet}OH + HCO_3^- \rightarrow H_2O + CO_3^{\bullet -} \quad \text{(II.17)}$$

Dissolved oxygen could be trapped by conduction band electron to form radicals such as ($O_2^{\bullet -}$); therefore, reducing the re-combination of electron and holes pairs. Furthermore, the super-oxide ion generated may also react with water molecules to form hydroxyl radicals to give added photocatalytical effect to oxidize pollutants (Ku et al., 2005; Eng et al., 2012). Besides oxygen

as oxidant, some additional oxidants such as hydrogen peroxide and oxalate can accelerate reaction rates (Faramarzpour et al., 2009; Gupta et al., 2012).

g) Presence of metal ions

It is necessary to examine the photodegradation in the presence of metal ions to better understand the effect of the environmental matrix (authentic natural waters) on the removal efficiency. Feng et al. (2014) found that the photodegradation of methylparaben compared to deionized water is inhibited in natural waters in the order: Liangzi Lake < Donghu Lake < Changjiang River ≈ Seawater. According to the study of Chen et al. (2011) whoreported on the photodegradation of propranolol by Fe(III)-citrate complexes, metal ions such Mg^{2+}, Ca^{2+}, Cu^{2+}, and Mn^{2+} can form complexes with citrate in competition with Fe(III), and thus decrease the photodegradation of substrates in the Fe(III)-citrate solution.

h) Effect of relative humidity on the degradation rate

Water vapour has a significant effect on the kinetics of photocatalytic degradation. In fact, many studies have shown the effect of water vapour. Several works reported that the rate of photocatalytic elimination of organic compounds (TCE, methanol and benzene) increased with the amount of water vapour (Kim and Hong, 2002; Hennezel et al., 1998). On the other hand, Martinez et al. (2011) reported a significant decrease of the degradation rates of NO with the decrease of the humidity. They comment that the photocatalytic reaction is limited by the competition between water and the pollutant on the photoactive sites only on materials with low adsorption capacities, such as glass. Regarding VOC for instance, water vapour has no influence as shown for 1-butanol (Wang et al., 1998; Augugliaro et al., 1999). Assadi et al. (2012) indicated that the relative humidity (RH) has great and complex effect on the removal of gaseous Trimethylamine (TMA) and isovaleraldehyde (ISOV). The presence of water vapour is beneficial at low concentration due to the formation of $^{\bullet}OH$ radicals which contribute to the increase of degradation; while at higher RH the competitive effect against the active sites becomes predominant (Monteiro et al., 2015); similar experimental result was also observed by Ku et al. (2005).

i) Effect of the nature of the reactor

The reactor geometries may also influence the degradation efficiency. Assadi et al. (2013) studied the degradation of gaseous isovaleraldehyde in two different reactor's configurations (planar reactor and cylindrical reactor) using TiO_2 deposited on a fiberglass support (GFT) photocatalyst. They found that with the same mean residence time and area of the photocatalyst

media for the two reactors, at low concentrations of isovaleraldehyde the planar reactor shows a higher selectivity (up to 25%) than the cylindrical reactor. Wang and Ku (2003) found a higher quantum yield for an optical fiber photoreactor compared to an annular photoreactor for the degradation of benzene. The decomposition of benzene rapidly decreases from 55 to 20% in the annular photoreactor after three operation cycles; while, conversions yield decreases from 85 to 20% in the optical fiber photoreactor after eight operation cycles. In the study of Behnajady et al. (2011), a tubular continuous-flow photoreactor with supported TiO_2-P25 on glass plates was constructed and used for the degradation of 4-nitrophenol. The results showed that the removal efficiency of the pollutant depends on the photoreactor length. Recently, many efficient configurations of reactors have been proposed. Tang et al. (2014) proposed a high efficient aqueous-film rotating disk photocatalytic fuel cell (RDPFC) compared with the conventional immersed rotating disk; it allows the cogeneration of hydrogen and electricity, simultaneously to dye degradation.

II.4.6. Effect of the semiconductor

a) Crystalline structure effect

Much effort has been devoted to develop visible-light-sensitive photocatalysts, including modification of photocatalyst by doping with elements such as N, C and S (Liu and Chen, 2008; Pan et al., 2013; Selvaraj et al., 2013; Nezamzadeh-Ejhieh and Shirzadi, 2014; Kerkez and Boz, 2015; Sonia et al., 2015). Generally, the doped semiconductor shows higher activity than the undoped counterpart owing to the introduction of localized state above the valence band (Pan et al., 2013; Chen et al., 2015; Ruzimuradov et al., 2015). The synthesis of TiO_2-SnO_2 heterostructures and their application to water decontamination based on the photodegradation of Rhodamine B (DeMendonça et al., 2014) shows that the heterostructures presented a higher photoactivity than commercial TiO_2 nanopowders, which is due to the prevention of recombination of photogenerated charges by increasing the SnO_2 proportion on these materials. Additionally, the longer lifetime observed might have been promoted by the increased contact area between the oxides. In order to reach higher photocatalytic activity, Behnajady and Tohidi (2015) synthesized ZnO-SnO_2 nanoparticles impregnated with Mg. The results indicate superior photocatalytic activity than TiO_2-P25 nanoparticles. Liu (2011) studied the effect of crystalline form of titanium dioxide on the photodegradation of ethylene-vinyl acetate copolymer/low density polyethylene composite. They found that the particle size and the crystal form of TiO_2 play a major role in controlling the photo-activity of TiO_2 which can be ordered from low to high as follows: micro rutile TiO_2>micro mixed crystals TiO_2 (rutile/anatase

=13/87)> micro anatase TiO_2; while nano mixed crystals TiO_2 (rutile/anatase =20/80) exhibited a high photocatalytic activity.

b) Size effect

Many researchers have reported the importance of controlling nanoparticle size of photocatalyst in order to achieve efficient photodegradation (Liu, 2011; Purwanto et al., 2011). The existence of an optimal size for titania in catalytic material has also been reported in several studies (Zhang et al., 1998; Baiju et al., 2007). When the photocatalyst size is reduced, the surface area increases which enhances the interfacial charge-carrier transfer rates. As a result, improvement in photocatalyst activity is observed. In addition to surface and volume recombination, the recombination of electrons/holes in the excited photocatalyst can occur (Zhang et al., 1998). When the particle size is very small, surface recombination is dominant. Thus, electrons/holes would recombine quickly and would not contribute to the photocatalytic process, resulting in a lower photocatalytic rate. At the optimal size, two parameters, surface area and the recombination process, should be optimized.

c) Surfaces and exposed faces effect

In a catalytic process, the specific surface area of the materials is of great importance, because the increase in the specific surface area generates an increase in the number of active sites on the material surface. It is important to point out that the created hydroxyl radicals come from groups, which are surface bound and not free in solution (De Mendonça et al., 2011). To improve the compatibility of catalyst with dye molecules in aqueous solution, prepared Bi_2S_3 nanostructures were surface modified via ligand exchange with the use of MPA as reported by (Zhang et al., 2010). In their work, Huang et al. (2013) reported the dependence of the dimension of nanostructured bismuth sulfide in the photodegradation of organic dyes; they found that the degree of degradation enhancement due to nanostructuration falls into the order of dots > sheets > rods. This could be attributed to the different dimensionalities reconcilable with UV absorption, namely specific surface area and crystal surface construction. On the other hand, the enhanced photocatalytic performance of heterostrucurated TiO_2/BiOCl under simulated-solar light may be attributed to the formation of the TiO_2/BiOCl heterojunction at the interface which could efficiently hinder the recombination of electron-hole pairs and facilitate the transfer of the photo-generated electrons and holes (Zhu et al., 2014).

II.5. Various designs of photocatalytic reactors

The photocatalytic process for both air and water treatment is examined in this review, since this does not imply a great difference (Tokode et al., 2015). Some papers use the term “fluid” to ovoid to distinguish if there is only one phase (liquid or gas) or a mixture of two phases. In some cases, and even if a gas phase is treated, water is used as reducing agent (Das et al., 2014). All pollutants degraded in an aqueous phase can also be destroyed in air, provided the presence of certain air humidity (Herrmann, 2010).

Generally, the main performance parameters of a photocatalytic reactor are the mass transfer rate, the kinetic reaction rate, and the reaction surface area. An ideal photocatalytic reactor should have a high specific surface area, an appropriate light directly irradiating on the reaction surface and a high mass transfer. Leblebici et al. (2015) compared 12 different photoreactors designs for wastewater treatment. The comparison showed that membrane integrated slurry reactors scored the highest among the compared designs. In addition, it was shown that with efficient light distribution, the microreactor technology can prove to be the new generation of wastewater treatment reactor.

II.5.1. Slurry photocatalytic reactor (Fig II.1)

The photocatalyst particles are suspended in the aqueous solution with the aid of mechanical stirring (Wei et al., 2011) or air sparging (Chong et al., 2011).Various slurry photoreactors have been used in photocatalytic decontamination, which include slurry annular reactor (Chong et al., 2009), photo-impinging streams cyclone reactor (Royaee et al., 2014), slurry bubble column reactor (Kamble et al., 2006), fountain reactor (Puma and Yue, 2001), air-lift loop photoreactor, pulse-baffle tube photochemical reactor, rotating tube reactor, cocurrent downflow contactor reactor and thin-film reactor(Dijkstra et al. 2003; Lasa et al., 2005). Such reactor can also be externally irradiated (Palmisano et al., 2015). Slurry photoreactivity systems can be operated in batch or continuous mode. Slurry reactors show some advantages, such as high surface area, high degradation rate, no mass transfer limitation and simple reactor structure (Mohammadi-Aghdam et al., 2014).

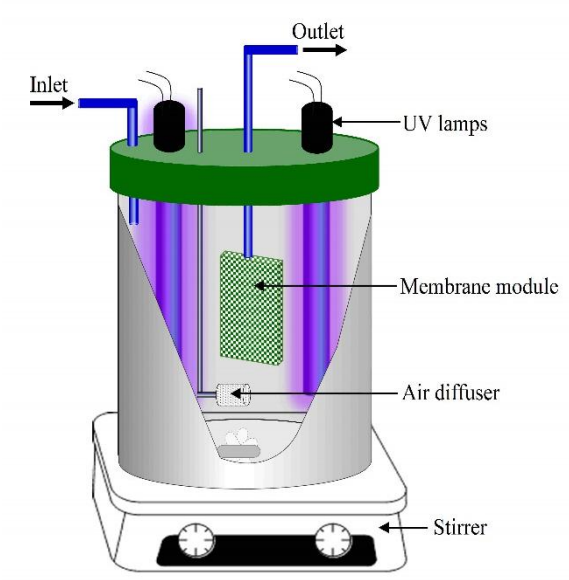

Figure II.1: Slurry photoreactor

However, they also show some drawbacks, since they suffer from light penetration limitationdue to the opacity of the slurry, fouling of catalystsdue to the decomposition of the catalyst particles, problem of fine catalyst separation from the treated liquid in view of catalyst recycling (Shah, 2014; Hassan et al., 2016) and low light utilization efficiency.

II.5.2. Photocatalytic membrane reactor (PMR)

In PMR, the catalyst is deposited on the membrane; this latter is made from polymers (polysulfone, polyamide, polyethersulfone, polyvinylidenefluoride, polyacrylonitrile…) (Molinari et al., 2002; Ma et al., 2014). The membrane is irradiated after its immersion inside the photoreactor. It mainly allows to confine the photocatalyst by means of the presence of the membrane, enabling to operate with high amounts of catalyst, to control the residence time of the pollutant in the reactor and also acting as a selective barrier for the species to be degraded (Huang et al., 2007; Choo et al., 2008).

The continuous membrane photoreactor associates both the advantages of classical photoreactors (catalyst in suspension) and membrane processes (separation at molecular level): to realize a continuous process (avoid the catalyst recovery step) with simultaneous product(s) separation from the reaction environment. Numerous configurations of photocatalytic membrane reactors have been proposed for the treatment of wastewaters by Molinari et al. (2002); they designed irradiated cells containing the catalyst deposited on a membrane. Wang et al. (2012) fabricated an original type of membrane photoreactor; they used a hybrid membrane photoreactor combining a photoreactor irradiated with visible-light-emitting diode (Vis-LED) and a cross-flow microfiltration (polyvinyldene fluoride (PVDF) MF membrane)

membrane module for the simultaneous degradation of penicillin G (PG) and the separation of visible-light responsive TiO_2 particles.

This type of reactor can also be combined with slurry photoreactor to give slurry membrane photoreactor (Laohaprapanon et al., 2015).

II.5.3. Rotating-drum photoreactor

The rotating disk photocatalytic reactor has three major components: a reactor vessel that has a semicircular form, a rotating disk loaded with TiO_2 catalyst and UV sources (**Figure II.2**). In this reactor, the mixing of the solution is achieved by rotation of the disk while the photocatalytic reactions occur on the UV-irradiated photocatalyst thin film, which is attached on the surface of the support (disk).

The degradation rates of the organic compounds can be controlled by many design parameters including the light intensity, the liquid flow rate and the level of the aqueous solution in the reaction vessel (Dionysiou et al., 2000), as well as the illuminated surface area of the catalyst, the rotational speed of the disk and the thickness of the carried liquid film on the rotating disk (Salu et al., 2011; Zhang et al., 2011).

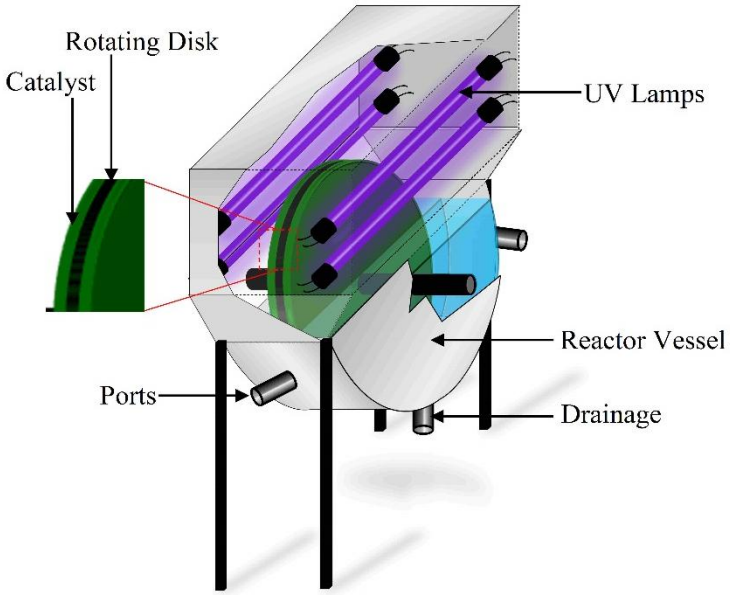

Figure II.2: Rotating-drum photoreactor

A new configuration of this type of photoreactor has been recently proposed (Tang et al., 2014); this configuration is named aqueous-film rotating disk photocatalytic fuel cell (RDPFC); it is characterized bysimultaneous production of hydrogen and electricity concomitantly with an efficient degradation of high concentrations of dye wastewater.

II.5.4. Annular photoreactor

The annular photocatalytic reactor consisted in two concentric cylinders that form an annular space with a certain distance surrounding a UV fluorescent lamp with an appropriate emitting wavelength range (**Figure II.3**). This geometry has the advantage of providing a symmetrical irradiation. The lamp is cooled by air flowing freely within the open central section of the reactor. These reactors may be also externally irradiated by UV fluorescent lamps (Palmisano et al., 2015). In annular photoreactors, the catalyst is suspended in the solution and is allowed to flow upwards in the annular space (Andreozzi et al., 2000; Chong et al., 2009) or supported on stainless steel sieve plate rings positioned horizontally in the annulus space (Souzanchi et al., 2013); it can also cover the inner side of the larger tube (Ku et al., 2005; Assadi et al., 2012). The flow is introduced in the annular space through inlet(s) surrounding the bottom and collected at outlet(s) surrounding the top so as to ensure a uniform flow. In addition, the bottom of the annular space is filled with glass beads to ensure a good homogenization before entering the irradiation section and the system works in a closed loop.

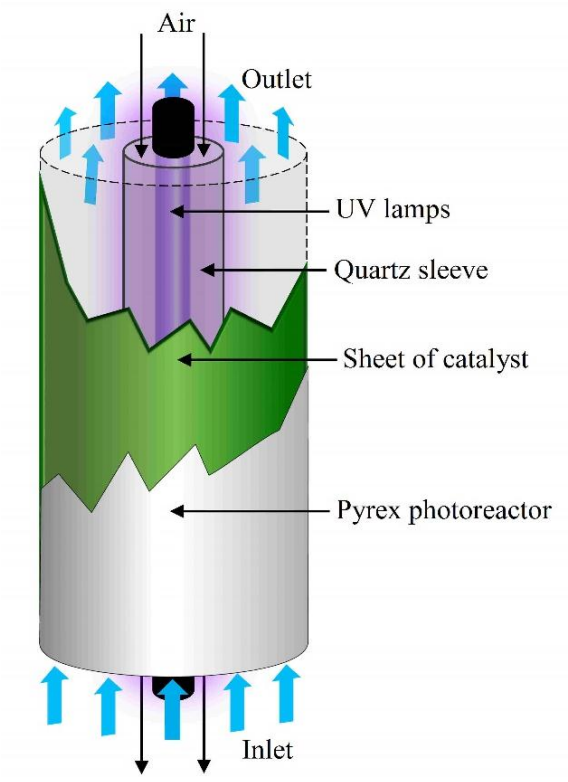

Figure II.3: Annular photoreactor

Zahraa et al. (2003) applied an aqueous suspension of TiO_2 for thedegradation of atrazine; they used an UV lamp longer than the annular reactor to obtain 80% of efficiency of the emitted light. Thomas et al. (2014) fabricated another type of annular photoreactor; they deposited the photocatalyst (TiO_2) on the fiberglass. In this reactor, the sheet of catalyst-deposited fiberglass

is rolled up and placed in the reactor so that it is plated on the inside of the external cylinder. Nevertheless, both faces of the sheet are in contact with the liquid and are sensitive to light, as the paper is permeable to both liquid and light. In a similar work, Behnajady et al. (2007) used a continuous-flow photoreactor with immobilized TiO_2 on glass plates for degrading a monoazo dye present in an aqueous phase. An annular photoreactor can also be packed with transparent cellulose acetate monolithic structures coated with a catalyst (Monteiro et al., 2015).

II.5.5. Closed-loop step photoreactor

Closed-loop step photoreactor consists of several parts: a tank, a pump, a spillway at the top and steps. The reactor is made of six regular steps of the same dimensions, covered with the photocatalytic media (containing TiO_2); this last is irradiated by three UV-lamps placed inside a cover (Brosillon et al., 2008; Chebli et al., 2010) (**Figure II.4**). The configuration of this reactor allows a uniform distribution of the water in the irradiated area and the thin film of liquid absorbs very little UV irradiation and as a consequence the photo-activation of the catalyst is higher (Brosillon et al., 2011). The high surface area also facilitates oxygen mass transfer from the air to the liquid phase resulting in a diminution of the electron–hole pair recombination, thus increasing the overall efficiency of the photocatalytic reaction.

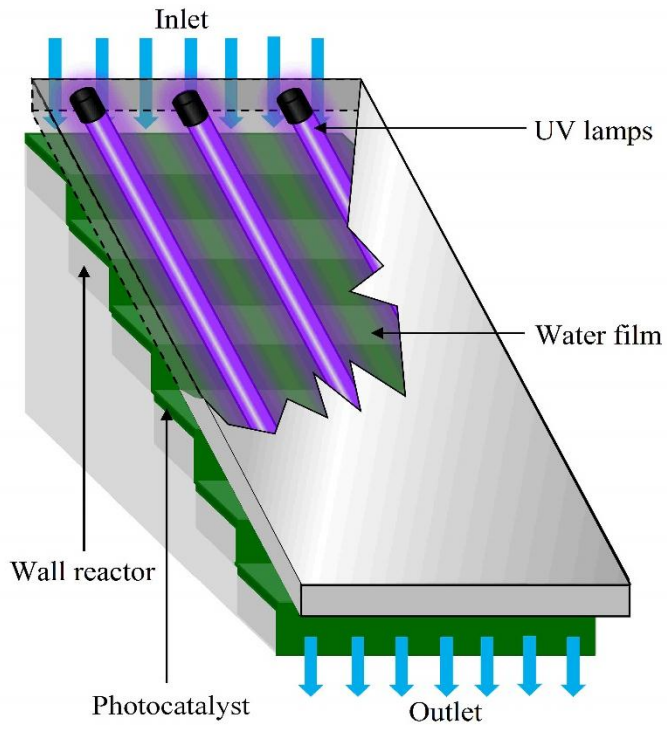

Figure II.4: Closed-loop Step photoreactor

II.5.6. Microphotoreactor

Microreactors are characterized by miniaturized dimensions which provide: (1) a reduced path for the light, decreasing photon transfer limitations and leading to high illumination homogeneity along the reactor (Coyle and Oelgemoller, 2008), (2) a high surface to volume ratio, which leads to the enhancement of heat and mass transfer (reduces mass transfer limitations) (Van Gerven et al., 2007). Several configurations of microphotoreactor have been reported by researchers (Eskandarloo et al., 2015). Among them, falling film microreactors utilized in G–L reactions, in which a thin falling liquid film flows by gravitational force along a microstructured surface while it is illuminated by UV light and exposed to a co-flowing gas (Coyle and Oelgemoller, 2008). But, these reactors can suffer from mass transfer limitations. In the dispersed phase microreactors, the gaseous reactant is dispersed in the liquid phase (e.g. slug flow, annular flow) flowing in the microchannel (Kreutzer et al., 2005; Lindstrom et al., 2007).

Recently porous photocatalytic membrane microreactors have been reported to benefits from a stable gas–liquid–solid (G–L–S) interface allowing a continuous supply of gaseous reactants and a reduced light path (Aran et al., 2011) (**Figure II.5**).

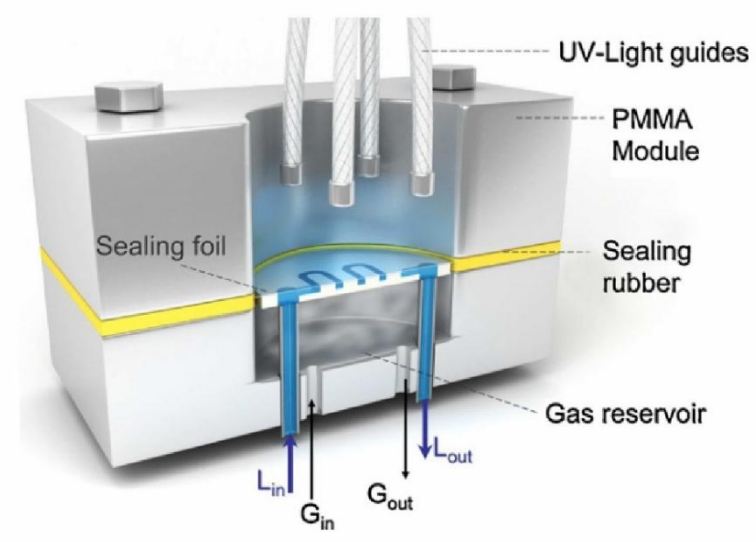

Figure II.5: Schematic representation of the fabricated porous photocatalytic membrane microreactor (PPMM) reactor module (cross-sectional view) (Aran et al., 2011)

II.6. Retrospective on research on the photocatalytic degradation of organic pollutants - Case study of synthetic dyes

The use of photocatalytic reactors for wastewater treatment and precisely for the degradation of synthetic dyes is not new (**Table II.1**). Dyes represent an important category of organic

compounds, which has a lot of applications in our daily life, in clothing, food, paper, leather, cosmetics, plastics, drugs, electronics and printing. The modern textile industry consumes about 80% of all synthetic dyes produced, with 700,000 tons of dyes applied to 40 million tons of fabric annually (Rajeshwar et al., 2008). Many researchers have already introduced diverse types of photocatalytic reactors for the degradation of a variety of compounds at different scales of operation. It should be noted that the studies considered here to illustrate the subject are only a few part of the wide literature available on this subject. As shown in **Table II.1**, percentages of decolorization are very variable. This is caused by the different designs of the photoreactors used and by the various experimental conditions (initial concentration and time of reaction), especially concerning the nature of catalyst as well as by the methods of process elaboration. Particularly, for the dye, Rhodamine B, tested by several researchers, the percentage of decolorization varied from 79.8 and 100%.

However, it is important to note that 12 hours were necessary to degrade 10 mg/L of Rhodamine B in the presence of TiO_2-coated beads to achieve 90% of dye decolorization (Li et al., 2014). There is a significant drawback for the suspended system, since there is a need to separate the TiO_2 nanoparticles after the photocatalytic reaction in view of their reuse. Recently considerable interest has been focused on sol–gel derived nanocomposites films using different kinds of substrates (Li et al., 2014; Mohammadi-Aghdam et al., 2014). The use of nanostructured titania supported over volcanic ashes (TVA) presents the advantage that it can be easily separated from water, thus avoiding solid–liquid separation. Moreover, its performance is not dependent on the solution pH and can maintain its capacity for dye degradation after several operation cycles, with however some increase in the contact time (Esparza et al., 2010). Overall, the use of solar-light driven supported catalyst (PdS/ZnS NPs doped PVAc hybrid electrospun nanofiber mat) might avoid the need of secondary operation like liquid–solid separation. Because of its hydrophobicity, it cans float on water and can be easily applied for polluted water treatment in open surface and can be used for potential pollutant treatment (Panthi et al., 2015).

The technology of heterogeneous photocatalysis based on the traditional UV lamps appears relatively limited due to a high-energy requirement associated to the high input power and low light efficiency (Wurtele et al., 2011). However, LEDs light sources represent an important improvement owing to some advantageous aspects, like high efficiency, compactness, lower power requirement, robustness, lower operating temperature, long life times, no disposal problems and no warm-up time (Rasoulifard et al., 2014). The works of Rasoulifard et al. (2015) revealed that UV-LEDs continuous photoreactor could be energy-efficiently applied for the degradation of low-levels of organic pollutants particularly synthetic dyes.

In addition, the high photoactivity of TiO_2 and metal-doped TiO_2 nanocatalysts supported over monolith channels for dyes photoreduction is obviously due to large illuminated surface area in monolith channels (Pinho et al., 2015), fast electron transfer with hindered recombination rates (Tahir et al., 2015a), high mobility of electron on the catalyst surface, efficient desorption of products and high photonic efficiency (Tahir et al., 2015b).

Table II.1: Some hazardous chemicals and photoreactor design

Photoreactor type	*Catalyst*	*Chemicals (init.conc.)*	*Decolorization (%)*	*Time needed*	*References*
immobilized photoreactor	ZnO nanowires	Methylene blue (5 mg/L)	99.4	120 min	Xue et al., (2015)
	S,N-codoped TiO_2	Methyl orange (7 mg/L)	96.0	3 h	Khalilian et al. (2015)
	Tu–TiO_2	Methyl orange (7 mg/L)	92.0	9 h	-
	meso-TiO_2 /SAC	Humic acid (20 mg/L)	80.3	10 h	Baek et al. (2013)
	TiO_2 PC-500	Phenazopyridine (10mg/L)	89.10	150 min	Fathinia et al. (2013)
Floating-bed photoreactor	TiO_2 nanoparticules	Furfural (0.5mmol/L)	99.6	120 min	Faramarzpour et al. (2009)
Annular Sieve-Plate photoreactor	Degussa P-25	Phenol (0.5mmol/L)	100	360 min	Souzanchi et al. (2013)
	-	Reactive Red 198 (50 mg/L)	100	35 min	Mahmoodi et al. (2006)
	TiO_2/β-SiC	Diuron (10 mg /L)	100	14 h	Kouamé et al. (2012)
double-cylindrical-shell (DCS)	TiO_2-coated beads	Rhodamine B (10mg/L)	90.4	12 h	Li et al., (2014)
	-	Methyl Orange (10mg/L)	/	/	-
Cylindrical multi-column (CMCPR)	TiO_2-coated beads	Methyl Orange (10mg/L)	96.5	3 h	Li et al.,(2015a)
	-	Amoxicillin (100mg/L)	57.7	3 h	-
	-	3-chlorophenol (25mg/L)	100	3 h	-
Membrane photocatalytic reactor	PP-g-PVBMC-POM	Acid orange 7 (0.02 g/L)	95	2 h	Ma et al.,(2014)
Thin-film	Fe-doped TiO_2	Methyl Orange (10mg/L)	35.3	3 h	Zhang et al. (2013)
a spiral photoreactor	TiO_2 film	4-tert-octylphenol (10 mg/L)	91.2	45 min	Wu et al. (2012)
optical fiber photoreactor	-	Benzene (20 ppmv)	80	4 h	Wang et al. (2003)
film-coated optical fiber	Ag/$H_3PW_{12}O_{40}$/TiO_2-1	Rhodamine B (20 mg/L)	98.8	3 h	Zhang et al. (2012)
	-	4-nitrophenol (10 mg/L)	97.1	3 h	-
	Degussa P-25	Methyl parathion (50 µg/L)	99.85	24 h	Senthilnathan et al. (2012)
	-	Acetone (ppmv)	100	200 min	Ku et al., (2005)
	-	Methyl Orange (10mg/L)	100	1.5 h	Xiao-gang et al. (2009)
	-	Dichlorvos (50 µg/L)	100	24 h	-
	-	Lindane (50 µg/L)	99.09	24 h	-
	N-doped TiO_2	Methyl parathion (50 µg/L)	99.54	24 h	-
	-	Dichlorvos (50 µg/L)	99.50	24 h	-
	-	Lindane (50 µg/L)	97.74	24 h	-
Rotating disk photocatalytic fuel cell	TiO_2 /Ti	Reactive brilliant red X-3B (300 mg/L)	100	2 h	Tang et al., (2014)
	-	Rhodamine B (100 mg/L)	100	2 h	-

Rotating disk photoreactor	titanium disk	Reactive brilliant red X-3B (20 mg/L)	90.4	2 h	-
	-	Rhodamine B (10 mg/L)	80.6	2 h	-
-	TiO_2-nanotube/Ti	Rhodamine B (20 mg/L)	90	3 h	Zhang et al., (2011)
Slurry	CdS-TiO_2-Au Anatase	Methyl Orange (10mg/L)	70.9	5 h	Lv et al. (2012)
	ZnO	Remazol Black B (50mg/L)	100	60 min	Gouvêa Carlos et al., (2000)
	-	Remazol Brilliant Blue R (50mg/L)	100	60 min	-
	-	Remazol Red F3B (150mg/L)	99	60 min	Akyol et al., (2005)
	-	Reactive Red 15 (100mg/L)	95	60 min	Khattab et al., (2012)
slurry membrane	-	Reactive Black 5 (75mg/L)	95	60 min	Laohaprapanon et al., (2015)
	TiO_2	Amoxicillin (104mg/L)	38.7	5 h	Elmolla et al. (2010)
	-	Phenoxy-acetic acid (200 mg/L)	100	1.5 h	Kamble et al. (2006)
	TiO_2 /AC-HP	3-chlorophenol (40mg/L)	98.0	5 h	El-Sheikh et al. (2007)
Annular	0.3wt%Pd/$CaSn(OH)_6$	Methylene blue (100 ppm)	100	30 min	Baeissa (2014)
Suspension	Degussa P-25	Dodecylbenzene sulfonate (µ87mmol/L)	100	90 min	Eng et al. (2012)
	-	Cetylpyridinium chloride (µ87mmol/L)	100	90 min	-
	-	Alizarin S (84.2 µmol/l)	100	3 h	Lachheb et al., (2002)
	-	Methyl Red (84.2 µmol/l)	100	3 h	-
	-	Methylene Blue (84.2 µmol/l)	100	3 h	-
	-	Congo Red (84.2 µmol/l)	100	3 h	-
	-	Methyl Red (84.2 µmol/l)	100	3 h	-
	-	Humic acid (10mg/L)	100	150min	Wei et al., (2011)
	-	Paraquat (100 mg/L)	90	3 h	Lee et al. (2003)
	-	Isoproturon (0.5mmol/L)	94.8	80 min	Haque et al. (2003)
	-	Acid Red 1 (0.025mmol/L)	≈90.0	≈250 min	Bernardini et al. (2010)
	-	Pirimiphos-methyl (31.8µmol/L)	>98.0	10 min	Herrmann et al. (1999)
	-	Acid orange 8 (0.25mmol/L)	75.0	90 min	Saquib et al. (2003a)
	-	Remazol Brilliant Blue (0.25mmol/L)	100	120 min	Saquib et al. (2002)
	-	Gentian violet (0.18 mmol/L)	100	90 min	Saquib et al. (2003b)
	-	*p*-chlorophenol (0.50 mmol/L)	98	150 min	Nguyen et al. (2015)
	-	Phenol (100 mg/L)	94	4 h	Royaee et al. (2014)
	TiO_2-M	Dimethyl terephthalate (0.25 mmol/L)	90.0	75 min	Rahman et al. (2003)
	-	Crystal violet (10^{-4} mol/L)	97.1	350 min	Djellabi et al. (2014)
	-	Methylene blue (10^{-4} mol/L)	93.2	-	-

	-	Rhodamine B (10^{-4} mol/L)	79.8	-	-
	-	Methyl orange (10^{-4} mol/L)	36.1	-	-
	-	Congo red (10^{-4} mol/L)	22.6	-	-
	TiO_2 nanotubes	Indigo carmine dye (5×10^{-5} mol/L)	100	60 min	Costa et al. (2009)
	N-doped TiO_2	Bisphenol-A (5.0 mg/L)	90	2 h	Subagio et al. (2010)
	C-N codoped TiO_2	Bisphenol A (5 ppm)	99	5 h	Wang et al. (2010)
	ZnAlTi (LDHs)	Methylene blue (10 mg/L)	99	2 h	Wang et al. (2014)
	m-$BiVO_4$ (RLS)	Rhodamine B (10 mg/L)	100	6 h	Hu et al., (2014)
	BiOBr–Mt	Rhodamine B (40 mg/L)	99	2 h	Xu et al., (2014)
	AgCl/Ag_3PO_4/GO-3%	Methylene blue (15 mg/L)	100	40 min	Cao et al., (2015)
	SnO_2/Zn_2SnO_4	Rhodamine B (10^{-5} mol/L)	100	100 min	Li et al., (2015b)
	TiO_2	Reactive Black 5 (1 ppm)	97	150 min	Chong et al., (2015)
	CdS microspheres	Methylene blue (3 mg/L)	≈100	3 h	Repo et al., (2013)
	-	Phenol red (3 mg/L)	≈100	3 h	-
	-	Methyl red (3 mg/L)	≈100	3 h	-
	Schwertmannite	Acid orange 7 (50 mg/L)	97.4	120 min	Guo et al., (2015)
	$BiVO_4$	Rhodamine B (10 mg/L)	100	6 h	Hu et al., (2014)
	$ZnFe_2O_4$ nanoplates	Rhodamine B (10 mg/L)	100	40 min	Han et al., (2014)
	TVA	Methylene blue (20 ppm)	100	1 h	Esparza et al., (2010)
	ZnO flowers	Malachite green (0.2 g/L)	90.87	100 min	Saikia et al., (2015)
	PdS/ZnS–PVAc henm	Methylene blue (10 ppm)	100	100 min	Panthi et al., (2015)
	amylose–HNT–TiO_2	4-nitrophenol (10 mg/L)	90	4 h	Zheng et al., (2015)
	-	Methylene blue (32 mg/L)	90	10 h	-
	Silica nanoparticles	Acridine orange (10^{-5} mol/L)	58	50 min	Selvaggi et al. (2015)

SAC: Spherical Activated Carbon; **LDHs**: Layered Double Hydroxides; **RLS**: Rod-Like Structures; **BiOBr–Mt**: BiOBr–montmorillonite composites; **GO**: graphene oxide-loaded; **TVA:** nanostructured titania supported over volcanic ashes; **henm:** PdS/ZnS–PVAc hybrid electrospun nanofiber mat.

II.7. Conclusion

The contamination of air and water bodies can affect the environment integrity and induce a real threat to human health. Photocatalysis process, considered as one of the advanced oxidation processes, can be an alternative for the treatment of industrial wastewaters before their discharge in natural ecosystems.

Diverse types of photoreactors used for liquid and gas phase oxidation and pollutant degradation are typically based on the slurry system; however, its application is severely constrained by low-efficient utilization of incident light and difficult separation of nano-sized particles of catalyst after reaction. The continuous membrane photoreactor associates both the advantages of separation at a molecular level, while avoiding the catalyst recovery step. In addition, the majority of the photochemical experiments are performed in the presence of new synthetic photocatalyst with solar light source or artificial light.

References

Akyol A., Bayramoglu M., 2005. Photocatalytic degradation of Remazol Red F3B using ZnO catalyst. J. Hazard. Mater. 124, 241-246.

Andreozzi R., Caprio V., Insola A., 2000. Photocatalytic oxidation of 4-nitropheno1 in aqueous TiO_2 slurries: An experimental validation of literature kinetic models. J. Chem. Technol. Biotechnol. 75(2), 131-136.

Aran H.C., Salamon D., Rijnaarts T., Mul G., Wessling M., Lammertink R.G.H., 2011. Porous Photocatalytic Membrane Microreactor (P2M2): A new reactor concept for photochemistry. J. Photochem. Photobiol. A: Chem. 225, 36-41.

Assadi A.A., Bouzaza A., Wolbert D., 2012. Photocatalytic oxidation of trimethylamine and isovaleraldehyde in an annular reactor: Influence of the mass transfer and the relative humidity. J. Photochem. Photobiol. A: Chem. 236, 61–69.

Assadi A.A., Palau J., Bouzaza A., Wolbert D., 2013. Modeling of a continuous photocatalytic reactor for isovaleraldehyde oxidation: Effect of different operating parameters and chemical degradation pathway. Chem. Eng. Res. Design, 91, 1307-1316.

Atiqur-Rahman M., Muneer M., Bahnemann D., 2003. Photocatalytic degradation of dimethyl terephthalate in aqueous suspensions of titanium dioxide, Res. Chem. Intermed. 29 (1), 35-50.

Atiqur-Rahman M., Muneer M., 2005. Photocatalysed degradation of two selected pesticide derivatives, dichlorvos and phosphamidon, in aqueous suspensions of titanium dioxide, Desalination 181, 161-172.

Augugliaro V., Coluccia S., Loddo V., Marchese L., Martra G., Palmisano L., Schiavello M., 1999. Photocatalytic oxidation of gaseous toluene on anatase TiO_2 catalyst: mechanistic aspects and FTIR investigation, Appl. Catal. B: Environ. 20, 15-27.

Baeissa E.S., 2014. Novel Pd/$CaSn(OH)_6$ nanocomposite prepared by modified sonochemical method for photocatalytic degradation of methylene blue dye. J. Alloys Compd. 590, 303-308.

Baek M.-H., Yoon J.-W., Hong J.-S., Suh J.-K., 2013. Application of TiO_2–containing mesoporous spherical activated carbon in a fluidized bed photoreactor-Adsorption and photocatalytic activity. Appl. Catal. A: General 450, 222-229.

Baiju K.V., Shukla S., Sandhya K.S., James J., Warrier K.G.K., 2007. Photocatalytic activity of Sol-Gel-derived nanocrystalline titania. J. Phys. Chem. C 111, 7612-7222

Behnajady M.A., Modirshahla N., Daneshvar N., Rabbani M., 2007. Photocatalytic degradation of an azo dye in a tubular continuous-flow photoreactor with immobilized TiO_2 on glass plates. Chem. Eng. J. 127, 167-176.

Behnajady M.A., Amirmohammadi-Sorkhabi S., Modirshahla N., Shokri M., 2011. Investigation of the efficiency of a tubular continuous-flow photoreactor with supported titanium dioxide nanoparticles in the removal of 4-nitrophenol: operational parameters, kinetics analysis and mineralization studies. Water Sci. Technol. 64(1), 56-62.

Bernardini C., Cappelletti G., Dozzi M. V., Selli E., 2010. Photocatalytic degradation of organic molecules in water: Photoactivity and reaction paths in relation to TiO_2 particles features. J. Photochem. Photobiol. A: Chem. 211, 185-192.

Braslavsky S.E., 2007. International union of pure and applied chemistry, organic and biomolecular chemistry division, subcommittee on photochemistry glossary of terms used in photochemistry, 3rd ed. (IUPAC recommendations 2006). Pure Appl. Chem. 79, (3), 293-465.

Brosillon S.., Djelal H., Merienne N., Amrane A., 2008. Innovative integrated process for the treatment of azo dyes: Coupling of photocatalysis and biological treatment, Desalination 222, 331-339.

Brosillon S.., Lhomme L.., Wolbert D.., 2011. Modelling of a falling thin film deposited photocatalytic step reactor for water purification: Pesticide treatment. Chem. Eng. J. 169, 216-225.

Burns R.A., 1999. Effect of inorganic ions in heterogeneous photocatalysis, J. Environ. Eng. 125, 77-85.

Byrne J.A., Eggins B.R., Brown N.M.D., McKinney B., Rouse M., 1998. Immobilisation of TiO_2 powder for the treatment of polluted water. Appl. Catal. B 17, 25-36.

Cao M., Wang P., Ao Y., Wang C., Hou J., Qian J., 2015. Preparation of graphene oxide-loaded Ag_3PO_4@AgCl and its photocatalytic degradation of methylene blue and O_2 evolution activity under visible light irradiation. Int. J. Hydrogen Energy 40, 1016-1025.

Chebli D., Fourcade F., Brosillon S., Nacef S., Amrane A., 2010. Supported photocatalysis as a pre-treatment prior to biological degradation for the removal of some dyes from aqueous solutions; Acid Red 183, Biebrich Scarlet, Methyl Red Sodium Salt, Orange II. J. Chem. Technol. Biotechnol.85 (4), 555-563.

Chen C.-Y., Kuo J.T., Yang H.A., Chung Y.C., 2013. A coupled biological and photocatalysis pretreatment system for the removal of crystal violet from wastewater. Chemosphere 92, 695-701.

Chen C.-Y., Yen S.-H., Chung Y.-C., 2014. Combination of photoreactor and packed bed bioreactor for the removal of ethyl violet from wastewater. Chemosphere 117, 494-501.

Chen G., Si X., Yu J., Bai H., Zhang X., 2015. Doping nano-Co_3O_4 surface with bigger nanosized Ag and its photocatalytic properties for visible light photodegradation of organic dyes. Appl. Surf. Sci. 330, 191-199.

Chen Y., Liu Z., Wang Z., Xue M., Zhu X., Tao T., 2011. Photodegradation of propranolol by Fe(III)-citrate complexes: kinetics, mechanism and effect of environmental media. J. Hazard. Mater. 194, 202-208.

Chong M.N., Cho Y.J., Poh P.E., Jin B., 2015. Evaluation of Titanium dioxide photocatalytic technology for the treatment of reactive Black 5 dye in synthetic and real greywater effluents. J. Cleaner Prod. 89, 196-202.

Chong M.N., Jin B., Chow C.W.K., Saint C., 2010. Recent developments in photocatalytic water treatment technology: a review. Water Res. 44 (10), 2997–3027.

Chong M.N., Jin B., Laera G., Saint C.P., 2011. Evaluating the photodegradation of Carbamazepine in a sequential batch photoreactor system: Impacts of effluent organic matter and inorganic ions. Chem. Eng. J. 174, 595-602.

Chong M.N., Jin B., Zhu H.Y., Chow C.W.K., Saint C., 2009. Application of H-titanate nanofibers for degradation of Congo Red in an annular slurry photoreactor. Chem. Eng. J. 150, 49-54.

Choo K.H., Chang D.I., Park K.W., 2008. Use of an integrated photocatalysis/hollow fiber microfiltration system for the removal of trichloroethylene in water. J. Hazard. Mater. 152, 183-190.

Colmenares J.C., Xu Y-J., 2016. Heterogeneous photocatalysis: From fundamentals to green applications. Springer, 415 pages.

Costa L.L., Prado A.G.S., 2009. TiO_2 nanotubes as recyclable catalyst for efficient photocatalytic degradation of indigo carmine dye. J. Photochem. Photobiol. A: Chem. 201, 45-49.

Coyle E.E., Oelgemoller M., 2008. Micro-photochemistry: photochemistry in microstructured reactors the new photochemistry of the future? Photochem. Photobiol. Sci. 7, 1313-1322.

Dalrymple O.K., Yeh D.H., Trotz M.A., 2007. Removing pharmaceuticals and endocrine disrupting compounds from wastewater by photocatalysis. J. Chem. Technol. Biotechnol. 82, 121-134.

Das S., Wan Daud W.M.A., 2014. Photocatalytic CO_2 transformation into fuel: A review on advances in photocatalyst and photoreactor. Renew. Sust. Energ. Rev. 39, 765-805.

Das M., Bhattacharyya K.G., 2015. Use of Raw and Acid-Treated MnO_2 as Catalysts for Oxidation of Dyes in Water: A Case Study with Aqueous Methylene Blue. Chem. Eng., Comm., 202(12), 1657-1667.

De Mendonca V.R., Lopes O. F., Fregonesi R. P., Giraldi T. R., Ribeiro C., 2014. TiO_2-SnO_2 heterostructures applied to dye photodegradation: The relationship between variables of synthesis and photocatalytic performance. Appl. Surf. Sci. 298, 182-191.

De Mendonça V.R., Ribeiro C., 2011. Influence of TiO_2 morphological parameters in dye photodegradation: A comparative study in peroxo-based synthesis. Appl. Catal. B: Environ. 105, 298-305.

Dhananjeyan M.R., Kiwi J., Thampi K.R., 2000. Photocatalytic performance of TiO_2 and Fe_2O_3 immobilized on derivatized polymer films for mineralization of pollutants. Chem. Commun., 1443-1444.

Dijkstra M.F.J., Koerts E.C.B., Beenackers A.A.C.M., 2003. Performance of immobilized photocatalytic reactors in continuous mode. AIChE J. 49, 734-744.

Dionysiou D.D., Balasubramanian G., Suidan M.T., Khodadoust A.P., Baudin I., Laine J.-M., 2000. Rotating disk photocatalytic reactor: development, characterization, and evaluation for the destruction of organic Pollutants in water. Water Res. 34(11), 2927-2940.

Dixit A., Mungray A.K., Chakraborty M., 2010. Photochemical oxidation of phenol and chlorophenol by UV/H_2O_2/TiO_2 process: a kinetic study. Inter. J. Chem. Eng. Appl. 1, 247-250.

Djellabi R., Ghorab M.F., Cerrato G., Morandi S., Gatto S., Oldani V., Di Michele A., Bianchi C.L., 2014. Photoactive TiO_2-montmorillonite composite for degradation of organic dyes in water. J. Photochem. Photobiol. A: Chem.295(1), 57-63.

Elmolla E.S., Chaudhuri M., 2010. Photocatalytic degradation of amoxicillin, ampicillin and cloxacillin antibiotics in aqueous solution using UV/TiO_2 and UV/H_2O_2/TiO_2 photocatalysis. Desalination 252, 46-52.

El-Sheikh A.H., Al-Degs Y.S., Newman A.P., Lynch D.E., 2007. Oxidized activated carbon as support for titanium dioxide in UV-assisted degradation of 3-chlorophenol. Separ. Purif. Technol. 54, 117-123.

Eng Y.Y., Sharma V.K., Ray A.K., 2012. Degradation of anionic and cationic surfactants in a monolithic swirl-flow photoreactor. Separ. Purif. Technol. 92, 43-49.

Eskandarloo H., Badiei A., Behnajady M.A., Ziarani G.M., 2015. UV-LEDs assisted preparation of silver deposited TiO_2 catalyst bed inside microchannels as a high efficiency microphotoreactor for cleaning polluted water. Chem. Eng. J. 270, 158-167.

Esparza P., Borges M.E., Díaz L., Alvarez-Galván M.C., Fierro J.L.G., 2010. Photodegradation of dye pollutants using new nanostructured titania supported on volcanic ashes. Appl. Catal. A: General 388, 7-14.

Faramarzpour M., Vossoughi M., Borghei M., 2009. Photocatalytic degradation of furfural by titania nanoparticles in a floating-bed photoreactor. Chem. Eng. J. 146, 79-85.

Fathinia M., Khataee A.R., 2013. Residence time distribution analysis and optimization of photocatalysis of phenazopyridine using immobilized TiO_2 nanoparticles in a rectangular photoreactor. J. Indus. Eng. Chem. 19, 1525-1534.

Feng X., Chen Y., Fang Y., Wang X., Wang Z., Tao T., Zuo Y., 2014. Photodegradation of parabens by Fe(III)-citrate complexes at circumneutral pH: Matrix effect and reaction mechanism. Sci. Total Environ. 472, 130-136.

Franco A., Neves M.C., Carrott M.M.L.R., Mendonca M.H., Pereira M.I., Monteiro O.C., 2009. Photocatalytic decolorization of methylene blue in the presence of TiO_2/ZnS nanocomposites. J. Hazard. Mater. 161, 545-550.

Garg V.K., Kumar R., Gupta R., 2004. Removal of malachite green dye from aqueous solution by adsorption using agro-industry waste: a case study of *Prosopis cineraria*. Dyes Pigments 62, 1-10.

Gmurek M., Bizukoj M., Mosinger J., Ledakowicz S., 2015. Application of photoactive electrospun nanofiber materials with immobilized meso-tetraphenylporphyrin for parabens photodegradation. Catal. Today 240, 160-167.

Gouvêa-Carlos A.K., Wypych F., Moraes S.G., Durán N., Nagata N., Zamora P.P., 2000. Semiconductor-assisted photocatalytic degradation of reactive dyes in aqueous solution. Chemosphere 40, 433-40.

Guo J., Dong C., Zhang J., Lan Y., 2015. Biogenic synthetic schwertmannite photocatalytic degradation of acid orange 7 (AO7) assisted by citric acid. Separ. Purif. Technol. 143, 27-31.

Gupta V.K., Jain R., Agarwal S., Nayak A., 2012. Photodegradation of hazardous dye quinoline yellow catalyzed by TiO2, Meenakshi Shrivastava. J. Colloid Interf. Sci. 366, 135-140.

Habib M.A., Ismail I.M.I., Mahmood A., Ullah M.R., 2012. Photocatalytic decolorization of Brilliant Golden Yellow in $TiO_2$and ZnO suspensions. J. Saudi Chem. Soc. 16(4), 423-429.

Han L., Zhou X., Wan L., Deng Y., Zhan S., 2014. Synthesis of $ZnFe_2O_4$ nanoplates by succinic acid-assisted hydrothermal route and their photocatalytic degradation of rhodamine B under visible light. J. Environ. Chem. Eng. 2, 123-130.

Haque M.M., Muneer M., 2003. Heterogeneous photocatalysed degradation of a herbicide derivative, isoproturon in aqueous suspension of titanium dioxide. J. Environ. Manag. 69, 169-176.

Hassan M., Zhao Y., Xie B., 2016. Employing TiO_2 photocatalysis to deal with landfill leachate: Current status and development. Chem. Eng. J. 285, 264–275.

Hennezel D., Pichat O.P., Ollis D.F., 1998. Benzene and toluene gas-phase photocatalytic degradation over H2O and HCl pretreated TiO_2: by-products and mechanisms. J. Photochem. Photobiol. A: Chem. 118, 197-204.

Herrmann J.M., 1999. Heterogeneous photocatalysis: fundamentals and applications to the removal of various types of aqueous pollutants. Catal. Today 53(1), 115-129.

Herrmann J.M., 2010. Environmental photocatalysis: Perspectives for China. Sci. China Chem. 53, (9), 1831-1843.

Herrmann J.M., Guillard C., Arguello M., Agüera A., Tejedor A., Piedra L., Fernández-Alba A., 1999. Photocatalytic degradation of pesticide pirimiphos-methyl Determination of the reaction pathway and identification of intermediate products by various analytical methods. Catal. Today 54, 353-367.

Hoffmann H.R., Martin S.T., Choi W., Bahnemann D.W., 1995. Environmental applications of semiconductor photocatalysis. Chem. Rev., 95, 69-96.

Houas A., Lachheb H., Ksibi M., Elaloui E., Guillard C., Herrmann J.M., 2001. Photocatalytic degradation pathway of methylene blue in water. Appl. Catal. B: Environ. 31(2), 145-57.

Hu L., Dong S., Li Y., Pi Y., Wang J., Wang Y., Sun J., 2014. Controlled fabrication of monoclinic $BiVO_4$ rod-like structures for natural-sunlight-driven photocatalytic dye degradation. J. Taiwan Instit. Chem. Eng. 45, 2462-2468.

Huang J., Huang J., Zhang H., Zhou X., Zhong X., 2013. Dimensionality-dependent performance of nanostructured bismuth sulfide in photodegradation of organic dyes. Mater. Chem. Phys. 138, 755-761.

Huang M., Xu C., Wu Z., Huang Y., Lin J., Wu J., 2008. Photocatalytic discolorization of methyl orange solution by Pt modified TiO_2 loaded on natural zeolite. Dyes Pigments 77, 327–334.

Huang X., Meng Y., Liang P., 2007. Operational conditions of a membrane filtration reactor coupled with photocatalytic oxidation. Sep. Purif. Technol. 55, 165–172

Kamble S.P., Sawant S.B., Pangarkar V.G., 2006. Photocatalytic mineralization of phenoxyacetic acid using concentrated solar radiation and titanium dioxide in slurry photoreactor. Chem. Eng. Res. Design 84(A5), 355-362.

Karimi L., Zohoori S., Yazdanshenas M.E., 2014. Photocatalytic degradation of azo dyes in aqueous solutions under UV irradiation using nano-strontium titanate as the nanophotocatalyst. J. Saudi Chem. Soc. 18, 581-588.

Karkmaz M., Puzenat E., Guillard C., Herrmann J., 2004. Photocatalytic degradation of the alimentary azo dye amaranth mineralization of the azo group to nitrogen. Appl. Catal. B: Environ. 51, 183-194.

Kerkez Ö, Boz I., 2015.Photodegradation of Methylene Blue with Ag_2O/TiO_2_under Visible Light: Operational Parameters. Chem. Eng. Comm. 202(4), 534-541.

Khalilian H., Behpour M., Atouf V., Hosseini S. N., 2015. Immobilization of S, N-codoped TiO_2 nanoparticles on glass beads for photocatalytic degradation of methyl orange by fixed bed photoreactor under visible and sunlight irradiation. Sol. Energy 112, 239-245.

Khattab I.A., Ghaly M.Y., Österlund L., Ali M.E.M., Farah J.Y., Zaher F.M., 2012. Photocatalytic degradation of azo dye Reactive Red 15 over synthesized titanium and zinc oxides photocatalysts: a comparative study. Desalin. Water Treat. 48, 120-129.

Kim S.B., Hong S.C., 2002. Kinetic study for photocatalytic degradation of volatile organic compounds in air using thin film TiO_2 photocatalyst. Appl. Catal. B: Environ. 35, 305-315.

Kouamé N.A., Robert D., Keller V., Keller N., Pham C., Nguyen P., 2012. TiO_2/β-SiC foam-structured photoreactor for continuous wastewater treatment. Environ. Sci. Pollut. Res. 19, 3727-3734.

Kreutzer M.T., Kapteijn F., Moulijn J.A., Heiszwolf J.J., 2005. Multiphase monolith reactors: chemical reaction engineering of segmented flow in microchannels. Chem. Eng. Sci. 60(22), 5895-5916.

Ku Y., Tseng K.-Y., Wang W.-Y., 2005. Decomposition of gaseous acetone in an annular photoreactor coated with TiO_2 thin film. Water Air Soil Pollut. 168, 313-323.

Lachheb H., Puzenat E., Houas A., Ksibi M., Elaloui E., Guillard C., Herrmann J.-M., 2002. Photocatalytic degradation of various types of dyes (Alizarin S, Crocein Orange G, Methyl Red, Congo Red, Methylene Blue) in water by UV-irradiated titania. Appl. Catal. B: Environ. 39, 75-90.

Laohaprapanon S., Matahum J., Tayo L., You S.-J., 2015. Photodegradation of Reactive Black 5 in a ZnO/UV slurry membrane reactor. J. Taiwan Instit. Chem. Eng. 000, 1-6.

Lasa H., Serrano B., Salaices M., 2005. Photocatalytic reaction engineering. Springer, New York.

Lee J.-C., Kim M.-S., Kim C.K., Chung C.-H., Cho S.M., Han G.Y., Yoon K.J., Kim B.-W., 2003. Removal of paraquat in aqueous suspension of TiO_2 in an immersed UV photoreactor. Korean J. Chem. Eng. 20(5), 862-868.

Li D., Zheng H., Wang Q., Wang X., Jiang W., Zhang Z., Yang Y., 2014. A novel double-cylindrical-shell photoreactor immobilized with monolayer TiO_2-coated silica gel beads for photocatalytic degradation of Rhodamine B and Methyl Orange in aqueous solution. Separ. Purif. Technol. 123, 130-138.

Li D., Zhu Q., Han C., Yang Y., Jiang W., Zhang Z., 2015a.Photocatalytic degradation of recalcitrant organic pollutants in water using a novel cylindrical multi-column photoreactor packed with TiO_2–coated silica gel beads.J. Hazard. Mater. 285, 398-408.

Li Z., Zhou Y., Mao W., Zou Z., 2015b. Nanowire-based hierarchical tin oxide/zinc stannate hollow microspheres : Enhanced solar energy utilization efficiency for dye-sensitized solar cells and photocatalytic degradation of dyes. J. Power Sourc. 274, 575-581.

Lichtfouse E., 2013. Green Materials for Energy, Products and Depollution, Environmental Chemistry for a Sustainable World 3. Springer Science C Business Media Dordrecht, 476 pages

Lindstrom H., Wootton R., Iles A., 2007. High Surface area titania photocatalytic microfluidic reactors. AIChE J. 53(3), 695-702.

Liu B., Yu Z., Song X., Yang F., 2010. Effects of sodiumdodecylbenzenesulfonate and sodium dodecyl sulfate on the *Mytilus galloprovincialis* biomarker system. Ecotoxicol. Environ. Safety 73, 835-841.

Liu S.X., Chen X.Y., 2008. A visible light response TiO_2 photocatalyst realized by cationic S-doping and its application for phenol degradation. J. Hazard. Mater. 152(1), 48-55.

Liu Z., 2011. Effect of crystal form and particle size of titanium dioxide on the photodegradation behaviour of ethylene-vinyl acetate copolymer/low density polyethylene composite. Polymer Degrad. Stability 96, 43-50.

Lv T., Pan L.K., Liu X.J., Sun Z., 2012. Visible-light photocatalytic degradation of methyl orange by CdS–TiO_2 –Au composites synthesized via microwave-assisted reaction. Electrochim. Acta 83, 216-220.

Ma S., Meng J., Li J., Zhang Y., Ni L., 2014. Synthesis of catalytic polypropylene membranes enabling visible-light-driven photocatalytic degradation of dyes in water. J. Memb. Sci. 453, 221-229.

Mahmoodi N.M., Arami M., Limaee N.Y., 2006. Photocatalytic degradation of triazinic ring-containing azo dye (Reactive Red 198) by using immobilized TiO_2 photoreactor: Bench scale study. J. Hazard. Mater. B133, 113-118.

Martinez T., Bertron A., Ringot E., Escadeillas G., 2011. Degradation of NO using photocatalytic coatings applied to different substrates. Building Environ. 46, 1808-1816.

Mohammadi-Aghdam S., Marandi R., Olya M.E., Mehrdad Sharif A.A., 2014. Kinetic modeling of BB41 photocatalytic treatment in a semibatch flow photoreactor using a nanocomposite film. J. Saudi Chem. Soc. 18, 317-326.

Molinari R., Palmisano L., Drioli E., Schiavello M., 2002.Studies on various reactor configurations for couplingphotocatalysis and membrane processes in water purification. J. Memb. Sci. 206, 399-415.

Monteiro R.A.R., Miranda S.M., Rodrigues-Silva C., Faria J. L., Silva A.M.T., Boaventura R.A.R., Vilar V.J.P., 2015. Gas phase oxidation of n-decane and PCE by photocatalysis using an annular photoreactor packed with a monolithic catalytic bed coated with P25 and PC500. Appl. Catal. B: Environ. 165, 306-315.

Nezamzadeh-Ejhieh A., Shirzadi A., 2014. Enhancement of the photocatalytic activity of Ferrous Oxide by doping onto the nano-clinoptilolite particles towards photodegradation of tetracycline. Chemosphere 107, 136-144.

Nguyen A.T., Juang R.-S., 2015. Photocatalytic degradation of p-chlorophenol by hybrid H_2O_2 and TiO_2 in aqueous suspensions under UV irradiation. J. Environ. Manag. 147, 271-277.

Ning X-A., Wang J-Y., Li R-J., Wen W-B., Chen C-M., Wang Y-J., Yang Z-Y., Liu J-Y., 2015. Fate of volatile aromatic hydrocarbons in the wastewater from six textile dyeing wastewater treatment plants. Chemosphere 136, 50-56.

Ojanperä I., 2000. Pesticides. In: Bogusz MJ (ed) Forensic science. Hanbook of analytical separations, Vol 2. Elsevier Science

Ollis D. F., Pelizzetti E., Serpone N., 1991. Photocatalyzed destruction of water contamination. Environ. Sci. Technol. 25, 1523-1529.

Padmesh T.V.N., Vijayaraghavan K., Sekaran G., Velan M., 2006. Biosorption of Acid Blue 15 using fresh water macroalga *Azolla filiculoides*: Batch and column studies. Dyes Pigments, 71, 77-82.

Palmisano G., Loddo V., Augugliaro V., Bellardita M., Roda G. C., Parrino F., 2015. Validation of a two-dimensional modeling of an externally irradiated slurry photoreactor. Chem. Eng. J. 262, 490-498.

Pan L., Zou J.-J., Wang S., Huang Z.-F., Zhang X., Wang L., 2013. Enhancement of visible-light-induced photodegradation over hierarchical porous TiO_2 by nonmetal doping and water-mediated dye sensitization. Appl. Surf. Sci. 268, 252-258.

Panthi G., Barakat N. A.M., Park M., Kim H.-Y., Park S.-J., 2015. Fabrication of PdS/ZnS NPs doped PVAc hybrid electrospun nanofibers: Effective and reusable catalyst for dye photodegradation. J. Industr. Eng. Chem. 21, 298-302.

Parra S., Stanca S.E., Guasaquillo I., Thampi K.R., 2004. Photocatalytic degradation of atrazine using suspended and supported TiO_2. Appl. Catal. B: Environ. 51, 107-116.

Pinho L.X., Azevedo J., Miranda S. M., Ângelo J., Mendes A., Vilar V.J.P., Vasconcelos V., Boaventura R.A.R., 2015. Oxidation of microcystin-LR and cylindrospermopsin by heterogeneous photocatalysis using a tubular photoreactor packed with different TiO_2 coated supports. Chem. Eng. J. 266, 100-111.

Puma L., Yue P., 2001. The modelling of a fountain photocatalytic reactor with a parabolic profile. Chem. Eng. Sci. 56(2), 721-726.

Purwanto A., Widiyandari H., Ogi T., Okuyama K., 2011. Role of particle size for platinum-loaded tungsten oxide nanoparticles during dye photodegradation under solar-simulated irradiation. Catal. Commun. 12, 525-529.

Qamar M., Muneer M., Bahnemann D., 2006. Heterogeneous photocatalysed degradation of two selected pesticide derivatives, triclopyr and daminozid in aqueous suspensions of titanium dioxide. J. Environ. Manag. 80, 99-106.

Rajeshwar K., Osugi M.E., Chanmanee W., Chenthamarakshan C.R., Zanoni M.V.B., Kajitvichyanukul P., Krishnan-Ayer R., 2008. Heterogeneous photocatalytic treatment of organic dyes in air and aqueous media. J. Photochem. Photobiol. C: Photochem. Rev. 9, 171-192.

Rasoulifard M., Fazli M., Eskandarian M., 2014. Kinetic study for photocatalytic degradation of Direct Red 23 in UV–LED/nano-TiO_2/$S_2O_8^{2-}$ process: Dependence of degradation kinetic on operational parameters. J. Indust. Eng. Chem. 20, 3695-3702.

Rasoulifard M.H., Fazli M., Eskandarian M. R., 2015. Performance of the light-emitting-diodes in a continuous photoreactor for degradation of Direct Red 23 using UV-LED/$S_2O_8^{2-}$ process. J. Indust. Eng. Chem. 24, 121-126.

Repo E., Rengaraj S., Pulkka S., Castangnoli E., Suihkonen S., Sopanen M., Sillanpää M., 2013. Photocatalytic degradation of dyes by CdS microspheres under near UV and blue LED radiation. Separat. Purif. Technol. 120, 206-214.

Rincoin A.G., Pulgarin C., 2004. New and future developments in catalysis: Solar photocatalysis. Appl. Catal. B 51, 283-302.

Royaee S.J., Sohrabi M., Shafeghat A., 2014. Wastewater treatment using photo-impinging streams cyclone reactor: Computational fluid dynamics and kinetics modelling. Korean J. Chem. Eng. 31(2), 240-247.

Ruzimuradov O., Sharipov K., Yarbekov A., Saidov K., Hojamberdiev M., Prasad R. M., Cherkashinin G., Riedel R., 2015. A facile preparation of dual-phase nitrogen-doped TiO_2–$SrTiO_3$ macroporous monolithic photocatalyst for organic dye photodegradation under visible light. J. Europ. Ceramic Soc. 35, 1815-1821.

Saikia L., Bhuyan D., Saikia M., Malakar B., Dutta D.K., Sengupta P., 2015. Photocatalytic performance of ZnO nanomaterials for self sensitized degradation of malachite green dye under solar light. Appl. Catal. A: General 490, 42-49.

Sakthivel S., Shankar M.V., Palanichamy M., Arabindoo B., Murugesan V., 2002. Photocatalytic decomposition of leather dye: comparative study of TiO_2 supported on alumina and glass beads. J. Photochem. Photobiol. A 148, 153-159.

Salu O.A., Adams A., Robertson P.K.J., Wong L.S., McCullagh C., 2011. Remediation of oily wastewater from an interceptor tank using a novel photocatalytic drum reactor. Critical Rev. Environ. Sci. Technol. 41(9), 807-878.

Saquib M., Muneer M., 2002. Semiconductor mediated photocatalysed degradation of an anthraquinone dye, Remazol Brilliant Blue R under sunlight and artificial light source. Dyes Pigments 53, 237-249.

Saquib M., Muneer M., 2003a. Titanium dioxide mediated photocatalyzed degradation of a textile dye derivative, acid orange 8, in aqueous suspensions. Desalination 155, 255-263.

Saquib M., Muneer M., 2003b. TiO_2-mediated photocatalytic degradation of a triphenylmethane dye (gentian violet), in aqueous suspensions. Dyes Pigments 56, 37-49.

Selvaggi R., Tarpani L., Santuari A., Giovagnoli S., Latterini L., 2015. Silica nanoparticles assisted photodegradation of acridine orange in aqueous suspensions. Appl. Catal. B: Environ. 168, 363-369.

Selvaraj A., Sivakumar S., Ramasamy A.K., Balasubramanian V., 2013. Photocatalytic degradation of triazine dyes over N-doped TiO_2 in solar radiation. Res. Chem. Intermed. 39(6), 2287-2302.

Senthilnathan J., Philip L., 2012. Elimination of pesticides and their formulation products from drinking water using thin film continuous photoreactor under solar radiation. Sol. Energy 86, 2735-2745.

Serpone N., Salinaro A., 1999. Terminology, relative photonic efficiencies and quantum yields in heterogeneous photocatalysis. Part I: suggested protocol. Pure Appl. Chem. 71(2), 303-320.

Shah M., 2014. Effective treatment systems for azo dye degradation: A joint venture between physico-chemical & microbiological process. Int. J. Environ. Bioremed. Biodegrad. 2(5), 231-242.

Shamsipur M., Hemmateenejad B., Jahani N.J., Majd K.M., 2015. Liquid chromatographic–mass spectrometric monitoring of photodegradation of diphenylamine using experimental design methodology. J. Photochem. Photobiol. A: Chem. 299, 210-217.

Silva C., Faria J., 2003. Photochemical and photocatalytic degradation of an azo dye in aqueous solution by UV irradiation. J. Photochem. Photobiol. A: Chem. 155, 133-143.

Sonia S., Jose Annsi I., Suresh Kumar P., Mangalaraj D., Viswanathan C., Ponpandian N., 2015. Hydrothermal synthesis of novel Zn doped CuO nanoflowers as an efficient photodegradation material for textile dyes. Mater. Lett. 144, 127-130.

Souzanchi S., Vahabzadeh F., Fazel S., Hosseini S.N., 2013. Performance of an Annular Sieve-Plate Column photoreactor using immobilized TiO_2 on stainless steel support for phenol degradation, Chem. Eng. J. 223, 268-276.

Subagio D.P., Srinivasan M., Lim M., Lim T.T., 2010. Photocatalytic degradation of bisphenol-A by nitrogen-doped TiO_2 hollow sphere in a vis-LED photoreactor. Appl. Catal. B : Environ. 95, 414-422.

Tahir B., Tahir M., Amin N.S., 2015a. Gold–indium modified TiO_2 nanocatalysts for photocatalytic CO_2 reduction with H_2 as reductant in a monolith photoreactor. Appl. Surf. Sci. 338, 1-14.

Tahir B., Tahir M., Amin N.S., 2015b. Performance analysis of monolith photoreactor for CO_2 reduction with H_2. Energy Conver Manage. 90, 272-281.

Tang C., Chen V., 2004. The photocatalytic degradation of reactive black 5 using TiO_2/UV in an annular photoreactor. Water Res. 38, 2775-2781.

Tang T., Li K., Ying D., Sun T., Wang Y., Jia J., 2014. High efficient aqueous-film rotating disk photocatalytic fuel cell (RDPFC) with triple functions: Cogeneration of hydrogen and electricity with dye degradation. Int. J. Hydrogen Energy 39, 10258-10266.

Tang W.Z., An H., 1995. UV/TiO_2 photocatalytic oxidation of commercial dyes in aqueous solutions. Chemosphere 31(9), 4157-70.

Terzian R., Serpone N., 1995. Heterogeneous photocatalyzed oxidation of creosote components: mineralization of xylenols by illuminated TiO_2 in oxygenated aqueous media, J. Photochem. Photobiol. A. 89, 163-175.

Thomas S., Alatrache A., Pons M.N., Zahraa O., 2014. Degradation of the herbicide isoproturon by a photocatalytic process. C. R. Chimie17(7–8), 824-831.

Thiruvenkatachari R., Vigneswaran S., Moon S., 2008. A review on UV/TiO_2 photocatalytic oxidation process. Korean J. Chem. Eng. 25(1), 64-72.

Tokode O., Prabhu R., Lawton L.A., Robertson P.K.J., Bahnemann D.W., 2015. UV LED sources for heterogeneous photocatalysis. Environ. Chem. 35, 159-180.

Tolvaj L., Molnar Z., Nemeth R., 2013. Photodegradation of wood at elevated temperature: Infrared spectroscopic study. J. Photochem. Photobiol. B: Biol. 121, 3236.

Van Gerven T., Mul G., Moulijn J., Stankiewicz A., 2007. A review of intensification of photocatalytic processes. Chem. Eng. Process. 46(9), 781-789.

Velmurugan R., Krishnakumar B., Swaminathan M., 2014. Synthesis of Pd co-doped nano-TiO_2–SO_4^{2-} and its synergetic effect on the solar photodegradation of Reactive Red 120 dye. Mater. Sci. Semicond. Process. 25, 163-172.

Wang J., Zhang G., Zhang Z., Zhang X., Zhao G., Wen F., Pan Z., Li Y., Zhang P., Kang P., 2006. Investigation on photocatalytic degradation of ethyl violet dyestuff using visible light in the presence of ordinary rutile TiO_2 catalyst doped with upconversion luminescence agent. Water Res. 40, 2143-2150.

Wang K.H., Tsai H.H., Hseieh Y.H., 1998. The Kinetics of photocatalytic degradation of trichloroethylene in gas phase over TiO_2 supported on glass bead. Appl. Catal. B: Environ. 17, 313-320.

Wang P., Lim T.-T., 2012, Membrane vis-LED photoreactor for simultaneous penicillin G degradation and TiO_2 separation. Water Res. 46, 1825-1837

Wang W., Ku Y., 2003. Photocatalytic degradation of gaseous benzene in air streams by using an optical fiber photoreactor. J. Photochem. Photobiol. A: Chem. 159, 47-59.

Wang X., Lim T.-T., 2010. Solvothermal synthesis of C–N codoped TiO_2 and photocatalytic evaluation for bisphenol A degradation using a visible-light irradiated LED photoreactor. Appl. Catal. B: Environ. 100, 355-364.

Wang X., Wu P., Huang Z., Zhu N., Wu J., Li P., Dang Z., 2014. Solar photocatalytic degradation of methylene blue by mixed metal oxide catalysts derived from ZnAlTi layered double hydroxides. Appl. Clay Sci. 95, 95-103

Wei Y., Chu H.Q., Dong B.Z., Li X., 2011. Evaluation of humic acid removal by a flat submerged membrane photoreactor, Chin. Sci. Bull. 56(32), 3437-3444.

Wu Y., Yuan H., Jiang X., Wei G., Li C., Dong W., 2012. Photocatalytic degradation of 4-tert-octylphenol in a spiral photoreactor system. J. Environ. Sci. 24(9), 1679-1685.

Wurtele M.A., Kolbe T., Lipsz M., Kulberg A., Weyers M., Kneissl M., Jekel M., 2011. Application of GaN-based ultraviolet-C light emitting diodes – UV LEDs – for water disinfection. Water Res. 45, 1481-1489.

Xiao-gang H., Hong-hui L., Zhong-lin Z., Cai-mai F., Shi-bin L., Yan-ping S., 2009. Modeling and experimentation of a novel labyrinth bubble photoreactor for degradation of organic pollutant. Chem. Eng. Res. Design 87, 1604-1611.

Xu C., Wu H., Gu F.L., 2014. Efficient adsorption and photocatalytic degradation of Rhodamine B under visible light irradiation over BiOBr/montmorillonite composites. J. Hazard. Mater. 275, 185-192.

Xue X., 2015. Piezo-potential enhanced photocatalytic degradation of organic dye using ZnO nanowires. Nano Energy, http://dx.doi.org/10.1016/j.nanoen.2015.02.029

Zahraa O., Sauvanaud L., Hamard G., Bouchy M., 2003. Kinetics of atrazine degradation by photocatalytic process in aqueous solution. Inter. J. Photoenergy 5, 87-93.

Zhang A., Zhou M., Han L., Zhou Q., 2011.The combination of rotating disk photocatalytic reactor and TiO_2 nanotube arrays for environmental pollutants removal. J. Hazard. Mater. 186, 1374-1383.

Zhang H., Wu P., Li Y., Liao L.F., Fang Z., Zhong X.H., 2010. Preparation of bismuth oxide quantum dots and their photocatalytic activity in a homogeneous system. Chem. Catal. Chem. 2, 1115-1121.

Zhang S., Chen L., Liu H., Guo W., Yang Y., Guo Y., Huo M., 2012. Design of $H_3PW_{12}O_{40}/TiO_2$ and $Ag/H_3PW_{12}O_{40}/TiO_2$ film-coated optical fiber photoreactor for the degradation of aqueous rhodamine B and 4-nitrophenol under simulated sunlight irradiation. Chem. Eng. J. 200-202, 300-309.

Zhang X., Yao J., Li D., Chen X., Wang H., Yeo L.Y., Friend J.R., 2014. Self-assembled highly crystalline TiO_2 mesostructures for sunlight-driven, pH-responsive photodegradation of dyes. Mater. Res. Bull. 55, 13-18.

Zhang Y.R., Li Q., 2013. Synthesis and characterization of Fe-doped TiO_2 films by electrophoretic method and its photocatalytic activity toward methyl orange. Solid State Sci. 16, 16-20.

Zhang Z., Wang C.C., Zakaria R., Ying J.Y., 1998.Role of particle size in nanocrystalline TiO2-based photocatalysts. J. Phys. Chem. B 102, 10871.

Zheng P., Du Y., Chang P.R., Ma X., 2015. Amylose–halloysite–TiO_2 composites: Preparation, characterization and photodegradation. Appl. Surf. Sci. 329, 256-261.

Zhu G., Hojamberdiev M., Tan C., Jin L., Xu C., Liu Y., Liu P., Zhou J., 2014. Photodegradation of organic dyes with anatase TiO_2 nanoparticles-loaded BiOCl nanosheets with exposed {001} facets under simulated solar light. Mater. Chem. Phys. 147, 1146-1156.

CHAPITRE III: Performance Photocatalytique du Polyester Imprégné de TiO_2 pour la Dégradation du Vert Cibacron : Implications du Prétraitement de Surface et de la Microstructure

---

Photocatalytic Performance of TiO_2 Impregnated Polyester for the Degradation of Reactive Green 12: Implications of the Surface Pretreatment and the Microstructure

Hichem Zeghioud [a,b], Nabila Khellaf [a,b], Abdeltif Amrane [c], Hayet Djelal [d], Walid Elfalleh [e], Aymen Amine Assadi[c], Sami Rtimi [f]

Journal of Photochemistry and Photobiology A: Chemistry 346 (2017) 493–501

[a] Department of Process Engineering, Faculty of Engineering, Badji Mokhtar University, P.O. Box 12, 23000 Annaba, Algeria.
[b] Laboratory of Organic Synthesis-Modeling and Optimization of Chemical Processes, Badji Mokhtar University, P.O. Box 12, 23000 Annaba, Algeria.
[c] ENSCR, CNRS, UMR 6226, Allée de Beaulieu, CS 50837, 35708 Rennes Cedex 7, France.
[d] Ecole des Métiers de l'Environnement, Campus de Ker Lann, 35170 Bruz, France.
[e] Unité de Recherche Catalyse et Matériaux pour l'Environnement et les Procédés (UR11ES85),Université de Gabès, Campus Universitaire Cité Erriadh, Gabès 6072,Tunisia.
[f] Ecole Polytechnique Fédérale de Lausanne, EPFL-STI-LTP, Station 12, CH-1015 Lausanne, Switzerland.

Préambule

Dans ce chapitre on a choisi des catalyseurs synthétiques supportés pour éviter le problème de la récupération ultérieur des nanoparticules du catalyseur pour une éventuelle réutilisation. Le semi-conducteur choisi c'est le TiO_2 imprégné sur du polyester. Mais durant la préparation deux techniques de prétraitement de surface (activation par plasma- Fréquence Radio (FR) et activation par Photons UV-C) de ce dernier pour crée des groupes polarisés ont été testé.

La caractérisation des catalyseurs fabriqués par IRTF, MET, imagerie microscopic et DRX a montré des microstructures, à des tailles cristallines et à des activités photocatalytiques légèrement différentes. Le colorant synthétique de textile Reactive Green (RG 12) est choisi comme une molécule modèle pour les tests photocatalytiques. Les tests desdeux catalyseurs n'ont montré aucune activité photocatalytique pour le polyester activé par plasma-FR en raison du mode de prétraitement. Cependant, la performance photocatalytique du catalyseur activé par UV-C a été étudiée en étudiant les conditions optimales de réaction de dégradation de RG 12 telles que la concentration initiale de polluant, la lumière appliquée (UV ou Visible), la quantité du catalyseur et la présence de peroxyde d'hydrogène à différentes concentrations.
Dans des conditions opératoires optimisées obtenues (dose de catalyseur de 5,18 g/L et concentration initiale en colorant de 2 mg/L), l'élimination du RG 12 atteint 100% sous lumière UV et 87,14% sous lumière visible en 115 min. Les résultats cinétiques ont montré que l'élimination de ce colorant récalcitrant suit presque un modèle de Langmuir-Hinshelwood (L-H) avec un coefficient de régression (R^2) de 0,926. L'activité du catalyseur s'est révélée stable pendant plus de cinq cycles de réutilisation.

Nomenclature

AOPs:	Advanced Oxidation Processes
DRX:	Diffraction des Rayons-X
FTIR:	Fourier Transform InfraRed Spectroscopy
IRTF	Infra-Raouge à Transformé de Fourier
L-H:	Langmuir-Hinshelwood
MET:	Microscope electronic a transmission
PES:	Polyester
RF:	Radio Frequency
RG-12:	Reactive Green 12
ROS:	Reactive Oxygen Species

TEM:	Transmission Electron Microscopy
UV:	Ultra Violet
WHO:	World Health Organization
XRD:	X-ray diffraction

Abstract

In the present work, we investigate the degradation of recalcitrant industrial textile dye (Reactive Green 12) in aqueous solution by TiO_2 impregnated polyester at room temperature. The TiO_2 loading on polyester was optimized using different polyester pretreatment (plasma surface activation and UV-C photons). The applied surface pretreatments led to slightly different microstructure, crystalline sizes and photocatalytic activities. Both catalysts tests showed no photocatalytic activity for plasma RF activated polyester due to the way of pretreatment. However, the photocatalytic performance of UV-C activated catalyst was investigated studying the optimal reaction conditions such as pollutant initial concentration, applied light (UV or visible), catalyst loading and the presence of hydrogen peroxide at different concentrations. Under optimized operating conditions namely catalyst dose of 5.18 g/L and initial dye concentration of 2 mg/L, the removal of Reactive green 12 reached 100% under UV light and 87.14% under visible light within 120 min. Moreover, the presence of hydrogen peroxide showed a positive impact on the degradation, since the time needed for total dye decreased to 80 min under UV light irradiation for a $[H_2O_2]_0$ to $[RG\text{-}12]_0$ ratio in the range 20–30. The kinetic results showed that the removal of this recalcitrant dye nearly followed a Langmuir-Hinshelwood (L-H) model with a regression coefficient (R^2) value of 0.926. The catalyst activity was found to be stable for more than five reuse cycles.

Keywords: Polyester, Photocatalytic degradation, Reactive green 12, UV-C, RF-Plasma, Textile dyes.

III.1. Introduction

Dyeing factories around the world are dumping millions of tons dye effluent into rivers, lakes and natural waters. Reactive dyes, which are known to have good practical applications, have been found to cause adverse effects not only to the humans but also to the environment, such as allergy, dermatitis, cancer, necrosis…etc. (Cardoso et al., 2011; De Lima al., 2011). A suitable and sustainable treatment method for the removal of these pollutants is needed today.

During the last decades, Advanced Oxidation Processes (AOPs) emerged as innovative technologies to treat wastewaters containing recalcitrant molecules (Zhu et al., 2004; Lee et al., 2003; Taborda et al., 200). Among them, Heterogeneous photocatalysis has attracted increased interest due to its simplicity, effectivity and the use of environmentally friendly and low-cost catalysts.

Recent developments in the photocatalytic degradations have been carried out using novel photo-catalysts at different forms and with diverse performance in the pollutants mineralization (Zhang et al., 2016a; Zhang et al., 2016b; Zhang et al., 2017).

The use of silver and strontium co-doped TiO_2 nanoparticles synthesized by a modified sol–gel route for the degradation of Direct Green-6 and Reactive Blue-160 under UV & visible light showed higher catalytic activity compared to undoped TiO_2, a complete mineralization of the dye molecules was also achieved and studied in details (Naraginti et al., 2015). Some studies reported on the exploitation of photocatalytic fuel cell with immobilized ZnO photoanode for the enhancement of the degradation of Reactive Green 19 and the generation of electricity at the same time (Lee et al., 2017). Recently, Yola et al., reported the synthesis of a novel composite containing silver nanoparticles (AgNPs) and colemanite ore waste (COW) that had been tested to remove reactive dyes (Yellow 86 and Reactive Red 2), they found a high photocatalytic activity for the degradation of the reactive dyes from single and binary dye solutions (Yola et al., 2014).

The use of nanoparticles/suspended photocatalysts poses the problem of the catalyst removal after the wastewater treatment. To overcome this problem, researchers supported the photocatalysts on different substrates. A variety of substrates had been tested as support for the catalyst such as glass, carbon fibers, polymers, etc. (Chen et al., 2016; Vild et al., 2016). In this study we are using polyester as support for TiO_2 because of its flexibility, relative stability, resistant to UV, and low-cost (Donelli et al., 2010). The low surface energy of polyester leads to poor TiO_2 nanoparticles adhesion. This is why a surface pretreatment/functionalization is needed to create surface polarity able to interact with TiO_2 nanoparticles. Sudrajat et al. (2010) reported the pretreatment of polyester surface with alkali before coating it with N-doped WO_3 photocatalyst. This led to the improvement of the polyester hydrophilicity and the prepared photocatalyst showed a high activity under solar light for the degradation of amaranth (Sudrajat and Babel, 2010). In another work, the use of a facile spray coating method to coated N-TiO_2 onto polyester filters showed an excellent photocatalytic performance for the removal of gaseous toluene under visible light (Zhang et al., 2016c).

Rtimi et al., recently reported the performance of TiO_2 impregnated on RF-Plasma pretreated polyester leading to *Escherichia coli* inactivation under visible light (Baghriche et al., 2013).

To the best of our knowledge, there is a lack of works dealing with the degradation of reactive dyes on coated polyester for wastewater treatment. It was therefore the purpose of this study and a recalcitrant industrial reactive dye (Reactive green 12) was considered as the target compound. The performance of TiO_2 impregnated on differently pretreated polyester surfaces (RF-plasma and UV-C photons) was consequently investigated for the removal of the dye under UV and visible light.

III.2. Experimental

III.2.1. Materials

Hydrogen peroxide (35 wt%, Acros), Reactive Green 12 dye (>99%, MW =1837 g mol^{-1}) procured from the textile manufacture of Constantine (Algeria) was used as received. The aqueous solutions were prepared using ultra-pure water with a resistance of 15.0 MΩ cm. Physico-chemical properties of RG-12 dye are shown in **Table III.1** and its structure is presented in **Figure III.1**.

Table III.1: Physicochemical properties of RG-12

Propriety	**Reactive green 12 (Cibacron Green LS-3B)**
Empirical formula	$C_{60}H_{29}Cl_3N_{16}NiO_{21}S.6Na$
Molecular weight (g/mol)	1837
Abbreviation	RG-12
Dyer class	Reactive dye
λ_{max} (nm)	615

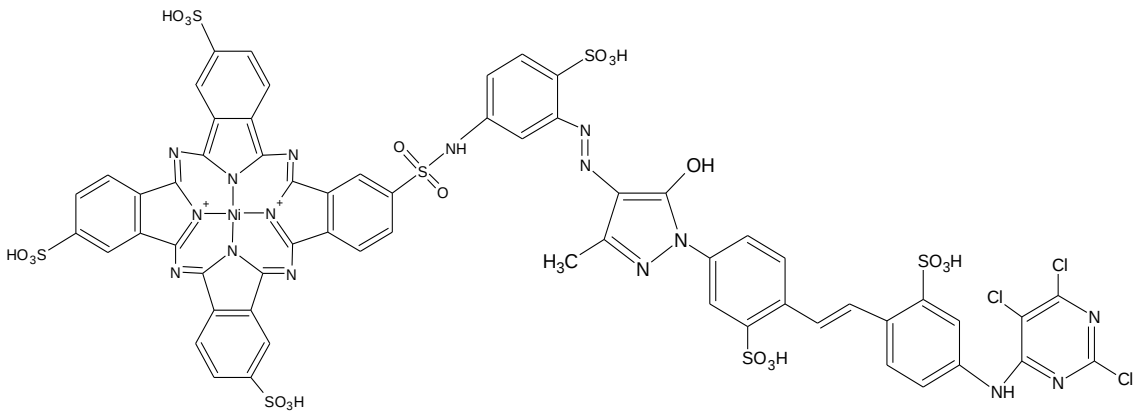

Figure III.1: Chemical structure of RG-12.

III.2.2. Polyester pretreatment using RF-plasma and vacuum UV-C photons

RF-plasma pretreatment of textiles consists on the application of electromagnetic radiation at low pressure (1 Torr). Vacuum enhances the capture length of the electron avoiding collision deactivation. Residual O_2 generates cations anions (O^-, O^+), radicals, excited sates, molecule-ions and electrons with high energy in a system where the local generated heat has a non–homogeneous distribution in a non-equilibrium situation. In the RF-cavity intense local heat develops breaking H- and intermolecular bonds in the textile fabrics at a pressure of 1 Torr. Intermolecular C-C bond scissions occur and the O_2 containing hydrophilic functional groups increase in the polyester leading to an improved wettability of these textiles as recently reported (Rtimi, 2016). In the presence of O_2, the principal species formed on the polyester surface are: $-COO^-$, percarboxylic species, -O-O-, phenolic and lactam species (Baghriche et al., 2013; Rtimi, 2016).

The UVC light excitation at 185 nm does not have the energy content to produce cationic O^+ and anionic oxygen O^- species, as it is the case of RF-plasma. This light only leads to excited O*: $O_2 + UVC \rightarrow 2O^*$. The optical absorption between the light and the textile positioned at 3 mm of the light source at 1 atm air is very low since εO_2 (185 nm) = 2.6 M^{-1} cm^{-1} and εN_2 (185 nm) = 0.3 M^{-1} cm^{-1} at 185 nm. Practically, no photons are lost in the optical pathway between the light source and the sample. Polyester fabrics pretreated by UVC introduced surface activation with more evenly distributed than pretreatment with RF-plasma. Vacuum-UVC light radiant energy at 185 nm is higher than 495 kJ/mol, the energy required for the reaction $O_2 \rightarrow 2O^*$. The absence of cationic or anionic oxygen leads to more uniform distribution in the activated sites on the polyester. This in turn leads more uniform charged/polar sites on the polyester surface able to bond TiO_2 (Rtimi, 2016).

III.2.3. Catalyst preparation

The titanium tetra-isopropoxide (TTIP, Sigma Aldrich) was dissolved in isopropanol in a 1:13 molar ratio to obtain TiO_2 colloidal suspensions. The formed solution was poured into a beaker with 50 ml of 0.1M HNO_3. The polyester samples of 10x10 cm of dimension were immersed into the acid TiO_2 precursor suspension and heated at 80°C during 120 min under continuous stirring in a reflux condenser. The obtained polyester fabrics were removed and rinsed; in order to remove the unbounded TiO_2 anultrasound bath treatment (for 2 min) was necessary. The ultrasonication was performed in an ultrasound bath Elgasonic at low intensity used for cleaning (50 w).

III.2.4. Photocatalytic activity

The photocatalytic activity of TiO_2 deposited on the polyester fabrics was evaluated by examining the degradation of 500 ml of the RG-12 dye solution in Schott Duran glass reactor under magnetic stirring. The reaction system includes a 9-Watt UV Philips Bulb lamp emitting a UV-vis light (λ=365 nm) with measured intensity of 20 W/m^2 with a (VLX 3 W) radiometer. For the catalyst activity test under visible-light, an S G23 9W (840) lamp (Sylvania) was used provided with a UV light filter. The solution was stirred in the dark for 30 min to establish adsorption–desorption equilibrium before irradiation. The concentration of dye solution (V=3 mL) was followed using a UV–vis spectrophotometer at regular time intervals. The effect of operating parameters like the initial dye concentration, the catalyst amount and the ratio of oxidizing agent on the photocatalytic decolorization were considered in the present study. The pollutant degradation kinetic was recorded using a Varian Cary®50 UV-vis Spectrophotometer, where the spectra were obtained at the wavelength range of 200–800 nm.

The decolorization efficiency (%) of RG-12 solution was calculated according to **Eq. III.1**:

$$\eta(\%) = \left(\frac{C_0 - C_t}{C_0}\right) \times 100 = \left(\frac{A_0 - A_t}{A_0}\right) \times 100 \qquad \text{(III.1)}$$

where A_0 and A_t are the initial intensity of absorbance at λ_{max} =615 nm and the intensity of absorbance peak at time t in UV-vis spectra of RG 12, respectively.

III.2.5. Surface characterization

FTIR spectra for bare and UVC pretreated polyester fabrics were taken in a Portmann AG spectrophotometer equipped with a Specac attachment (45° one pass diamond crystal). Spectra were taken by 256 scans with a resolution of 10 cm^{-1} between 900 and 4000 cm^{-1}.

Fibers from the TiO_2impregnated polyester (noted as “P” in the figure) samples were embedded in epoxy (noted as “E” in the figure) resin N°45359 (purchased from Fluka) and thin sectioned using an ultra-microtome then visualized using a Philips CM-12 operated at 120 KV.

The crystalline structure of the TiO_2 impregnated polyester was investigated by X-ray diffraction (XRD) INEL Model XRG instrument, power 3.5 KW (Cu Ka radiation with wavelength λ=1.5418 A°) and coupled with a detector CPS120 to record peaks from 10° to 100°.

III.3. Results and discussion

III.3.1. Characterization of materials

a) Effect of the surface treatment and electron microscopy imaging of TiO_2 impregnated polyester

Figure III.2 shows the FTIR of the pretreated polyester with UVC. Main bands in the polyester chain can be assigned to: stretching of C–O–C at 1160–1020 cm^{-1}, vibrational stretching of –C=O at 1730–1760 cm^{-1}, stretching of $–CH_2$ and C–H groups at 2950–2900 cm^{-1}, and –OH stretching bond at: 3450–3500 cm^{-1}. FTIR Spectra show the formation of ester group when treating polyester with UVC photons as shown in **Figure III.2**, spectrum 2. The little shift observed for CH_2 and C–H groups can be attributed to the chain elongation leading to bonds session. Local high temperature generated during the pretreatment causes yellowish colour centres attributed to the segmentation of the polyester as shown below in **Figure III.3**.

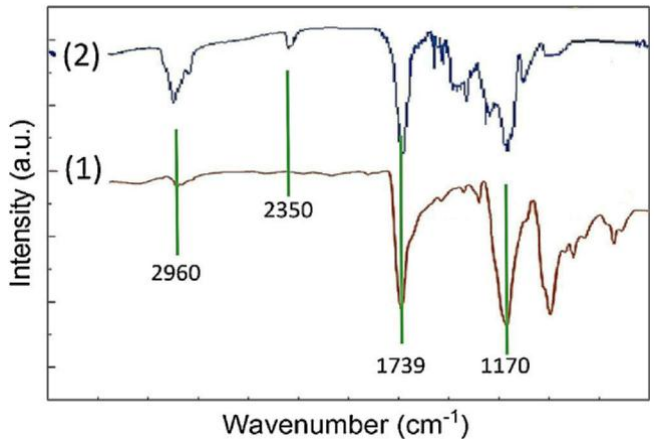

Figure III.2: FTIR spectra of bare polyester and UVC pretreated polyester. For more details, see Experimental section

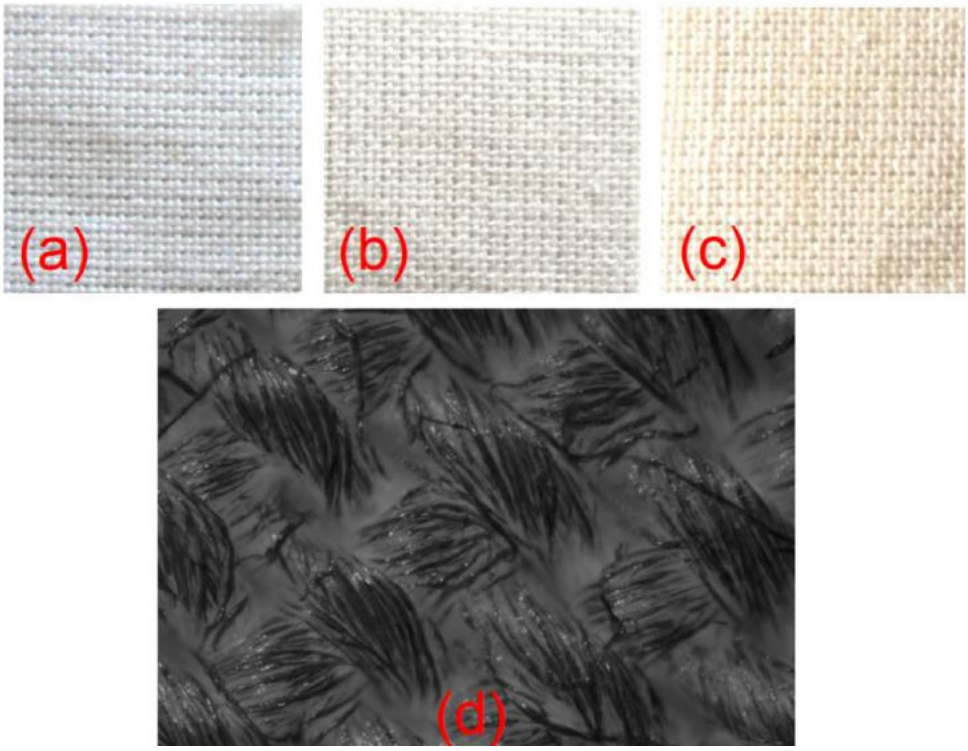

Figure III.3: Visual perception and optical imaging of: (a) bare polyester fabric, (b) UVC pretreated polyester fabric, (c) TiO_2 impregnated polyester (pretreated with UVC) and (d) optical microscopy imaging of TiO_2 impregnated polyester pretreated with UVC. (For interpretation of the references to colour in the text, the reader is referred to the web version of this article)

Figure III.4 shows the morphological properties of the samples of TiO_2 impregnated on polyester fibre. The polyester fibres seem to be wholly covered by the TiO_2 particles/aggregates. It can also be observed that the catalyst particle in RF-Plasma activated polyester are more compact and attached to the fibre surface and the density of TiO_2 particle is very high compared to UVC activated polyester, this result may be due to the diversity of polar species created during the activation process which leads to an important electrostatic force of attraction in polyester surface as previously reported by Baghriche et al. (2013).

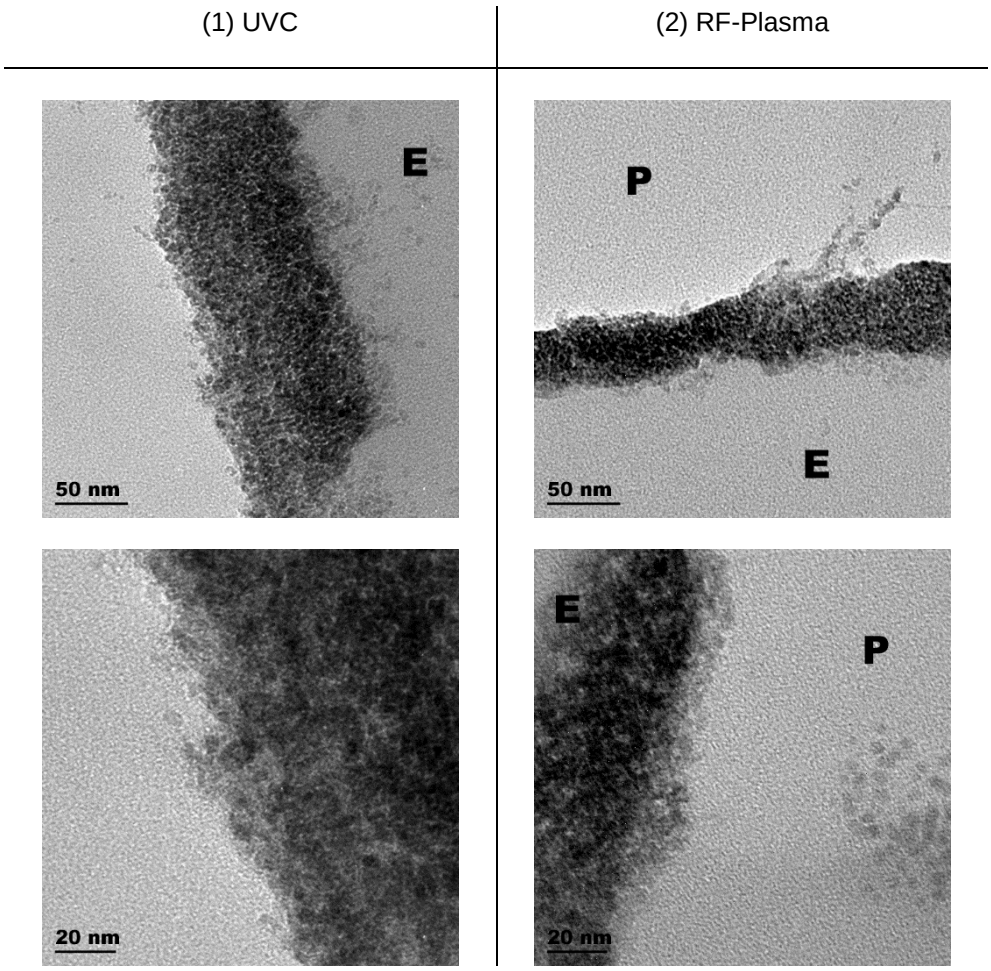

Figure III.4: TEM images of TiO_2 impregnated polyester using different surface pretreatment: (1) UVC and (2) RF-Plasma (for more details, see experimental section).

b) X-ray diffraction (XRD) analysis of TiO_2 impregnated polyester pretreated differently

Figure III.5 shows the XRD of TiO_2 crystal phases on polyester. Two peaks at $2\theta = 15°$ and 16.5° were seen and attributed to the polyester/substrate (Sudrajat and Babel, 2010), a small broad peak at $2\theta = 34.3°$ indicated the presence of Rutile form of TiO_2 (Zhang et al., 2016c). A high sharp narrow peak at $2\theta = 22.9°$ for the Polyester-TiO_2 indicated an efficient crystallization of an Anatase form of TiO_2; similar results were found in the literature (Baghriche et al., 2013; Rtimi, 2016; Rtimi et al., 2016).

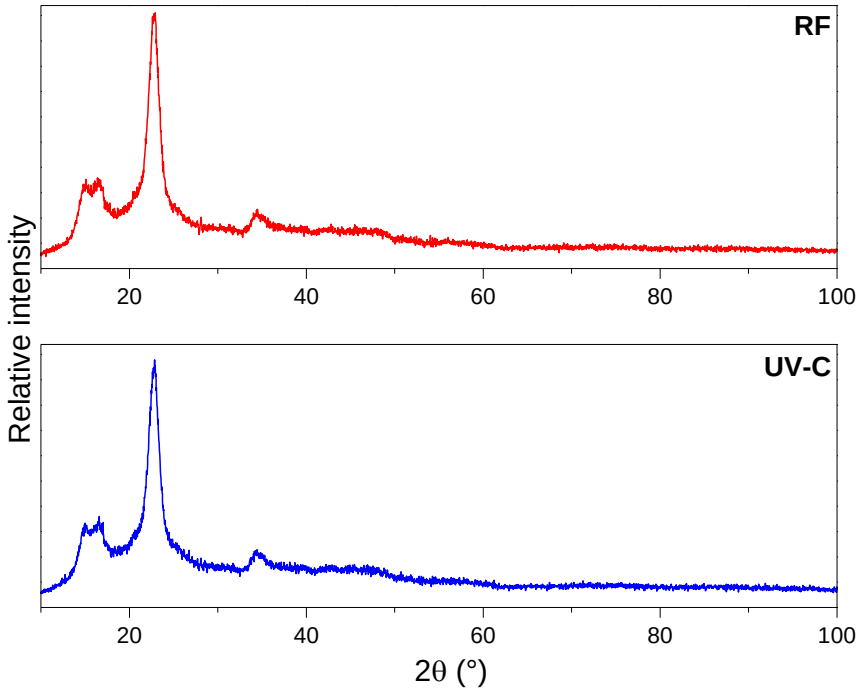

Figure III.5: XRD patterns of TiO_2-impregnated polyester pretreated via RF-plasma and UVC

The Scherrer equation (Merkus, 2009) was used to estimate the crystalline size of TiO_2 on polyester as a function of the treatment of polyester prior to the impregnation (**Eq. III.2**).

$$D = \frac{K\lambda}{\beta Cos\theta} \quad \text{(III.2)}$$

Where D is the apparent crystal size, K is a form-factor (Scherrer- constant), which takes into account the size distribution of different reflecting planes, and for cubic crystal and/orunknown crystal shape K = 0.9 is recommended (Klug and Alexander, 1974). B is the peak width at half maxima in radians (in 2θ) and θ is the Bragg angle.

The application of this equation gave a grain size of 4.88 nm for the catalyst RF-plasma-activated polyester and 5.22 nm for the catalyst UV-C activated polyester. This result is consistent with the observation from TEM showing different behavior of TiO_2 aggregates at the surface of polyester with respect to the pretreatment process e.g. plasma or UV-C photons (**Figure III.4**). It is essential to indicate that the applicability of the Scherrer-Formula is restricted in the range of 100–200 nm for a significant physical interpretation of results.

III.3.2. Catalysts activity

In order to evaluate the photocatalytic activity in dye removal for the synthetic catalysts (TiO_2 impregnated on UV-C and RF-Plasma activated polyesters), tests were carried out under both UV and visible light during 2 h. As shown in **Figure III.6**, the TiO_2 impregnated on UV-C activated polyester has a good activity under both UV and Visible light. However, the TiO_2 impregnated on RF-activated polyester did not shown significant photocatalytic activity under visible light. This can be attributed to the fact that pre-treating the polyester which UVC creates damages generating yellowish colour centres. These latter could be generated due to the local high temperature heating leading to the segmentation of polyester, creating beneficial polar groups facilitating the TiO_2 binding. These colour centres enhanced the visible light absorption leading to the observed photocatalytic activity of the TiO_2-polester (UVC pretreated) under visible light.

Figure III.6 shows that TiO_2 deposited on UV-C pretreated polyester Exhibit 87% RG-12 dye removal under visible light and total removal under UV light within 2 h. The polar sites on the UV-C pretreated polyester are also important for the electrostatic attraction forces between the dye and the impregnated polyester. Since the UV-C pretreated sample showed better RG-12 removal, we will not go further with the RF-plasma pretreated sample.

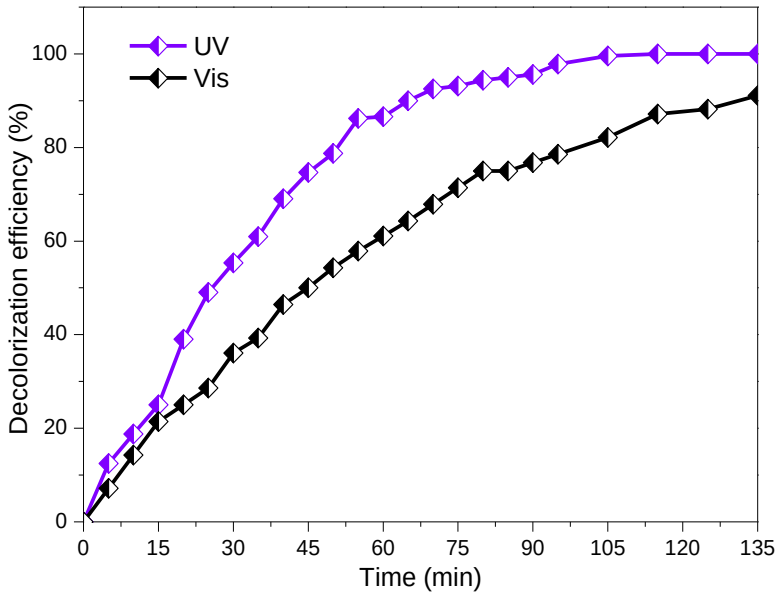

Figure III.6: Photocatalytic degradation of RG-12 under UV and Visible light on TiO_2-polyester UV-C pretreated (RG-12 initial concentration: 2 mg/L; catalyst dosage: 5.176 g/L; natural pH~ 6.5)

III.3.3. Effect of initial dye concentration

In order to understand the effect of the dye concentration on the degradation efficiency, different initial RG-12 concentrations from 1 to 10 mg/L were studied at room temperature (2.59 g/L TiO_2, natural pH). As shown in **Figure III.7**, at initial concentrations of 1 and 2 mg/L, around 100% and 99% of the RG 12 were removed within 120 min, respectively; and, the removal yields of RG-12 were found to decrease significantly with increasing initial concentration of the dye. This relationship between the photo-degradation rate and the initial concentrations of RG-12 could be explained differently (Tang and Chen, 2004; Nam et al., 2002). The concentrations of 1 and 2 mg/L can be therefore considered optimal due to the squat optical density of the dye allowing TiO_2 particles to absorb maximum exciting photons to generate higher concentrations of Reactive Oxygen Species (ROS) at the surface of the semiconductor. Contrarily, higher RG-12 concentrations show strong absorption of the applied light, limiting consequently the diffusion step of the photo-exited species to the TiO_2 surface (Kumawat et al., 2012; Vidya et al., 2016). In principle, the dye covers TiO_2 particles irrespective of the dye concentration. However, in the case of low dye concentrations, the transparency of the solution is sufficiently large that light can penetrate at the surface of the photocatalyst, which can generate active species. Azo-dyes contain sulfonate groups increasing the water solubility, as well as hydroxyl and amide groups responsible for their relative stability. The initial reaction corresponds to the oxidation of water molecules leading to the formation of physic-sorbed hydroxyl radicals on the catalyst surface (Cat(•OH)):

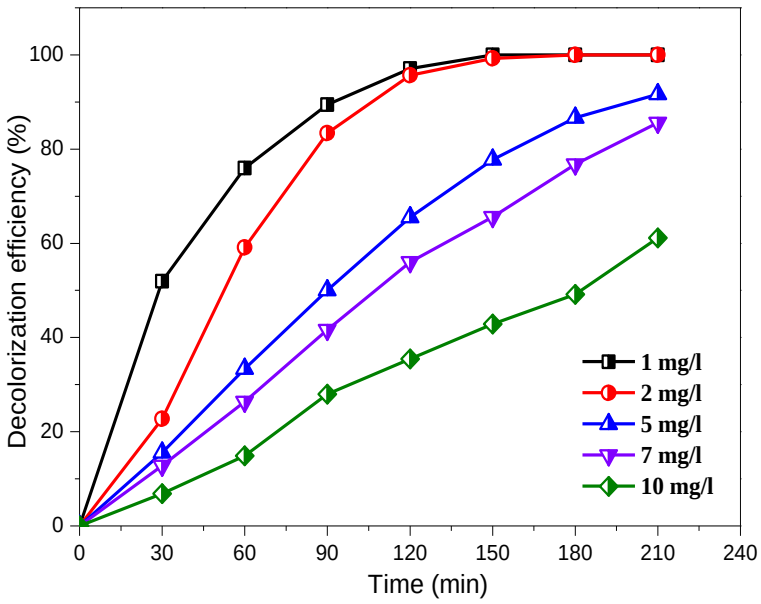

Figure III.7: Photocatalytic degradation of RG-12 at different initial concentrations (catalyst dosage: 2.588 g/L; natural pH)

Azo-dyes contain sulfonate groups increasing the water solubility and hydroxyl and amide group responsible for their relative stability. The initial reaction corresponds to the oxidation of water molecules leading to the formation of physi-sorbed hydroxyl radicals on the catalyst surface (Cat(*OH)):

$$Cat(^{\bullet}OH) \rightarrow CatO + H^{+} + e^{-} \quad \text{(III.3)}$$

If higher oxidation states are available for a metal oxide, superoxide (CatO) may be formed above the standard potential of O_2 (E0 = 1.23 V vs. SHE).

$$Cat\text{-}(^{\bullet}OH) \rightarrow CatO + H^{+} + e^{-} \quad \text{(III.4)}$$

The CatO/Cat redox couple acts as a mediator in the oxidation of organic pollutants **Eq. III.5** followed with the side reaction of oxygen evolution via chemical decomposition of the higher oxide species presented in **Eq. III.6**.

$$CatO + R \rightarrow Cat + RO \quad \text{(III.5)}$$

$$CatO \rightarrow Cat + \tfrac{1}{2}\, O_2 \quad \text{(III.6)}$$

Reaction of direct oxidation of Cat(•OH) to O_2 as shown in **Eq. III.7** competes with reaction of its dimerization into H_2O_2 by **Eq. III.8**:

$$Cat(^{\bullet}OH) \rightarrow Cat + \tfrac{1}{2}\, O_2 + H^{+} + e^{-} \quad \text{(III.7)}$$

$$2\ Cat(^{\bullet}OH) \rightarrow 2\ Cat + H_2O_2 \quad \text{(III.8)}$$

III.3.4. Effect of catalyst loading

To evaluate the effect of TiO_2 loaded on the polyester on the degradation efficiency of RG-12, a range of concentrations (from 1.29 to 5.18 g/L) were tested for 2 mg/L of initial dye concentration. **Figure III.8** shows that the degradation efficiency of RG-12 was enhanced from 82.93% to 100% by increasing the catalyst concentration from 1.29 to 5.18 g/L within 120 min under UV light. It is readily seen that increasing the amount of TiO_2 fasten the removal rate of RG-12. This can be due to the increase of the catalytic active sites which leads to increase ROS production ($^{\bullet}OH$, HO_2, …) (Zeghioud et al., 2016). Above this catalyst concentration the rate of degradation was seen to be lower and this can be attributed to the TiO_2 particulate aggregation and hence reducing the surface to volume characteristic. This latter reduces the contact between the TiO_2 and the organic dye.

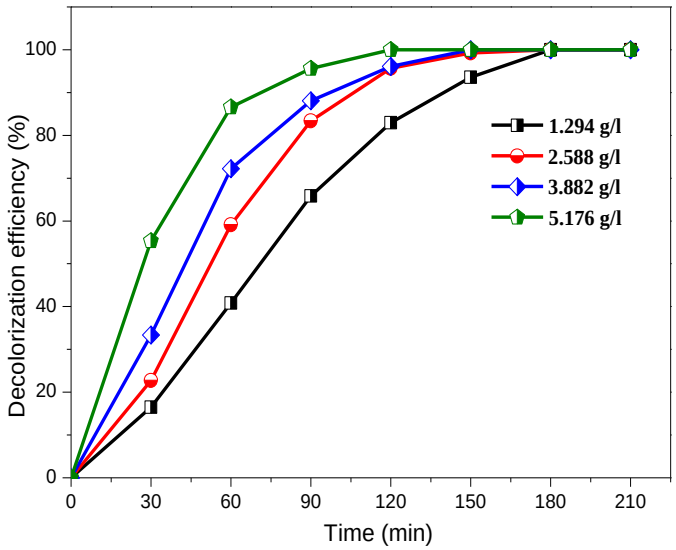

Figure III.8: Photocatalytic degradation of RG-12 at different catalyst loadings (RG-12 initial concentration: 2 mg/L; natural pH)

III.3.5. Effect of various oxidation processes for RG-12 degradation

To enhance the RG-12 degradation, H_2O_2 was added during the removal process. **Figure III.9** shows that no RG-12 degradation was observed by photolysis, while in the presence of H_2O_2, 51.5% RG-12 removal was observed within 135 min.

The effect of hydrogen peroxide concentration on the TiO_2 photocatalytic RG-12 degradation was carried out by varying the molar ratio $R=[H_2O_2]_0/[RG\ 12]_0$ from 0 to 40, with $[RG\ 12]_0$ = 1.09 mmol and a TiO_2 loading of 2.59 g/L. It is readily seen that until a molar ratio R of 20, the presence of H_2O_2 inhibited the photocatalytic process, while an obvious positive impact of H_2O_2 on the catalyst activity can be observed for R values in the range 20–30. An increase of R beyond 30 led to decreasing the RG-12 degradation efficiency. It has been recently reported that photo-activated TiO_2 and doped-TiO_2 led to photocatalytic activity under anaerobic conditions. This was attributed to the valence band hole (h^+) oxidative potential leading to organic molecules degradation as recently reported (Baghriche et al., 2013; Rtimi, 2016; Rtimi et al., 2016).

At high peroxide concentrations, the following reactions illustrated in **Eq. III.9-III.10** occur (Neppolian et al., 2003; Wang and Hong, 1999):

$$H_2O_2 + {}^{\bullet}OH \rightarrow H_2O + HO_2^{\bullet} \qquad \text{(III.9)}$$

$$HO_2^{\bullet} + {}^{\bullet}OH \rightarrow H_2O + O_2 \qquad \text{(III.10)}$$

The latter reactions inhibited the kinetic of photo-degradation by consumption of the two important and necessary radicals •OH and HO_2• (Qourzal et al., 2007).

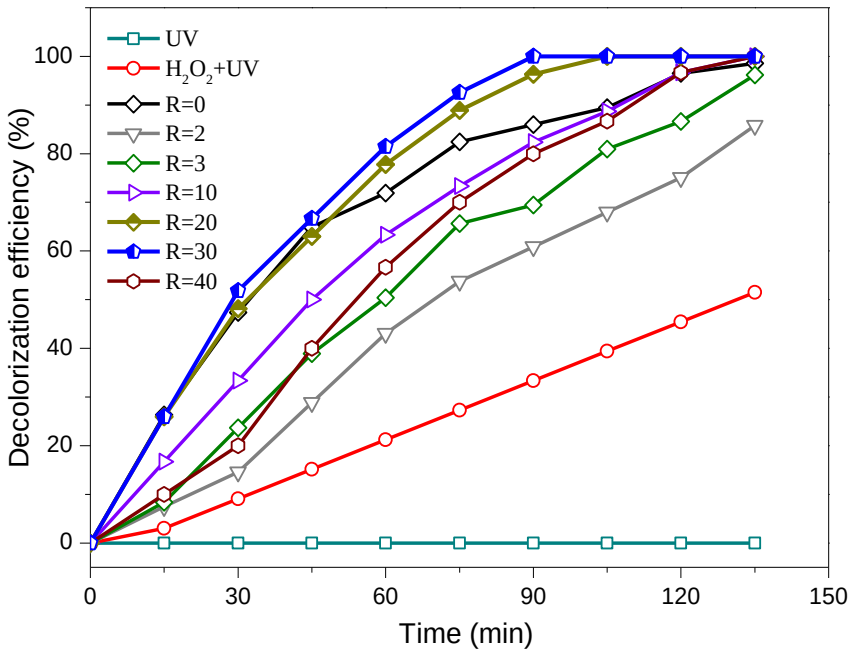

Figure III.9: Photocatalytic degradation of RG-12 at different $[H_2O_2]_0/[RG\ 12]_0$ molar ratio (RG-12 initial concentration: 2 mg/L; catalyst dosage: 2.59 g/L; natural pH)

III.3.6. Dye degradation kinetics

The rate value of pseudo-first-order (k_1) reaction could be determined from the slope of the straight-line plot of $\ln(C_o/C)$ vs. time as shown in **Figure III.10**. As shown by the high R^2 accuracy factor (**Table III.2**), the rate of pseudo-first-order reaction (*k1*) was found to increase inversely proportional to the dye concentration. This is quite common in photocatalytic degradation of dyes (Xu and Langford, 2000). The variation of k_1 with the initial concentration of RG-12 shows that the photocatalytic reaction was not strictly first-order, even though the plot linearity of $\ln(C_0/C)$ versus time is quite well (Bouzaza and Laplanche, 2002). Among the variety of kinetic models describing the photo-degradation reaction, Langmuir-Hinshelwood (L-H) model is the most widely used for dyes removal studies (Doll and Frimmel, 2004), because it involves the relation between radicals and substrate molecules in either absorbed or dissolved status (Konstantinou and Albanis, 2004). The L-H model can be simplified to the following expression (**Eq. III.11**):

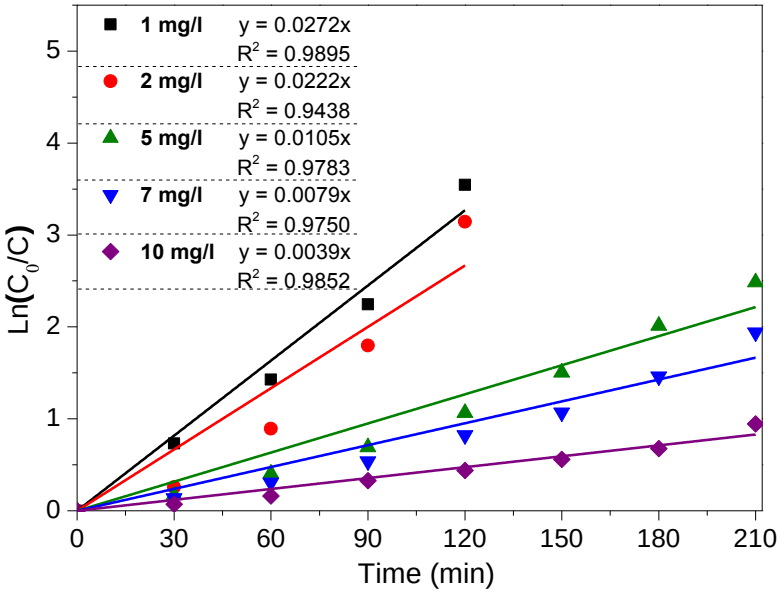

Figure III.10: Apparent first-order kinetics for RG-12 at different initial concentration (catalyst dosage: 2.588 g/L; natural pH)

Table III.2: Variation of the pseudo-first-order rate constant (k_1) at various initial concentration of RG-12 (C_0).

C_0 (mg/L)	k_1 (min^{-1})	R^2
1	0.0272	0.9895
2	0.0222	0.9438
5	0.0105	0.9783
7	0.0079	0.9750
10	0.0039	0.9852

$$\frac{1}{r_0} = \frac{1}{k} + \frac{1}{kK} \cdot \frac{1}{C_0} \qquad \text{(III.11)}$$

Where k denotes the reaction rate constant for the process (mg L^{-1} min^{-1}), K is the adsorption coefficient of reactants (L mg^{-1}), C_0 is the initial concentration of dye (mg/L) and r_0 is the initial rate of disappearance of dye (mg L^{-1} min^{-1}).

Figure III.11 shows the variation of RG-12 dye reciprocal initial concentration versus reciprocal of reaction rate, and their linear regression. The linear transform of this expression yielded k = 0.035 mg L^{-1} min^{-1} and K = 0.796 L mg^{-1}. Using the L-H model, Aboul-Gheit et al. (Xu and Langford, 2000) recently investigated the removal of Black B dye in the presence of two prepared nano-TiO_2 catalysts (A600 and A700); they found k = 0.83 and 0.34 (mg L^{-1} h^{-1}) and K = 0.02 and 0.03 (L mg^{-1}) for A600 and A700 catalysts, respectively (Aboul-Gheit et al., 2014). Moreover, Singh et al. found k = 1.78 mg L^{-1} min^{-1} and K = 0.06 L mg^{-1}, for Acid Red

dye degradation with activated carbon-TiO_2 composite (Singh et al., 2016). The obtained kinetic constant in our case appears therefore to be very low compared to the literature. This can be due to the molecular weight of the pollutant and thus the slow photocatalytic degradation pathway/ kinetics. Moreover, the low value of intensity UV lamp can explain this difference in L-H model constants.

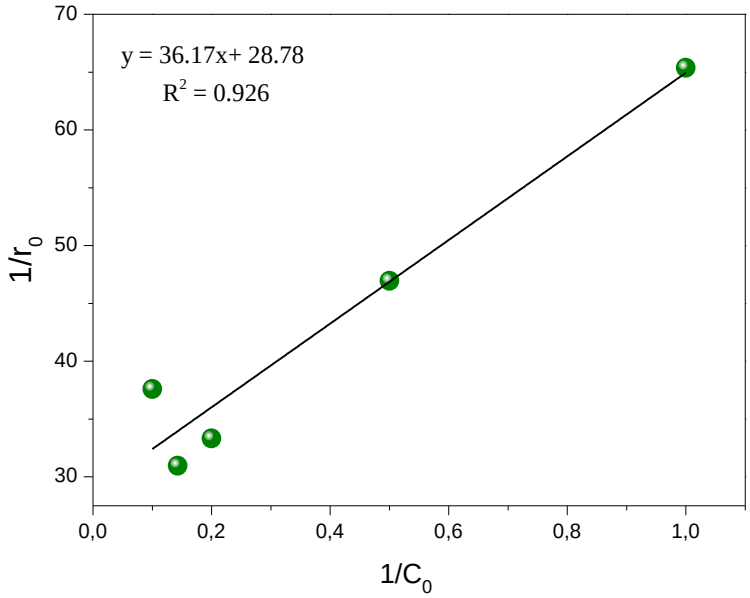

Figure III.11: Linear correlation of $1/r_0$ versus $1/C_0$

III.3.7. Recycling and photo-stability of the catalyst for decolorization of RG-12

In the perspective of an economical large-scale application, it is important to study the dependence of removal efficiency on the catalyst stability on long-term. The recycle degradation test was undertaken in order to evaluate the photocatalytic reusability, stability and reusability of the catalyst under the same conditions of pollutant concentration, catalyst dosage and light wavelength.

Figure III.12 shows that the removal efficiency of RG-12 on TiO_2 impregnated polyester was stable, showing total pollutant degradation within in 120 min for each cycle and after five consecutive experiments. The impregnated polyester fabrics were washed after each experiment to remove the byproducts before another cycle started. It has been shown by Nesic et al. that TiO_2- PES fabrics pretreated with UVC showed TiO_2 release below the tolerated concentration fixed by the WHO; and the level of Ti-release showed in their study was considered not to be cytotoxic to mammalian cells (Nesic et al., 2014).

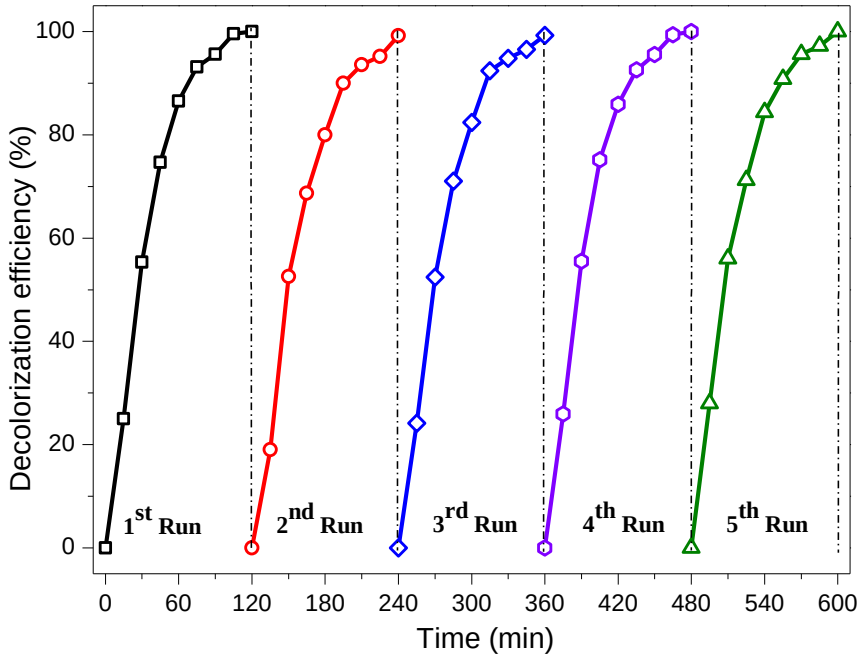

Figure III.12: Five recycling runs of the catalyst for Photocatalytic degradation of RG-12 (RG-12 initial concentration: 2 mg/L; catalyst dosage: 5.176 g/L; natural pH)

The prepared fabrics exhibited high stability showing their potential application for environmental remediation under light (Elfalleh et al., 2017). Recently, many studies reported on the visible light activated Titania (VLA-TiO_2) for pollutants degradation such as Cyanotoxins (Pelaez et al., 2009; Pelaez et al., 2012). Many mechanisms were proposed and some of them showed controversial interpretations (Dozzi et al., 2013; Serpone, 2006; Rtimi and Kiwi, 2017).

III.4. Conclusions

RF-Plasma and UV-C activated polyester were successfully prepared and led to the creation of surface polar groups. The TiO_2 impregnated on RF-Plasma activated polyester did not show fast photocatalytic activity for RG-12 dye removal contrary to UV-C activated polyester catalyst. This was attributed to the TiO_2 aggregation on the surface of RF-plasma activated polyester. TiO_2 impregnated on polyester active photocatalyst showed photo-catalytic degradation of RG-12 organic reactive dye under both UV and Visible light. The photocatalytic efficiency was found to be reliant significantly to initial concentration, catalyst quantity and light wavelength. Kinetics modelling of RG-12 dye removal was accurately fitted using the L-H model. The photo-catalyst showed excellent stability and preserved its photocatalytic activity for more than five reuse cycles. This latter observation opens potential industrial application justified by the good reusability and the TiO_2 adhesion on the polyester surface.

References

Aboul-Gheit A.K., El-Desouki D.S., El-Salamony R.A., 2014. Different outlet for preparing nano-TiO_2 catalysts for the photodegradation of Black B dye in water, Egypt. J. Pet. 23, 339–348.

Baghriche O., Rtimi S., Pulgarin C., Roussel C., Kiwi J., 2013. RF-plasma pretreatment of surfaces leading to TiO_2 coatings with improved optical absorption and OH-radical production, Appl. Catal. B: Environ. 130–131, 65–72.

Bouzaza A., Laplanche A., 2002. Photocatalytic degradation of toluene in the gas phase: comparative study of some TiO_2 supports, J. Photochem. Photobiol. A: Chem. 150, 207–212.

Cardoso N.F., Lima E.C., Calvete T., Pinto I.S., Amavisca C.V., Fernandes T.H.M., Pinto R. B., Alencar W.S., 2011. Application of aqai stalks as biosorbents for the removal of the dyes Reactive Black 5 and Reactive Orange 16 from aqueous solution, J. Chem. Eng. Data 56, 1857–1868.

Chen H.-K., Chen W.-F., Koshy P., Adabifiroozjaei E., Liu R., Sheppard L.R., Sorrell C.C., 2016. Effect of tungsten-doping on the properties and photocatalytic performance of titania thin films on glass substrates, J. Taiwan Inst. Chem. Eng. 67, 202–210.

de Lima R.O.A., Bazo A.P., Salvadori D.M.F., Rech C.M., Oliveira D.P., Umbuzeiro G.A., 2007. Mutagenic and carcinogenic potential of a textile azo dye processing plant effluent that impacts a drinking water sourceMutat, Res. Genet. Toxicol. Environ. Mutagen. 626, 53–60.

Doll T.E., Frimmel F.H., 2004. Kinetic study of photocatalytic degradation of carbamazepine, clofibric acid, iomeprol and iopromide assisted by different TiO_2 materials–determination of intermediates and reaction pathways, Water Res. 38, 955–964.

Donelli I., Freddi G., Nierstrasz V.A., Taddei P., 2010. Surface structure and properties of poly-(ethylene terephthalate) hydrolyzed by alkali and cutinase, Polym. Degrad. Stab. 95, 1542–1550.

Dozzi M.V., Selli E., 2013. Doping TiO_2 with p-block elements: effects on photocatalytic activity, J. Photochem. Photobiol. C: Photochem. Rev. 14, 13–28.

Elfalleh W., Assadi A.A., Bouzaza A., Wolbert D., Kiwi J., Rtimi S., 2017. Innovative and stable TiO_2 supported catalytic surfaces removing aldehydes under UV-light irradiation, J. Photochem. Photobiol. A: Chem. 343, 96–102.

Ghanbari M., Ansari F., Niasar M.S., 2017. Simple synthesis-controlled fabrication of thallium cadmium iodide nanostructures via a novel route and photocatalytic investigation in degradation of toxic dyes, Inorg. Chim. Acta 455, 88–97.

Klug H.P., Alexander L.E., 1974. X-ray Diffraction Procedures, Wiley, New York.

Konstantinou I.K., Albanis T.A., 2004. TiO_2-assisted photocatalytic degradation of azo dyes in aqueous solution: kinetic and mechanistic investigations, Appl. Catal. B 49, 1–14.

Kumawat R., Bhati I., Ameta R., 2012. Role of some metal ions in photogedradation of Rose Bengal dye, Indian J. Chem. Technol. 9, 191– 194.

Lee H.-S., Hur T., Kim S., Kim J.-H., Lee H.-I., 2003. Effects of pH and surface modification of TiO_2 with SiOx on the photocatalytic degradation of a pyrimidine derivative, Catal. Today 84, 173–180.

Lee S.-Li, Ho Li-N., Ong S.-A., Wong Y.-S., Voon C.-H., Khalik W.F., Yusoff N.A., Nordin N., 2017. A highly efficient immobilized ZnO/Zn photoanode for degradation of azo dye Reactive Green 19 in a photocatalytic fuel cell, Chemosphere 166, 118– 125.

Merkus H.G., 2009. Particle Size Measurements: Fundamentals, Practice, Quality, Springer, Berlin.

Nam W., Kim J., Han G., 2002. Photocatalytic oxidation of methyl orange in a three-phase fluidized bed reactor, Chemosphere 47, 1019–1024.

Naraginti S., Thejaswini T.V.L., Prabhakaran D., Sivakumar A., Satyanarayana V.S.V., 2015. Enhanced photo-catalytic activity of Sr and Ag co-doped TiO2 nanoparticles for the degradation of Direct Green-6 and Reactive Blue- 160 under UV & visible light, Spectrochim. Acta Part A 149, 571–579.

Neppolian B., Kanel S.R., Choi H.C., Shankar M.V., Arabindoo B., Murugesan V., 2003. Photocatalytic degradation of reactive yellow 17 dye in aqueous solution in the presence of TiO_2 with cement binder, Int. J. Photoenergy 5, 45–49.

Nesic J., Rtimi S., Laub D., Roglic G., Pulgarin C., Kiwi J., 2014. New evidence for TiO_2 uniform surfaces leading to complete bacterial reduction in the dark: critical issues, Colloids Surf. B : Biointerfaces 123, 593–599.

Pelaez A., De la cruz M., Stathatos E., Falaras P., Dionysios D.D., 2009. Visible light-activated N-Fcodoped TiO_2 nanoparticles for the photocatalytic degradation of microcystin-LR in water, Catal. Today 144, 19–25.

Pelaez M., Nolan N.T., Pillai S.C., Seery M.K., Falaras P., Kontos A.G., Dunlop P.S.M., Hamilton J.W.J., Byrne J.A., O'Shea K., Entezari M.H., Dionysiou D.D., 2012. A review on the visible light active titanium dioxide photocatalysts for environmental applications, Appl. Catal. B: Environ. 125, 331–349.

Qourzal S., Tamimi M., Assabbane A., Ait-Ichou Y., 2007. Influence de certains ions inorganiques, de l'éthanol et du peroxyde d'hydrogène sur la photominéralisation du b-naphtol en présence de TiO_2, C. R. Chimie 10, 1187–1194.

Rtimi S., 2016. Indoor light enhanced photocatalytic ultra-thin films on flexible non-heat resistant substrates reducing bacterial infection risks, Catalysts 7 (2017) 57.

Rtimi S., Giannakis S., Bensimon M., Pulgarin C., Sanjines R., Kiwi J., 2016. Supported TiO2 films deposited at different energies: implications of the surface compactness on the catalytic kinetics, Appl. Catal. B: Environ. 191, 42– 52.

Rtimi S., Kiwi J., 2017. Bactericide effects of transparent polyethylene photocatalytic films coated by oxides under visible light, Appl. Catal. B Environ. 213, 62–73.

Serpone N., 2006. Is the band gap of pristine TiO2 narrowed by anion- and cation-doping of titanium dioxide in second-generation photocatalysts? J. Phys. Chem. B 110, 24287.

Singh P., Vishnu M.C., Sharma K.K., Borthakur A., Srivastava P., Pal D.B., Tiwary D., Mishra P.K., 2016. Photocatalytic degradation of Acid Red dye stuff in the presence of activated carbon-TiO_2 composite and its kinetic enumeration, J. Water Process Eng. 12, 20–31.

Sudrajat H., Babel S., 2016. An innovative solar photoactive system N-WO3@polyester fabric for degradation of amaranth in a thin-film fixed-bed reactor, Sol. Energy Mater. Sol. Cells 149, 294–303.

Taborda A.V., Brusa M.A., Grela M.A., 2001. Photocatalytic degradation of phthalic acid on TiO2 nanoparticles, Appl. Catal. A: Gen. 208, 419–426.

Tang C., Chen V., 2004. The photocatalytic degradation of reactive black 5 using TiO2/UV in an annular photoreactor, Water Res. 38, 2775–2781.

Vidya C., Chandra Prabha M.N., Antony Raj M.A.L., 2016. Green mediated synthesis of zinc oxide nanoparticles for the photocatalytic degradation of Rose Bengal dye, Environ. Nanotechnol. Monit. Manage. 6, 134–138.

Vild A., Teixeira S., Kühn K., Cuniberti G., Sencadas V., 2016. Orthogonal experimental design of titanium dioxide-Poly(methyl methacrylate) electrospun nanocomposite membranes for photocatalytic applications, J. Environ. Chem. Eng. 4, 3151–3158.

Wang Y., Hong C.S., 1999. Effect of hydrogen peroxide, periodate and persulfate on photocatalysis of 2-chlorobiphenyl in aqueous TiO2 suspensions, Water Res. 33, 2031–2036.

Xu Y., Langford C.H., 2000. Variation of Langmuir adsorption constant determined for TiO2-photocatalyzed degradation of acetophenone under different light intensity, J. Photochem. Photobiol. A 133, 67–71.

Yola M.L., Eren T., Atar N., Wang S., 2014. Adsorptive and photocatalytic removal of reactive dyes by silver nanoparticle-colemanite ore waste, Chem. Eng. J. 242, 333–340.

Zeghioud H., Khellaf N., Djelal H., Amrane A., Bouhelassa M., 2016. Photocatalytic reactors dedicated to the degradation of hazardous organic pollutants: kinetics, mechanistic aspects and design–a review, Chem. Eng. Commun. 203, 1415–1431.

Zhang L., Tan P.Y., Lim C.K., Guo X., Tse M.S., Tan O.K., Chang V.W.C., 2016c. N–TiO_2–coated polyester filters for visible light—photocatalytic removal of gaseous toluene under static and dynamic flow conditions, J. Environ. Chem. Eng. 4, 357–364.

Zhang X., Shao C., Li X., Miao F., Wang K., Lu N., Liu Y., 2016b. 3D MoS_2 nanosheet/TiO_2 nanofiber heterostructures with enhanced photocatalytic activity under UV irradiation, J. Alloys Compd. 686, 137–144.

Zhang Y., Park M., Kim H.-Y., Park S.-J., 2016a. In-situ synthesis of grapheme oxide/ BiOCl heterostructured nanofibers for visible-light photocatalytic investigation, J. Alloys Compd. 686,106–114.

Zhu X., Feng X., Yuan C., Cao X., Li J., 2004. Photocatalytic degradation of pesticide pyridaben in suspension of TiO2: identification of intermediates and degradation pathways, J. Mol. Catal. A: Chem. 214, 293–300.

CHAPITRE IV: Prise en Compte et Rôle des Espèces Réactives et leur Contribution à L'élimination des Effluents Textiles par Photocatalyse sous Lumière UV et Visible : Dynamique et Mécanisme

---

Reactive Species Monitoring and their Contribution for Removal of Textile Effluent with Photocatalysis under UV and Visible Lights: Dynamics and Mechanism

Hichem ZEGHIOUD[1,2], Aymen Amine ASSADI[3], Nabila KHELLAF[1,2], Hayet DJELAL[4], Abdeltif AMRANE[3], Sami RTIMI[5]

En revision dans *Journal of Photochemistry and Photobiology A: Chemistry (Janvier 2018)*

[1] Department of Process Engineering, Faculty of Engineering, Badji Mokhtar University, P.O. Box 12, 23000 Annaba, Algeria
[2] Laboratory of Organic Synthesis-Modeling and Optimization of Chemical Processes, Badji Mokhtar University, P.O. Box 12, 23000 Annaba, Algeria
[3] Université de Rennes 1, ENSCR, CNRS, UMR 6226, Allée de Beaulieu, CS 50837, 35708 Rennes Cedex 7, France
[4] Ecole des Métiers de l'Environnement, Campus de Ker Lann, 35170 Bruz, France.
[5] Ecole Polytechnique Fédérale de Lausanne, EPFL-STI-LTP, Station 12, CH-1015 Lausanne, Switzerland.

Préambule

Dans cette partie, différents catalyseurs supportés ont été préparé en jouant sur le semiconducteur (TiO_2 et TiO_2 dopé avec Cu) et le support (polyester et cellulose). Les activités photocatalytiques ont été étudiées pour le traitement de la solution du colorant Vert Cibacron (RG-12) sous irradiation UV et visible à l'aide des trois catalyseurs ; TiO_2 dopé au Cu et TiO_2 imprégné (1) sur cellulose et (2) sur polyester activé par UV-C.

Les résultats obtenus ont révélé que le TiO_2 imprégné sur un polyester activé par UV-C présentait des performances prometteuses par rapport à l'autre catalyseur synthétisé. De plus, la dispersion des sites actifs sur le polyester prétraité par UV-C a été optimisée en testant deux configurations dans lesquelles le catalyseur est différemment dispersé. Dans le cas où le catalyseur est moins dispersé, la photodégradation a donné de bons résultats sous lumière UV et visible pour l'élimination du Vert Cibacron.

La dernière configuration choisie a été testé pour la dégradation de trois colorants textiles de même concentration molaire à savoir : le Reactive Green (RG 12), l'Ecarlate Solophényl (ES) et le Marine Cibanone (MC). Le RG 12 a été choisi comme polluant modèle pour la suite de l'étude à cause de son comportement vis-à-vis de la solubilité, l'adsorption, la dégradation et la désorption.

Le suivi du degré de minéralisation du RG 12 par le suivi du COT (Carbone Organique Totale) a permis de voir que la minéralisation est inversement proportionnelle à la concentration initiale du polluant. Ceci peut être expliqué par l'effet compétitif entre les sous-produits et la molécule mère vis-à-vis les sites actifs disponibles pour les fortes concentrations en polluant. Une dégradation totale a été enregistrée pour les concentrations 1 et 2 mg/L après 120 min. Ceci peut être expliqué par l'existence de deux phases dans l'élimination du polluant ; la première consiste en l'exploitation de la totalité des espèces réactives dans la fragmentation de la molécule mère en sous-produits jusqu'à la fin. Dans la deuxième phase, les espèces oxydantes générées transforment les sous-produits intermédiaires en CO_2, H_2O et autres minéraux.

Dans le but de simuler un cas plus au moins réel, des mélanges binaires de même concentrations molaire de RG 12 et ES ont été utilisés dans la photodégradation catalytique. Dans un système multi-composant, le rendement de décoloration dépend de la structure des molécules, leur taille et le nombre de sous-produits résultants. La présence du colorant ES a induit un effet inhibiteur sur la vitesse de décoloration du RG 12 à cause de l'effet compétitif entre les molécules de colorants vis-à-vis des sites actifs disponibles sur le catalyseur.

Le rôle et la contribution des espèces oxydantes réactives (EOR) : $^{\bullet}OH$, $O_2^{\bullet-}$ et h^+ ont été également examinés avec les catalyseurs à base de TiO_2 (imprégné sur polyester et sur cellulose) sous différentes sources de lumière. Les résultats obtenus ont montré que l'anion radicalaire superoxyde ($O_2^{\bullet-}$) jouait un rôle clé dans la dégradation photocatalytique du colorant RG 12 pour les deux catalyseurs supportés exposés à la lumière UV. Néanmoins, ces radicaux ($O_2^{\bullet-}$) ont changé de comportement en passant d'un effet promoteur à un effet inhibiteur lors du changement de la lumière. Les radicaux hydroxyles ($^{\bullet}OH$) ont joué un rôle primordial dans la dégradation photocatalytique du RG 12 sous irradiation visible.

Nomenclature

BET:	Brunauer, Emmett and Teller
DR-89:	Direct Red 89
EPT:	Electrical Percolation Threshold
NDIR:	Non-Dispersive Infra-Red
RF:	Radio Frequency
RG-12:	Reactive Green 12
ROS:	Reactive Oxygen Species
TOC:	Total organic Carbon
UV:	Ultra Violat
VB-20:	Vat Blue 20

Abstract

In this study, the photocatalytic activities were investigated for the treatment of Reactive Green 12 (RG-12) solution under UV and visible irradiation using Cu doped TiO_2, and TiO_2 impregnated on (1) cellulose and (2) UV-C activated polyester catalysts. The obtained results revealed that TiO_2 impregnated on UV-C activated polyester showed promising performances compared to the other synthesized catalysts. Moreover, the dispersion of active sites on UV-C pretreated polyester was optimized and tested for RG-12 removal in the binary mixture; the presence of Direct Red 89 (DR-89) dye had an inhibiting effect on the rate of RG-12 decolorization process because of the competitive effect between dye molecules toward the available active sites. The role and contribution of reactive oxidizing species (ROS): $^{\bullet}OH$, $O_2^{\bullet-}$and h^+ was also examined with the three catalysts under different light sources; it was found that the superoxide radical anion played the key role in RG-12 photocatalytic degradation for

both TiO_2 supported catalysts. Nevertheless, the behavior of $O_2^{\bullet-}$ radicals was found to be changed from promoting effect to inhibitory effect when changing light from UV to visible.

Keywords: Photocatalytic surface, Pollutant degradation, Batch reactor, Radical scavengers, Dye mixture, Visible light.

IV.1. Introduction

It is well known that heterogeneous photocatalysis is based on the study of the relationship between a solid semiconductor and light in fluid environment. The illumination of catalyst surface leads to an excitation of electrons by absorption of photons energy in the valence band, which drives them to move into the conduction band leaving behind a positive hole (h^+) (Rtimi et al., 2017). Many efforts have been made by researchers to facilitate this shifting and limit the e^-/h^+ recombination rate.

A diversity of investigations focused on using different semiconductors (TiO_2, ZnO, CeO_2, CdS…) in order to find the most profitable and efficient photocatalyst (Kandiel et al., 216; Wang et al., 2016; Kim et al., 2016; Li et al., 2016). To enhance the activity under UV and/or visible light of these latter, many metal-oxide photocatalyst composites and complexes were elaborated and tested such as Metal-HQS complex-TiO_2 nanocomposites (Huang et al., 2016), Ternary ZnO/AgI/Ag_2CO_3 nanocomposites (Golzad-Nonakaran and Habibi-Yangjeh, 2016), CeO_2/$Bi_4Ti_3O_{12}$ composite (Liu et al., 2016), ternary CdS/MoS_2/MWCNTs hybrid photocatalysts (Jo and Sagaya Selvam., 2016) and CeO_2/TiO_2 nanotube…etc. (Lu et al., 2016). Some workers consider another way to promote the photocatalytic activity; by introducing localized states above the valence band with the help of doping elements like N, C, Cu, Cr and S, etc. (Zeghioud et al., 2016; Koh et al., 2017; Pham et al., 2015).The subsequent photocatalytic process was in the majority of the cases due to a synergetic effect between the dopant oxidation states and the electrons transferred from the treated solution toward TiO_2 particles (Pérez-Larios et al., 2016), the reduction in the band gap energy and the inhibition in electrons-holes recombination (Koh et al., 2017) and the enhancement of hydrophilicity (Pham et al., 2015). Nevertheless, to achieve an excellent photocatalytic activity with doped catalyst, the ratio of dopant must be optimized (Bhatia et al., 2016; Sutka et al., 2016).

From an economic point of view, it is essential to find a visible and/or solar light active photocatalyst (Golzad-Nonakaran and Habibi-Yangjeh., 2016; Rtimi et al., 2015; Zhu et al., 2016; Borges et al., 2016) for future extrapolation to industrial scale. Many oxidants can be used if there is a need to improve the activity of these catalysts such as O_2, H_2O_2 and $K_2S_2O_8$ (Neppolian et al., 2003; Faramarzpour et al., 2009; Gupta et al., 2012).

The current trend in photocatalysis development is to: i) control the radicals and reactive oxidizing species (ROS) generated during the activation process like $^{\bullet}OH$, $O_2^{\bullet-}$, h^+ and $H^{\bullet}$ and ii) to favor the conditions for ROS to promote the catalytic effect and at the same time preventing and/or to limit the effect of inhibitory species (Rodríguez et al., 2015; Ismail et al., 2016; Villa et al., 2015).

In this paper, three persistent industrial organic textile dyes (Reactive Green 12, Direct Red 89 and Vat Bleu 20) were chosen as target pollutants in textile wastewater. In this aim, to enhance the photocatalytic decolorization/degradation under different light sources, three different photocatalysts were investigated in terms of degradation and mineralization of the three dyes and their mixture.

Moreover, a special attention was paid to understand the contribution of actives species such as $^{\bullet}OH$, $O_2^{\bullet-}$ and h^+, using several scavengers in different operating conditions.

IV.2. Experimental

IV.2.1. Materials

Potassium dichromate (>99 wt. %, Carlo Erba), Ethylene diamine tetra-acetic acid (>99 wt.%, Prolabo), 2-Propanol (>99.5%, Sigma-Aldrich) were used without further purification. The aqueous solutions were prepared using ultra-pure quality of water with a resistance of 15.0 MΩ cm. All dyes were used as received. The chemical structures are presented in **Figure IV.1** and some physicochemical properties of the studied textile dyes are summarized in **Table IV.1**.

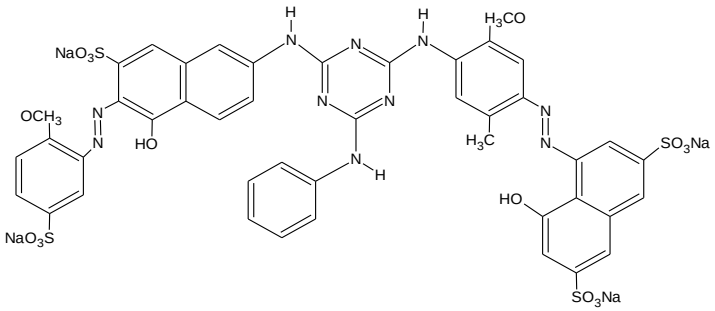

(a)

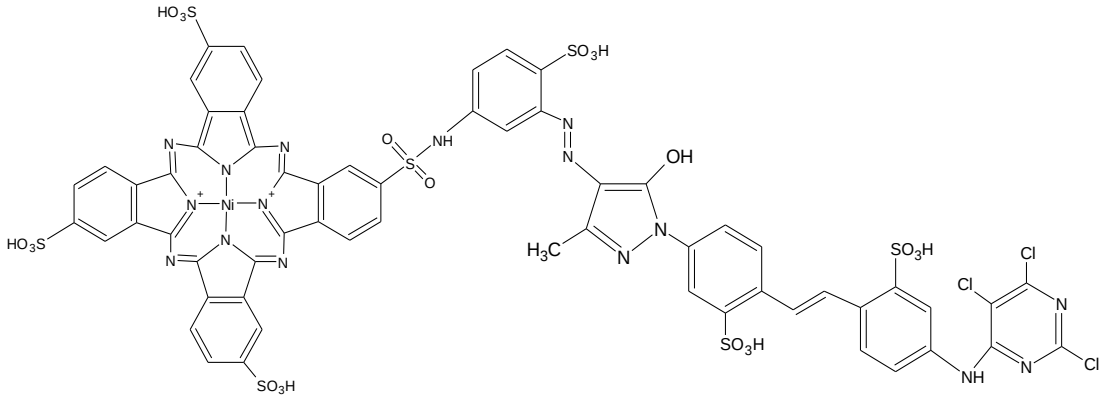

(b)

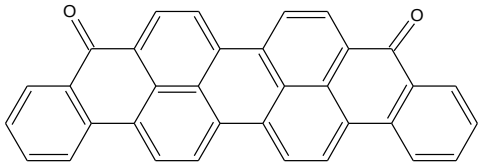

(C)

Figure IV.1: Chemical structures of: **(a)** DR-89; **(b)** RG-12 and **(c)** VB-20

Table IV.1: Physicochemical properties of the studied textile dyes

Property	Vat Blue 20 (VB-20)	Direct Red 89 (DR-89)	Reactive Green 12 (RG-12)
Empirical formula	$C_{34}H_{16}O_2$	$C_{44}H_{22}N_{10}Na_4O_{16}S_4$	$C_{60}H_{29}Cl_3N_{16}NiO_{21}S.6Na$
Molecular weight (g/mol)	456	1372	1837
λ_{max} (nm)	580	494	615
pH (50 mg/L in H_2O)	7.60	7.10	6.90

IV.2.2. Catalysts preparation

a) TiO_2 impregnated on UV-C activated polyester

The polyester used corresponds to the polyester Dacron, type 54 spun, plain weave ISO 105-F04 (Baghriche et al., 2013). Due to low surface energy, polymer fabrics (polyester, polyethylene...) exhibit low ability to bind inorganics. Some research groups recently reported on the polyester surface pretreatment leading to the formation of polar groups facilitating the TiO_2 binding to the surface (Baghriche et al., 2013; Rtimi et al., 2014). High-energy photons (commonly UVC light) and Radio Frequency plasma (RF-plasma) were used to this end as recently reported (Rtimi et al., 2014).

In UV-C pretreatment process, the light excitation at 185 nm does not have enough energy content to produce cationic O^+ and anionic oxygen O^- species contrarily to RF-Plasma treatment of textiles. This light only leads to excited O*: $O_2 + UVC \rightarrow 2O^*$. The optical absorption between the light and the textile positioned at 3 mm of the light source at 1 atm of air is very low since εO_2 (185 nm) = 2.6 M^{-1} cm^{-1} and εN_2 (185 nm) = 0.3 M^{-1} cm^{-1} at 185 nm. From a practical point of view, we can say that no photons are lost in the optical pathway between the light source and the sample (Rtimi et al., 2014). Polyester fabrics pretreated by UVC introduced surface activation more evenly distributed than pretreatment with RF-plasma. Vacuum-UVC light radiant energy at 185 nm is higher than 495 kJ/mol, the energy required for the reaction $O_2 \rightarrow 2O^*$. The absence of cationic or anionic oxygen leads to more uniform distribution of active sites on the polyester surface.

A TiO_2 colloïdal suspension was prepared by dissolving titanium tetra-isopropoxide (TTIP, Sigma Aldrich) in isopropanol in a 1:13 molar ratio. The formed solution was poured into a beaker with 50 mL of 0.1M HNO_3. The sheets of polyester samples of 10cmx10cm of dimension were immersed into the acid TiO_2 precursor suspension and heated at 80 °C during 120 min under continuous magnetic stirring in a reflux condenser. The polyester prepared was removed and rinsed by DI-H_2O. To eliminate the unbounded TiO_2 particles an ultrasound bath treatment was needed.

b) Cu doped TiO_2 impregnated polyester

$Cu(NO_3)_2$ and TiO_2 (P25 aerosol, Evonik) were dissolved in distilled water to obtain a certain concentration suspension, $Cu(NO_3)_2$ was used as Cu precursor. The concentration of TiO_2 in the suspension was 5 g/L, the molar ratio of Cu was 0.2%. After stirred for 4h, small amount of methanol was added into the beaker as sacrificial agent. Then, the polyester fabrics were impregnated in a covered beaker. The system was then purged in N_2 for 30 min to remove O_2 in the suspension. Then the system was illuminated under solar simulated light for 120 min to photo-corrode the textile leading to more TiO_2-Cu binding to the surface. Then, the impregnated polyester fabrics were removed and rinsed 3 times with DI-H_2O and put in incubator at 110 °C overnight. The films were gently washed with de-ionized water before use.

c) TiO_2 impregnated on cellulose fibers

The photocatalytic media provided by Ahlstrom Company, under reference Alhström 1048, is a non-woven textile composed of cellulose fibers coated with a mix of catalysts (TiO_2 Millennium PC 500,), zeolite and silica and their mass per square meter are 16.5, 3.4 and 13.3

g/m^2, respectively. The BET surface area of the TiO_2 was measured by N_2 adsorption and was found equal to 317 m^2/ g. The thickness of the catalyst layer is equal to 250 µm. The median diameter of deposited pellets on the medium is 1.4 µm.

d) UV-Vis Pollutant analysis and Total Organic Carbon (TOC) measurement

The UV-vis spectra of all samples were recorded using a Varian Cary®50 UV-vis Spectrophotometer; the spectra were obtained at the wavelength range of 200–800 nm.
TOC was measured by TOC-$V_{CPH/CPG}$ Total Organic Analyzer Schimadzu. The combustion and conversion of Organic Carbon compounds resulted in obtaining CO_2, which was identified by non-dispersive Infra-Red Detector (NDIR).

IV.2.3. Photocatalytic experiments

For all experiments the photocatalytic removal of dyes with different synthetic catalysts was followed by the investigation of the degradation of 500 mL of dyes solution in Schott Duran glass reactor under magnetic stirring. In the case of UV irradiation, a 9-Watt UV Philips Bulb lamp emitting a UV-vis light (λ=365 nm). An S G23 9W (840) lamp (Sylvania) was used as a visible-light source for the catalyst activity examination under visible-light. Each lamp is placed in the center of the glass cell, yielding an irradiation intensity of 20 W/m^2 as detected with a Radiometer (VLX- 3W equipped with a sensor CX 365, ALYS Technologies, Switzerland). Before each experiment, the solution was stirred in the dark for 30 min to establish adsorption–desorption equilibrium in the system before the lamp illumination. Samples of 3 ml taken at regular time intervals were analyzed with the help of a UV–vis spectrophotometer to monitor the kinetics progression of the catalytic process.
The decolorization efficiency (%) of dyes solution can be calculated according to **Eq. IV.1**.

$$\eta(\%) = \left(\frac{C_0 - C_t}{C_0}\right) \times 100 = \left(\frac{A_0 - A_t}{A_0}\right) \times 100 \qquad \text{(IV.1)}$$

Where A_0 and A_t are the initial intensity of the absorbance peak at λ_{max} of each studied dye and the intensity of the absorbance peak at a given time t, respectively.
The removal rate of the dyes was calculated according to **Eq. IV.2**.

$$rate = \left(\frac{C_0 - C_t}{t}\right) = \frac{\eta(\%) \times C_0}{100 \times t} \qquad \text{(IV.2)}$$

IV.3. Results and discussion

Different operating conditions can influence the dye removal on a photocatalytic surface, such as photocatalyst nature, support and uniformity of the dispersion. The initial pollutant concentration in mono-compounds and/or in mixture can drastically affect the process performance. These parameters will be investigated in details in the next sections.

IV.3.1. Photo-enhanced activity of the three supported photocatalysts

The activity of different supported catalysts in the degradation of 2 mg/L of RG-12 was examined under both UV and visible light. As shown in the **Figure IV.2a**, the TiO_2 impregnated on cellulose and the Cu doped TiO_2 impregnated on textile were active under UV light while no activity was recorded under visible light. On the other hand, the TiO_2 impregnated on UV-C activated/pre-treated polyester showed significant RG-12 decolorization under both UV and visible lights. Under visible light, TiO_2 impregnated polyester (UVC pre-treated) shows fast decolorization kinetics up to 60 min, then the kinetics slow down due to the surface saturation. This can also be due to the accumulation of the dye degradation by-products prior to their mineralization as shown in trace 3.

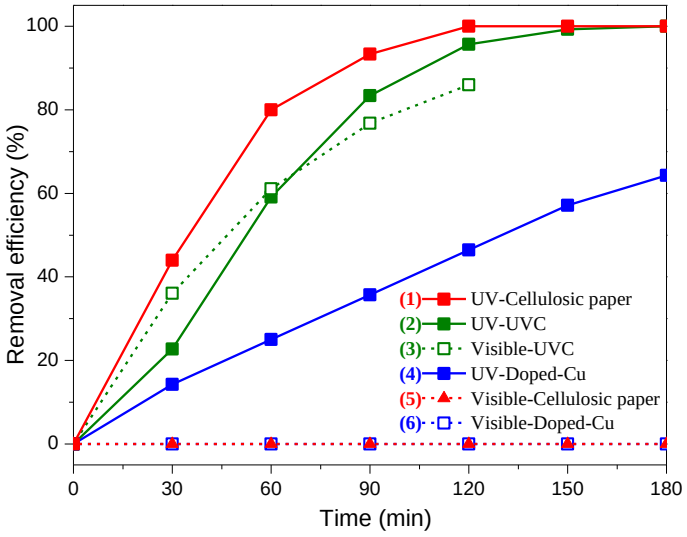

Figure IV.2a: Photocatalytic degradation of RG-12 with various catalysts under UV and visible lights (initial concentration: 2 mg/L; natural pH): (1) TiO_2 impregnated on cellulose under UV, (2) TiO_2 impregnated on polyester under UV, (3) TiO_2 impregnated on polyester under visible, (4) Cu doped TiO_2 impregnated polyester under UV, (5) TiO_2 impregnated on cellulose under visible and (6) Cu doped TiO_2 impregnated polyester under visible

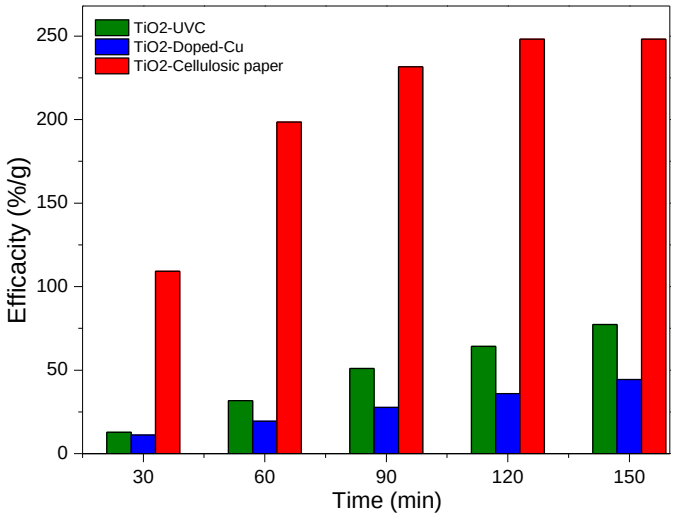

Figure IV.2b: Degradation efficiency time-courses of various catalysts for RG-12 decolorization under UV light (initial concentration: 2 mg/L; natural pH)

For a more significant comparison, time-courses of the activity of each catalyst related to the mass unit under UV light are displayed in **Figure IV.2b**. The figure shows that TiO_2 impregnated on cellulose had the highest photocatalytic activity under UV light, its efficiency reached 248.1%/g; while the Cu doped TiO_2 was the less active photocatalyst with 44.3%/g efficiency. However, in the case of TiO_2 impregnated on UV-C activated polyester photocatalyst, the efficiency reached 77.3%/g under UV light and 66.5%/g under visible light. These differences in the photocatalytic activities can be attributed to the method of preparation of the catalysts and the activation of the supports. Indeed, at the light of these results the TiO_2 impregnated on UV-C activated polyester was selected for the subsequent experiments as the most profitable photocatalyst in this study.

IV.3.2. Effect of TiO_2 dispersion

In the aim of optimizing the photocatalytic activity of the catalyst, two dispersion modes of TiO_2 on the support were tested. In each case, the same amount of TiO_2 was dispersed on one or two sheets of polyester (sheet dimension 10cmx10cm). It can be first noted that when the amount of TiO_2 was dispersed on two sheets, no photocatalytic activity was obtained under visible light. Nevertheless, a slight activity under UV light was noted, i.e. 12.3% dye removal in 210 min of irradiation (**Figure IV.3**). However, when the same amount of TiO_2 was dispersed only on one sheet (Sheet concentrated with TiO_2), 23.5% (in 210 minutes) and 100% (in 180 minutes) of RG 12 was degraded under visible and UV light, respectively (**Figure IV.3**).

This trend can be explained by the fact that the dispersed active site on the polyester sheet may be similar to the case of extrinsically conducting polymers, where the electrons require certain

concentration of inclusions (carbon fibres for example) in polymeric matrix known as Electrical Percolation Threshold (EPT) to enable them to move from one particle of inclusion to another (Wang et al., 2016). In the case of visible light, the excited electrons have only low energy, which makes difficult the exchange between the semiconductor particles and leads to less reactive oxidizing species.

It seems that at low concentration, TiO_2 dispersion penetrates inside the polyester fibers and become non-accessible for light hence are not active to generate ROS. Hence, saturating the polyester with TiO_2 titanium on a single sheet is more effective than putting a single layer on each sheet. This could be explained by the fact that the photocatalytic support is so porous that the titanium oxides of a layer are trapped into the pores and are not subsequently accessible. Thus, a supplementary layer is needed in order to enhance the availability of active sites.

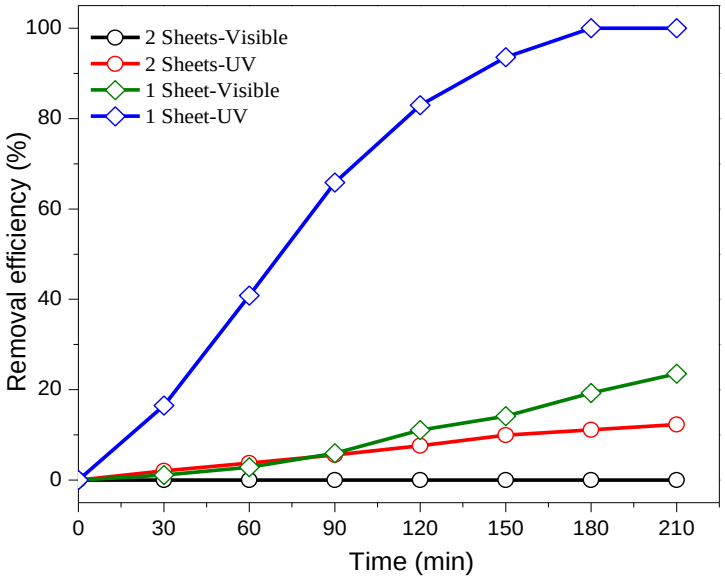

Figure IV.3: Photocatalytic degradation of RG-12 for two different dispersion modes of TiO_2 on polyester under UV and visible lights (initial concentration: 2 mg/L; UVC catalyst dosage: 1.29 g/L; natural pH)

IV.3.3. Degradation of three textile dyes in mono-compenent system (VB-20, RG-12, DR-89).

Based on the finding on RG12 degradation previously shown, we chose to pursue our investigation using TiO_2 impregnated on UV-C activated polyester active under UV and visible light irradiation. **Figure IV.4** shows the removal efficiency of different recalcitrant textile dyes (VB-20, RG-12, DR-89) as a function of time. As shown in **Figure IV.4**, the VB-20 dye was fully removed within 60 min followed by RG-12 dye in 180 min. However, only 90.9% of DR-

89 dye was degraded within 210 min. The quick degradation of VB-20 dye can be explained by a small molecule size which facilitated the mass transfer and the adsorption on the catalyst surface.

The DR-89 dye showed better adsorption on the catalyst surface than RG-12 (data not shown in this study). However, its degradation rate was the lower than RG-12. This can be attributed to the two azo groups in the chemical structure, as well to more of hydroxyl and amide groups, which make the molecule more stable compared to RG-12 having only one azo group. Consequently, and owing to the difficult desorption of DR-89 from the catalyst surface (data not shown in this study), the RG-12 dye was taken as a molecule model for the subsequent stages of the present work.

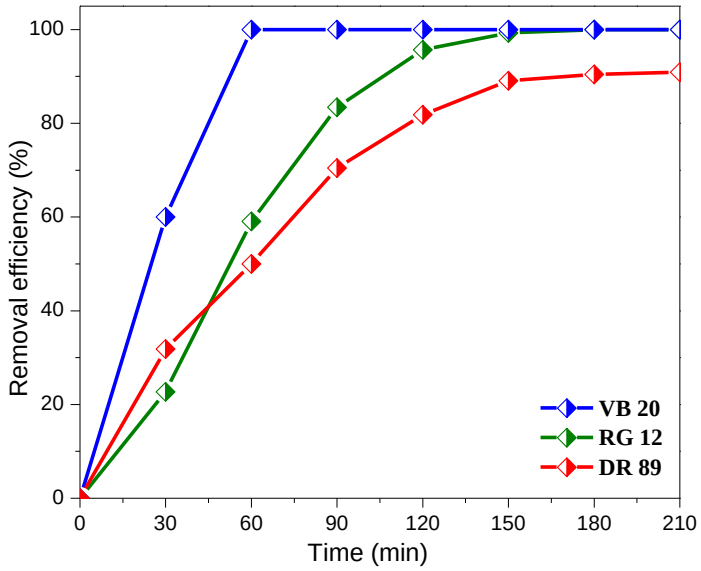

Figure IV.4: Photocatalytic degradation of dyes at the same molar initial concentration, 1.09 µmol/L (catalyst dosage: 2.58 g/L; natural pH)

IV.3.4. Mineralization of RG-12 in mono-compound system

It is well known that the degradation yield is not the sole criterion to be considered to judge about the performance of a photocatalyst for the treatment of hazardous organic pollutants, because of the probability of by-product toxicity resulting from the photocatalytic oxidation. The mineralization efficiency *vs* the initial concentration of RG-12 was therefore examined following the Total Organic Carbon (TOC) resulting from the photocatalytic mineralization of the dye as shown in **Figure IV.5**.

It can be readily seen from **Figure IV.5** that after 210 min, the mineralization of dye molecules was nearly complete with the UV-C-pretreated catalyst for 1 and 2 mg/L of RG 12 initial concentrations. This result may be clarified by the photocatalytic decolorization of dye

molecules until 100% value of removal efficiency (approximately within 120 min) as a priority step; then the by-products were converted until the final state under the forms of CO_2, H_2O and other minerals. For initial concentrations up to 2 mg/L the majority of the photo-generated ROS were consumed in the degradation step of the molecules and only few percentages were involved in the mineralization step. Moreover, Kouloumbos et al. (2003) also observed during the first minutes of irradiation that 70% of the initial concentration of diazinon was converted into intermediates compounds while the recovery of CO_2 during this time was negligible. Thereafter none of these products was detected after 30 min of irradiation.

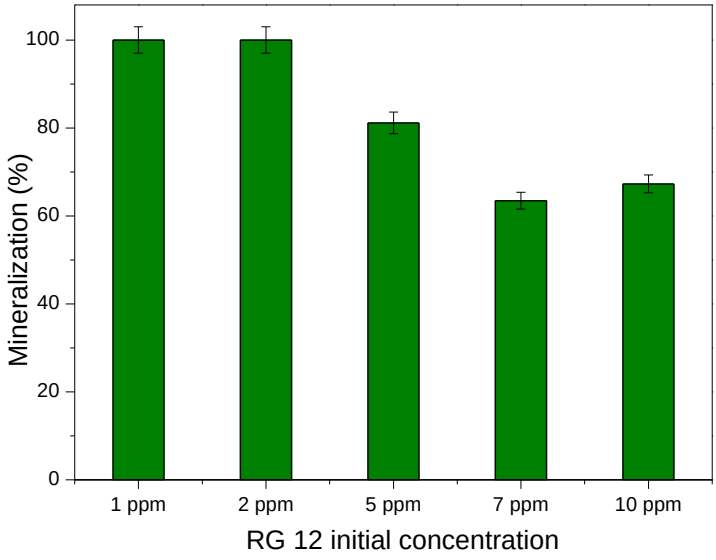

Figure IV.5: Mineralization vs initial concentration of RG-12 removal under UV light (UV-C catalyst dosage: 5.18 g/L; time of photocatalysis: 210 min; natural pH)

The photocatalytic oxidation scheme of each pollutant consists of the simultaneous carboxylic function removal and new function carried on a 'n-1' carbon molecule. That degradation pathway in series leads to a complete mineralization of the pollutant (Assadi et al., 2012). This seems that the intermediates by products of RG-12 were easily photocatalytic degraded.

We note (**Figure IV.5**) that when the inlet concentration of RG-12 increases, the % of mineralization decreases. This means that the quantity of the intermediate by-products generated is more important. So, the increase of the inlet concentration leads to a lower availability of the active sites. Assuming that the photocatalytic process is a series of successive reactions, the competition toward the active sites of the catalyst becomes more important. So, the by-products formed cannot be degraded. This result is similar to what has been observed in the literature, for example in the work of Assadi et al. (2012) and Stephan et al. (2011).

IV.3.5. Competitive effect in binary system (RG-12 + DR-89)

In this part of the study different molar ratios of dyes (r= $[RG\text{-}12]_0/[DR\text{-}89]_0$) were considered, taking into account that the catalyst surface received the same molar quantity of pollution for each ratio ($[RG\text{-}12]_0 + [DR\text{-}89]_0$=Cst). The corresponding results are displayed in **Figure IV.6**. Increasing the initial concentration of DR-89 improved the rate and the efficiency of decolorization owing to the increasing amount of dye molecules adsorbed on the catalyst surface per time unit. Removal efficiency showed a minimum value for r=1; the decrease observed for increasing ratio from 0.33 to 1 can be attributed to the competitive effect for adsorption of dyes on the catalyst surface and the better interaction between DR-89 and the catalyst, as discussed in the section IV.3.3 (Assadi et al., 2012). The increase in the decolorization efficiency for ratios above 1 can be attributed to the existence of mass transfer limitations due to the higher amount of RG-12 molecules if compared to DR-89.

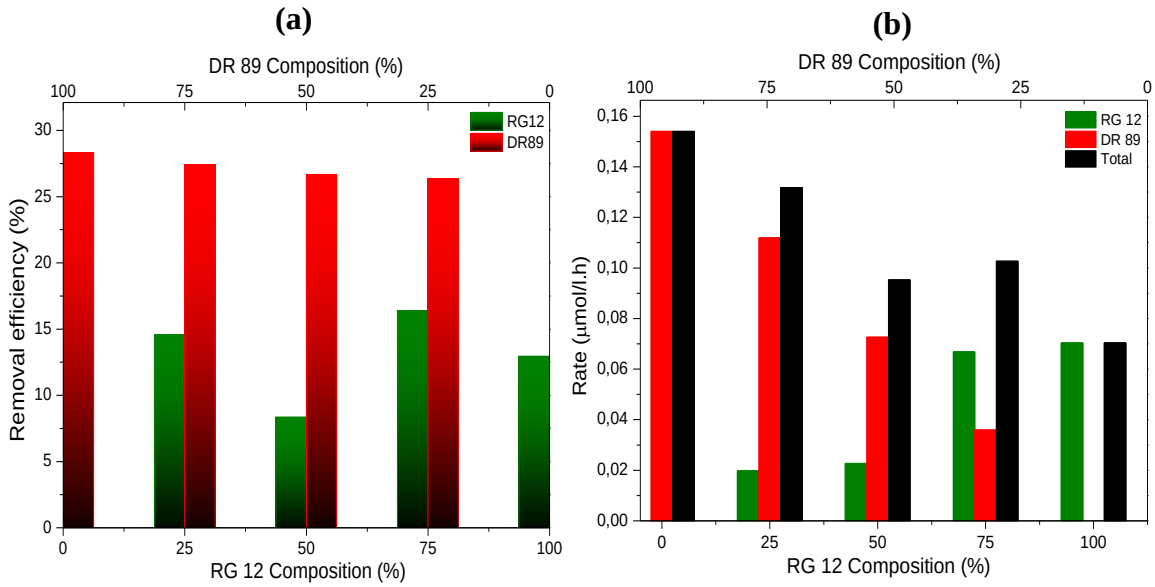

Figure IV.6: Removal efficiency **(a)** and photocatalytic degradation rates **(b)** of RG-12 and DR-89 and at different $[RG\text{-}12]_0/[DR\text{-}89]_0$ ratio and for the same quantity of pollution under visible light ($[RG\text{-}12]_0+[DR\text{-}89]_0$=2.18 µmol/L; UV-C catalyst dosage: 2.58 g/L; natural pH)

Nevertheless, for composition interval [75-100%], the removal efficiency of RG-12 increases when going from pure RG-12 solution to a mixture solution and *vice-versa* when it comes to DR-89. Regti et al. (2016) explained this trend in binary mixture of Basic Blue 41 (BB41) and Basic Yellow 28 (BY28) by the fact that BB41 attraction to the interfaces is stronger than that of BY28 and that the presence of both dyes in solution enhance a competitive adsorption in the system (Baghriche et al., 2017).

In addition, the decolorization efficiency of RG-12 in pure solution was less than in r=3 multicomponent system, this result can be attributed to molecular structure (Daifullah and Mohamed, 2004), and molecular size which leads to very high number of decolorization by-products. Meanwhile these last enter into competition with RG-12 molecules against the available active sites, similar results were recently reported by Abou Saoud et al. (2017).

As shown in the **Figure IV.6b** the rate of decolorization of RG-12 increased with increasing dye concentration in binary system. When it is clear that RG-12 is slightly better degraded in a monocomponent system than multicomponent system whereas very significant differences is observed for DR-89, similar result was found for the degradation of Butyraldehyde (Buty) and dimethyl disulphide (DMDS) in binary mixture (Abou Saoud et al., 2017).

IV.3.6. Species scavenger's investigations

In order to understand the contribution of reactive oxidizing species in the removal of RG-12, a number of experiments were carried out for different photocatalysts and different types of light sources in the presence of different radical scavengers such as *iso*-propyl alcohol for $^{\bullet}OH$ radicals (Zsilák et al., 2014), EDTA for h^{+} (Wang et al., 2016), and potassium dichromate for $O_2^{\bullet-}$ (Zhao et al., 2017). The effect of the addition of these various radical scavengers on the photocatalytic phenomenon of RG-12 was then studied.

a) ROS Scavengers under UV light

It should be noted that in the case of UV-C polyester catalyst and before each radical scavenger experiment, the catalyst was washed under magnetic sttiring using ultra-pure water for one hour repeated three times. Contrarily, for TiO_2/cellulose catalyst, a new and similar sheet was used for each experiment (**Figure IV.7**).

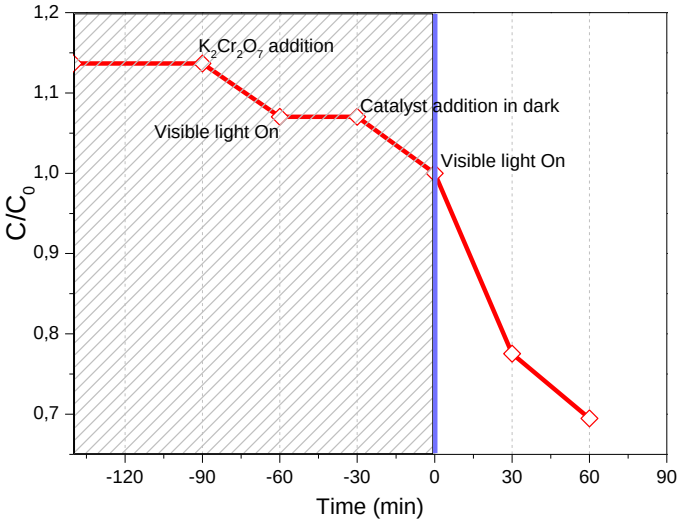

Figure IV.7: Example of the different steps for $O_2^{\bullet-}$ scavenger experiments for RG-12 degradation under visible light (initial concentration: 2 mg/L; UV-C catalyst dosage: 1.29 g/L; natural pH)

- **h^+ scavengers**

EDTA was used as scavengers to probe the creation and the role of photo-generated hole (h^+) throughout RG-12 photocatalytic degradation. While 50 mg of EDTA was added to 500 mL of pollutant solution, a quick reaction with the holes occurred, leading to reduce strongly the photocatalytic removal efficiency from 100% to 53.3% within 180 min as shown in **Figure IV.8a**.

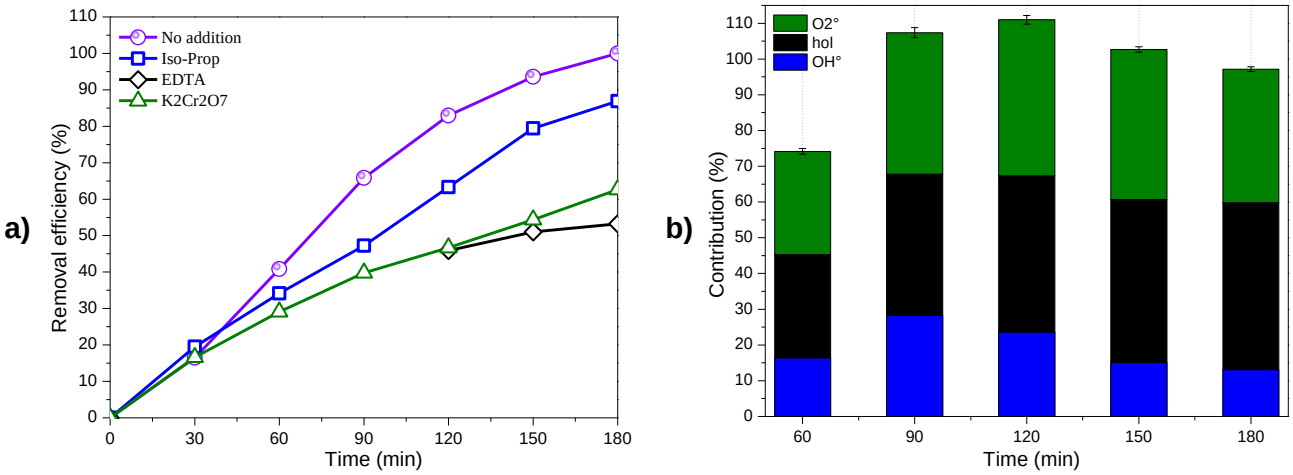

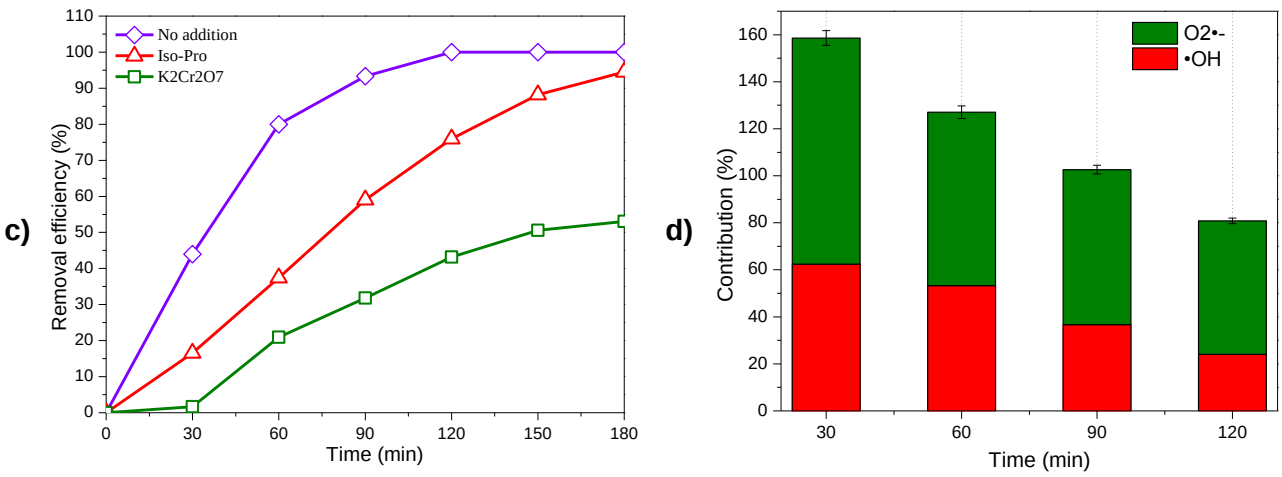

Figure IV.8: Effect of diverse additives (**a & c**) and contribution of various actives species (**b and d**) on RG-12 removal efficiency using UV-C polyester (a and b) and TiO_2/cellulosic paper (c & d) catalysts under UV light (initial concentration: 2 mg/L; catalyst dosage: 0.4 g/L; natural pH)

Wang et al. (2016) have reported that the use of EDTA as holes' scavenger resulted in a small decrease of the removal efficiency of triclocarban. The obtained results can be clarified by the following reactions:

$$h^+ + H_2O \rightarrow HO^\bullet + H^+ \quad \text{(IV.3)}$$

$$h^+ + OH^- \rightarrow HO^\bullet \quad \text{(IV.4)}$$

$$h^+ + Dye \rightarrow Dye^{\bullet+} \rightarrow Degradationproduct \quad \text{(IV.5)}$$

Two reasons may account for the sharp decrease in the removal efficiency. First, the holes (h^+) generate directly a high amount of hydroxyl radicals by reaction with H_2O and OH^-, according to **Eq. IV.3** and **Eq. IV.4**, respectively (Zeghioud et al., 2016). Secondly, the generated holes from excited catalyst can directly oxidize the molecules of dyes (**Eq. IV.5**) (Rtimi et al., 2016). Moreover, the consumption of holes according to the first and/or the second process leads to reduce e^-/h^+ recombination rate, increasing consequently e^- life time, to generate more ROS from e^- (their effect will be investigated in the $O_2^{\bullet-}$ scavengers section –IV.3.6). Time-courses of the radical's contribution for the UV-C polyester catalyst are given in **Figure IV.8c**.

- **$^\bullet$OH scavengers**

In order to evaluate the participation and the role of hydroxyl radicals ($^\bullet$OH) in RG-12 disappearance, 1 mL of iso-propyl alcohol was added to 500 mL of dye solution. From **Figure**

IV.8a and **Figure IV.8c**, considerable diminution in the degradation efficiency was recorded after alcohol addition, from 100% to 86.9% after 180 min of reaction for UV-C polyester catalyst, and from 100% to 75.9% after 120 min for TiO_2/Cellulose catalyst. This result was explained by the instantaneous radicals scavenging and the consumption of $^{\bullet}OH$ by iso-propyl alcohol (**Eq. IV.6**) (Buxton et al., 1988).

$$(CH_3)_2CHOH + HO^{\bullet} \rightarrow (CH_3)_2C\ ^{\bullet}OH + H_2O \quad \text{(IV.6)}$$

The maximum contributions of $^{\bullet}OH$ radicals under UV excitation reached 28.2% (after 90 min) and 62.4% (after 30 min) for UV-C polyester and TiO_2/cellulose catalysts, respectively (**Figure IV.8b** and **Figure IV.8d**). It is essential to note that $^{\bullet}OH$ plays an important role in the RG 12 decolorization process (**Eq. IV.7**), but the amount of this radical produced in the medium and which is really involved in pollutant oxidation can differ significantly, owing to the possible existence of a variety of recombination reactions between $^{\bullet}OH$ and other radicals (**Eq. IV.8-IV.10**) (Torres-Luna et al., 2013).

$$HO^{\bullet} + \text{pollutant} \rightarrow\rightarrow\rightarrow CO_2 + H_2O \quad \text{(IV.7)}$$

$$HO^{\bullet} + HO^{\bullet} \rightarrow H_2O_2 \quad \text{(IV.8)}$$

$$HO^{\bullet} + O_2^{\bullet -} \rightarrow O_2 + OH^- \quad \text{(IV.9)}$$

$$HO^{\bullet} + OH^- \rightarrow O^{\bullet -} + H_2O \quad \text{(IV.10)}$$

- **$O_2^{\bullet -}$scavengers**

The possible contribution of $O_2^{\bullet -}$ on RG-12 photocatalytic removal has been checked in the presence of radical acceptors such as potassium dichromate ($K_2Cr_2O_7$). This latter was used instead of benzoquinone because of the high reaction rate of potassium dichromate with hydrated electrons (3.3×10^{10}) compared to benzoquinone one (1.35×10^{9}) (Anbar and Neta, 1967).

It was observed that the decolorization kinetic of RG-12 was widely inhibited when 50 mg of potassium dichromate was added to 500 mL of dye aqueous solution. Indeed, after $O_2^{\bullet -}$ scavenging the removal efficiency decreased from 100% to 62.6% within 180 min with UV-C polyester catalyst and from 100% to 43.2% within 120 min with TiO_2/cellulose photocatalyst (**Figure IV.8a** and **Figure IV.8c**, respectively). It is in agreement with the observations made by Zhao et al. (2017) related to the degradation of tetracycline hydrochloride.

The highest contributions of $O_2^{\bullet-}$ radicals reached 43.7% after 120 min of reaction and 96.2% after 30 min for UV-C polyester catalyst and TiO_2/cellulose catalyst, respectively (**Figure IV.8b** and **Figure IV.8d**).

Superoxide radical has been recommended to play the main role in the photocatalytic degradation of some pollutants. Besides, the effective creation of this radical ion would mean the limitation of free electrons/holes recombination rate by the consumption of photo-generated e^- (**Eq. IV.11**) (Zeghioud et al., 2016; Zhao et al., 2017). An exhaustive explanation of the obtained results may be attributed to the scavenging of $O_2^{\bullet-}$ radicals and the production of hydroxyl radicals from this latter according to the following reactions:

$$(O_2)_{ads} + e_{cb}^- \rightarrow O_2^{\bullet-} \quad \text{(IV.11)}$$

$$O_2^{\bullet-} + pollutant \rightarrow\rightarrow\rightarrow CO_2 + H_2O \quad \text{(IV.12)}$$

$$O_2^{\bullet-} + H^+ \rightarrow HO_2^{\bullet} \quad \text{(IV.13)}$$

$$HO_2^{\bullet} + pollutant \rightarrow CO_2 + H_2O \quad \text{(IV.14)}$$

$$O_2^{\bullet-} + H_2O_2 \rightarrow HO^{\bullet} + OH^- + O_2 \quad \text{(IV.15)}$$

$$O_2^{\bullet-} + 2H^+ + e_{cb}^- \rightarrow H_2O_2 \quad \text{(IV.16)}$$

$$H_2O_2 + e_{cb}^- \rightarrow 2HO^{\bullet} \quad \text{(IV.17)}$$

$$H_2O_2 + h\nu \rightarrow 2HO^{\bullet} \quad \text{(IV.18)}$$

First, superoxide radical anion can directly oxidize the pollutant molecule via **Eq. IV.12** (Tachikawa et al., 2007), and/or react with H^+ to generate hydroperoxyl radical $^{\bullet}OOH$ (**Eq. IV.13**). This later can also oxidize the molecules of dye via **Eq. IV.14** (Emilioet al., 2006).

Secondly, superoxide radical anion can generate hydroxyl radical; directly by means of **Eq. IV.15** (Ilisz et al., 1998), and/or indirectly by the generation of H_2O_2 (**Eq. IV.16**) as intermediate and the decomposition of this latter according to **Eq. IV.17** and/or **Eq. IV.18** (Ilisz et al., 1998; Li et al., 2012).

b) Scavengers when visible light was used

- **•OH scavengers**

Changing the light wavelength from UV to visible did not modify the trend regarding the contribution of •OH radicals; the removal efficiency decreased from 23.5% in absence of radicals' scavenger to 13.0% in the presence of iso-propyl alcohol (**Figure IV.9a**).

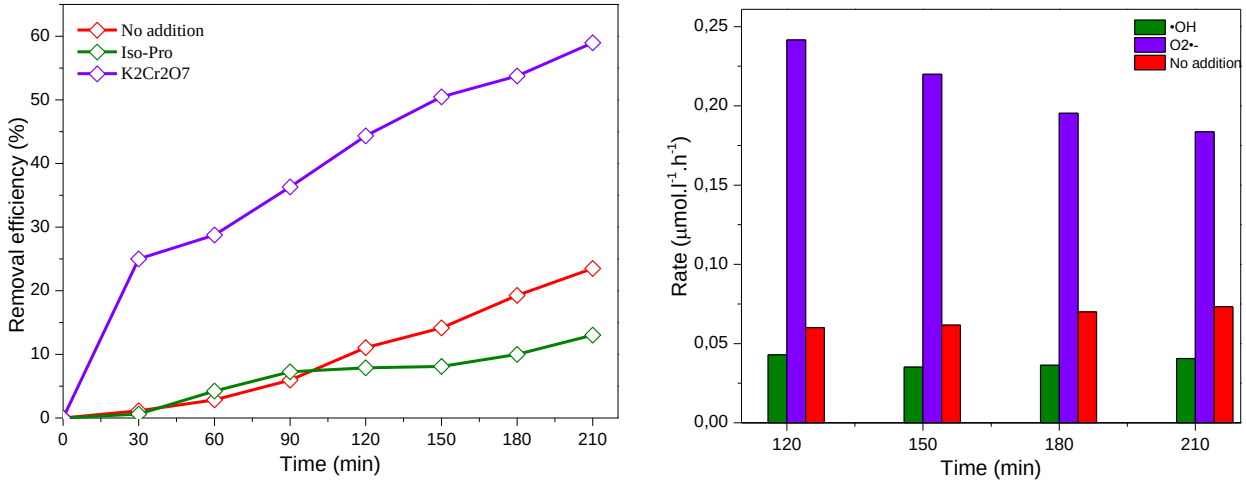

Figure IV.9: (a) Effect of diverse additives on RG-12 removal efficiency under visible light; **(b)** Rate of RG-12 degradation after the addition of various ROS scavengers under visible light (initial concentration: 2 mg/L; UV-C catalyst dosage: 1.29 g/L; natural pH)

- **$O_2^{\bullet -}$ scavengers**

A significantly faster decolorization of RG-12 was found with visible light experiment run in the presence of $O_2^{\bullet -}$ radical scavenger for the same conditions applied for UV irradiation (**Figure IV.9a**), contrarily to the trend observed in the case of UV light for which a positive contribution of the $O_2^{\bullet -}$ radicals was observed (**Figure IV.8a**).

In order to assure that the trend change observed in $O_2^{\bullet -}$ radicals scavenger experiment is only due to the change in type of irradiation light, different combinations were tested to find the step responsible for the huge rise in the removal efficiency (**Figure IV.7**); firstly, the addition of potassium dichromate in the dark was accompanied by a small decrease in RG-12 concentration followed by an equilibrium state in spite of the excitation by visible light. Another balance concerns adsorption/desorption equilibrium, which was established after catalyst addition after 30 min (in the dark); a dramatically decrease in pollutant concentration was quickly observed after light irradiation which indicated that the photocatalytic reaction was the only step

responsible for the reduction of dye concentration in the presence of $O_2^{\bullet-}$ scavengers under visible irradiation.

The contradictory results obtained regarding the impact of the $O_2^{\bullet-}$ radical under visible light if compared to UV excitation can be explained in the light of the following reactions:

$$O_2^{\bullet-} + HO^{\bullet} \rightarrow OH^- + O_2 \quad \text{(IV.9)}$$

$$OH^- + HO^{\bullet} \rightarrow H_2O + O^{\bullet-} \quad \text{(IV.10)}$$

$$O^{\bullet-} + O_2^{\bullet-} + H_2O \rightarrow 2OH^- + O_2 \quad \text{(IV.19)}$$

Indeed, in alkaline medium and under visible light, the $O_2^{\bullet-}$ radical anion became inhibitor of the photocatalytic process due probably to the inactivation of hydroxyl radical via two roots: the first one, the reaction of $O_2^{\bullet-}$ directly with $^{\bullet}OH$ radical takes place according to **Eq. IV.9**. In the second root, OH^- acts as scavenger of hydroxyl radicals leading to the creation of single oxygen ($O^{\bullet-}$) radicals (**Eq. IV.10**), which have a high chemical reactivity for the generation of a supplementary amount of OH^- by means of **Eq. IV.19** (Torres-Luna et al., 2013).

Another possible explanation of the increase in observed removal efficiency is that under visible irradiation there is no much hydrated electrons generated during photocatalyst activation step to consume to react with potassium dichromate, which leads this latter to play the role of oxidant and attack RG-12 molecules and consequently more decolorization efficiency.

As shown in the **Figure IV.9b**, the evolutions of the photocatalytic reaction rates with time after the addition of ROS scavengers are slightly different one to each other in the case of $H^{\bullet}$ and $O_2^{\bullet-}$, when the both rates decrease with time the rate of $^{\bullet}OH$ case is almost constant. Seems that a very high amount of $^{\bullet}OH$ radicals was produced but a small quantity only was really participated in the reaction and a significant part is consumed by scavenging reactions with other species such as $O_2^{\bullet-}$ as illustrated by **Eq. IV.9**. Similar results were reported by Daifullah and Mohamed (2004) in the self-scavenging of $^{\bullet}OH$ radicals by excess H_2O_2.

IV.4. Conclusion

TiO_2 impregnated on UV-C activated polyester catalyst, Cu doped TiO_2 catalyst and TiO_2 impregnated on cellulose fibres catalyst were successfully synthesized and tested for RG-12 photodegradation under both UV and visible illumination. UV-C activated polyester catalyst

showed a good photocatalytic activity for RG-12 decolorization under various light sources. The photocatalytic removal efficiency of RG-12 was found to be significantly dependent on the semiconductor dispersion and the competitive effect in binary mixture of two pollutants (RG-12 and DR-89) and resulted by products. The effect of the addition of various radicals' scavengers on RG-12 photocatalytic process was investigated with different photocatalysts and under various light sources (visible light and UV irradiation). The obtained results suggested that $O_2^{\bullet -}$ and $^{\bullet}OH$ radicals play an important role in the photodegradation process of RG-12. It was found that the superoxide radical anion is the key specie which had; i) the most promoter effect in RG-12 decolorization under UV light, ii) the most inhibitory effect in RG-12 removal under visible light. TiO_2 impregnated on UV-C activated polyester catalyst was therefore found to be efficient for the degradation and mineralization of RG-12.

References

Abou Saoud W., Assadi A. A., GuizaM., Bouzaza A., Ouederni A., Soutrel I., Wolbert D., Rtimi S., 2017. Study of synergetic effect, catalytic poisoning and regeneration using dielectric barrier discharge and photocatalysis in a continuous reactor: Abatement of pollutants in air mixture system, Applied Catalysis B: Environmental. 213, 53-61.

Anbar M., Neta P., 1967. A Compilation of Specific Bimolecular Rate Constants for the Reactions of Hydrated Electrons, Hydrogen Atoms and Hydroxyl Radicals with Inorganic and Organic Compounds in Aqueous Solution, International Journal of Applied Radiation and Isotopes, 18, 493-523.

Assadi A. A., Bouzaza A., Wolbert D., 2012. Photocatalytic oxidation of trimethylamine and isovaleraldehyde in an annular reactor: Influence of the mass transfer and the relative humidity, Journal of Photochemistry and Photobiology A: Chemistry, 236, 61-69.

Baghriche O., Rtimi S., Pulgarin C., Kiwi J., 2017. Polystyrene CuO/Cu_2O uniform films inducing MB degradation under sunlight, Catalysis Today, 284, 77–83.

Baghriche O., Rtimi S., Pulgarin C., Roussel C., Kiwi J., 2013. RF-plasma pretreatment of surfaces leading to TiO_2 coatings with improved optical absorption and OH-radical production, Applied Catalysis B: Environmental, 130–131, 65–72.

Bhatia S., Verma N., Bedi R.K., 2016. Optical application of Er-doped ZnO nanoparticles for photodegradation of direct red 31 dye, Optical Materials, 62,392-398.

Borges M.E., Sierra M., Cuevas E., García, R.D., Esparza, P., 2016. Photocatalysis with solar energy: Sunlight-responsive photocatalyst based on TiO_2 loaded on a natural material for wastewater treatment, Solar Energy, 135, 527–535.

Buxton G.V., Greenstock C.L., Helman W.P., Ross A.B., 1988. Critical review of rate constants for reactions of hydrated electrons: hydrogen atoms and hydroxyl radicals (OH/O^{-}) in aqueous solution, J. Phys. Chem. Ref. Data, 17, 513–886.

Daifullah A., and Mohamed M.M., 2004, Degradation of benzene, toluene ethylbenzene and p-xylene (BTEX) in aqueous solutions using UV/H_2O_2 system, J. Chem. Technol. Biotechnol. 79, 468-474.

Emilio C. A., Litter M. I., Kunst M., Bouchard M., Colbeau-Justin C., 2006. Phenol photodegradation on platinized-TiO_2 photocatalysts related to charge-carrier dynamics, Langmuir. 22, 3606-3613.

Faramarzpour M., Vossoughi M., Borghei M., 2009. Photocatalytic degradation of furfural by titania nanoparticles in a floating-bed photoreactor, Chem. Eng. J. 146, 79–85.

Golzad-Nonakaran B., Habibi-Yangjeh A., 2016. Ternary ZnO/AgI/Ag_2CO_3 nanocomposites: Novel visible-light-driven photocatalysts with excellent activity in degradation of different water pollutants, Materials Chemistry and Physics. 184, 210-221.

Gupta V.K., Jain R., Agarwal S., Nayak A., 2012. Photodegradation of hazardous dye quinoline yellow catalyzed by TiO_2, Meenakshi Shrivastava, J. Colloid Interf. Sci. 366, 135–140.

Huang, Y., Shang Q., Wang D., Yang S., Guan H., Lu Q., Tsang S. C., 2016. Effects of electronic structure and interfacial interaction between metal-quinoline complexes and TiO_2 on visible light photocatalytic activity of TiO_2, Applied Catalysis B: Environmental, 187, 59–66.

Ilisz I., Föglein K., Dombi A., 1998. The photochemical behaviour of hydrogen peroxide in near UV-irradiated aqueous TiO_2 suspensions, J. Mol. Catal A Chem. 135, 55–61.

Ishibashi K., Fujishima A., Watanabe T., Hashimoto K., 2000. Detection of the Active Oxidative Species in TiO_2 Photocatalysis by Using the Fluorescence Technique, Electrochem. Comm, 2, 207-210.

Ismail L., Rifai A., Ferronato C., Fine L., Jaber F., Chovelon J.-M., 2016. Towards a better understanding of the reactive species involved in the photocatalytic degradation of sulfaclozine, Applied Catalysis B: Environmental, 185, 88–99.

Jo W.-K., Sagaya Selvam N.C, 2016. Fabrication of photostable ternary CdS/MoS_2/MWCNTs hybrid photocatalysts with enhanced H_2 generation activity, Applied Catalysis A: General. 525, 9–22.

Kandiel T.A., Ahmed A.Y., Bahnemann D., 2016. TiO_2(B)/anatase heterostructure nanofibers decorated with anatase nanoparticles as efficient photocatalysts for methanol oxidation, Journal of Molecular Catalysis A: Chemical, 425, 55–60.

Kim T.-H., Seon H., Park D.-W., 2016. Synthesis of CeO_2 nanocrystalline powders using DC non-transferred thermal plasma at atmospheric pressure, Advanced Powder Technology, 27, 2012–2018.

Koh P. W., Hatta M. H. M, Teng Ong S., Yuliati L., Lee S. L., 2017. Photocatalytic degradation of photosensitizing and non-photosensitizing dyes over chromium doped titania photocatalysts under visible light, Journal of Photochemistry and Photobiology A: Chemistry, 332, 215–223.

Kouloumbos V. N., Tsipi D. F., Hiskia A. E., Nikolic D., Van Breemen R. B., 2003. Identification of Photocatalytic Degradation Products of Diazinon in TiO_2 Aqueous Suspensions Using GC/MS/MS and LC/MS with Quadrupole Time-of-Flight Mass Spectrometry, J. Am. Soc. Mass Spectrom. 14, 803–817.

Li C.-m., He Y., Tang Q., Wang K.-t., Cui X.-m., 2016. Study of the preparation of CdS on the surface of geopolymer spheres and photocatalyst performance, Mater. Chem. Physics. 178, 204-210.

Li W., Li D., Lin Y., Wang P., Chen W., Fu X., Shao Y., 2012. Evidence for the active species involved in the photodegradation process of methyl orange on TiO_2, J. Phys. Chem C. 116, 3552–3560.

Liu Y., Zhu G., Gao J., Hojamberdiev M., Lu H., Zhu R., Wei X., Liu P., 2016. A novel $CeO_2/Bi_4Ti_3O_{12}$ composite heterojunction structure with an enhanced photocatalytic activity for bisphenol A, J. Alloys Comp. 688, 487-496.

Lu X., Li X., Qian J., Miao N., Yao C., Chen Z., 2016. Synthesis and characterization of CeO_2/TiO_2 nanotube arrays and enhanced photocatalytic oxidative desulfurization performance, J. Alloys Comp. 661, 363-371.

Neppolian B., Kanel S.R., Choi H.C., Shankar M. V., Arabindoo B., Murugesan V., 2003. Photocatalytic degradation of reactive yellow 17 dye in aqueous solution in the presence of TiO_2 with cement binder, Inter. J. Photoenergy, 5, 45-49.

Pérez-Larios A., Hernández-Gordillo A., Morales-Mendoza G., Lartundo-Rojas L., Mantilla Á., Gómez R., 2016. Enhancing the H_2 evolution from water–methanol solution using Mn^{2+}–Mn^{+3}–Mn^{4+} redox species of Mn-doped TiO_2 sol–gel photocatalysts, Catalysis Today, 266, 9–16.

Pham T.-T., Nguyen-Huy C., Lee H.-J., Nguyen-Phan T.-D., Son T. H., Kim C.-K., Shin E. W., 2015. Cu-doped TiO_2/reduced graphene oxide thin-film photocatalyst: Effect of Cu content upon methylene blue removal in water, Ceramics International, 41, 11184–11193.

Rodríguez E. M., Márquez G., Tena M., Álvarez P. M., Beltrán F. J., 2015. Determination of main species involved in the first steps of TiO_2 photocatalytic degradation of organics with

the use of scavengers: The case of ofloxacin, Applied Catalysis B: Environmental, 178, 44–53.

Rtimi S., Giannakis S., Sanjines R., Pulgarin C., Bensimon M., Kiwi J., 2016. Insight on the photocatalytic bacterial inactivation by co-sputtered TiO_2-Cu in aerobic and anaerobic conditions, Applied Catalysis B: Environmental, 182, 277-285.

Rtimi S., Nesic J., Pulgarin C., Sanjines R., Bensimon M., Kiwi J., 2014. Effect of surface pretreatment of TiO_2 films on interfacial processes leading to bacterial inactivation in the dark and under light irradiation, Interface Focus, 5, 2014-2046.

Rtimi S., Pulgarin C., Kiwi J., 2017. Recent developments in accelerated antibacterial inactivation on 2D Cu-Titania surfaces under indoor visible light, Coatings, 7, 20.

Rtimi S., Pulgarin C., Sanjines R., Kiwi J., 2015. Kinetics and mechanism for transparent polyethylene-TiO_2 films mediated self-cleaning leading to MB dye discoloration under sunlight irradiation, Applied Catalysis B: Environmental. 162, 236–244.

Rtimi S., Pulgarin C., Sanjines R., Kiwi J., 2016. Accelerated self-cleaning by Cu promoted semiconductor binary-oxides under low intensity sunlight irradiation, Applied Catalysis B: Environmental.180, 648–655.

Stephan B., Ludovic L., Dominique W., 2011. Modelling of a falling thin film deposited photocatalytic step reactor for water purification: Pesticide treatment, Chemical Engineering Journal, 169, 216–225.

Sutka A., Kaambre T., Parna R., Juhnevica I., Maiorov M., Joost U., Kisand V., 2016. Co doped ZnO nanowires as visible light photocatalysts, Solid State Sciences. 56, 54-62.

Tachikawa T., Fujitsuka M., Majima T., 2007. Mechanistic Insight into the TiO_2 Photocatalytic Reactions: Design of New Photocatalysts, J. Phys. Chem. C. 111, 5259-5275.

Torres-Luna J.R., Ocampo-Pérez R., Sánchez-Polo M., Rivera Utrilla J., Velo-Gala I., Bernal-Jacome L.A., 2013. Role of $HO^{\bullet}$ and $SO_4^{\bullet -}$ radicals on the photodegradation of remazol red in aqueous solution, Chemical Engineering Journal, 223,155–163.

Villa K., Murcia-López S., Andreu T., Morante J. R., 2015. Mesoporous WO_3 photocatalyst for the partial oxidation of methane to methanol using electron scavengers, Applied Catalysis B: Environmental. 163, 150–155.

Wang J., Sun Y., Feng J., Xin L., Ma J., 2016. Degradation of triclocarban in water by dielectric barrier discharge plasma combined with TiO_2/activated carbon fibers: Effect of operating parameters and byproducts identification, Chemical Engineering Journal, 300, 36-46.

Wang J., Xia Y., Dong Y., Chen R., Xiang L., Komarneni S., 2016. Defect-rich ZnO nanosheets of high surface area as an efficient visible-light photocatalyst, Applied Catalysis B: Environmental. 192, 8–16.

Wang Y., Shan J.W., Weng G.J., 2016. Percolation threshold and electrical conductivity of graphene-based nanocomposites with filler agglomeration and interfacial tunneling, Journal of applied Physics, 118, 065101_1-065101_10.

Zeghioud H., Khellaf N., Djelal H., Amrane A., Bouhelassa M., 2016. Photocatalytic Reactors Dedicated to the Degradation of Hazardous Organic Pollutants: Kinetics, Mechanistic Aspects and Design-A Review, Chemical Engineering Communications, 203, 1415–1431.

Zhao Y., Lin C., Bi H., Liu Y., Yan Q., 2017. Magnetically Separable $CuFe_2O_4$/AgBr Composite photocatalysts: Preparation, characterization, photocatalytic activity and photocatalytic mechanism under visible light, Applied Surface Science 392, 701–707.

Zhu H.-Y., Jiang R., Fu Y.-Q., Li R.-R., Yao J., Jiang S.-T., 2016. Novel multifunctional $NiFe_2O_4$/ZnO hybrids for dye removal by adsorption, photocatalysis and magnetic separation, Applied Surface Science, 369, 1–10.

Zsilák Z., Fónagy O., Szabó-Bárdos E., Horváth O., Horváth K., HajósP., 2014. Degradation of industrial surfactants by photocatalysis combined with ozonation, Environ Sci Pollut Res. 21, 11126–11134.

CHAPITRE V: Combinaison d'un Procédé Photocatalytique et d'un Traitement Biologique pour l'Amélioration de la Dégradation d'un Polluant Textile, Reactive Green 12

Combining Photocatalytic Process and Biological Treatment for Enhancing the Degradation of a Textile Pollutant, Reactive Green 12

Hichem ZEGHIOUD[1,2], Nabila KHELLAF[1,2], Abdeltif AMRANE[3], Hayet DJELAL[4], Aymen Amine ASSADI[3], Sami RTIMI[5], Mohammed BOUHELASSA[6]

Soumis à *Environmental Science and Pollution Research* (Mars 2018)

[1] Department of Process Engineering, Faculty of Engineering, Badji Mokhtar University, P.O. Box 12, 23000 Annaba, Algeria
[2] Laboratory of Organic Synthesis-Modeling and Optimization of Chemical Processes, Badji Mokhtar University, P.O. Box 12, 23000 Annaba, Algeria
[3] Université de Rennes 1, ENSCR, CNRS, UMR 6226, Allée de Beaulieu, CS 50837, 35708 Rennes Cedex 7, France
[4] Ecole des Métiers de l'Environnement, Campus de Ker Lann, 35170 Bruz, France.
[5] Ecole Polytechnique Fédérale de Lausanne, EPFL-STI-LTP, Station 12, CH-1015 Lausanne, Switzerland.
[6] Faculty of Process Engineering, LIPE, Constantine 3 University, Algeria.

Préambule

L'objectif du présent chapitre est le couplage du procédé de dégradation photocatalytique de solutions de Reactive Green (RG 12) et du traitement biologique avec boues activées en vue d'améliorer la dégradation du polluant et/ou diminuer le temps de traitement par photocatalyse. Dans l'étape de préparation des échantillons photocatalysés à partir des solutions de 10 ppm de RG 12, nous avons choisi les conditions opératoires obtenues dans la partie optimisation (Chapitre III) : quantité de catalyseur, type d'irradiation et volume reactionnel. Le catalyseur est celui qui a presenté de bonnes performances (chapitre IV), à savoir TiO_2 impregné sur polysester traité par UV-C ; la durée de l'opération de photocatalyse est de 4 et 8 h.

La biodégradabilité des solutions non-traitées par photocatalyse et celles photocatalysées pendant 4 et 8 h est évaluée par la mesure de la DCO et de la DBO_5. Les résultats ont révélé une faible biodégradabilité des différentes solutions avec un taux d'élimination de 11,7% de la solution traitée pendant 8 h par photocatalyse. La combinaison du traitement photocatalytique pendant 4 et 8 h et du traitement biologique pendant 7 jours a conduit à une décoloration de 59.6% et 74.9%, respectivement. Une réduction significative de la matière organique a également été enregistée à l'aide de la mesure de l'Indice de Permanganate (la méthode de la DCO avec des tubes prêts à l'emploi s'est montrée inefficace vis-à-vis de la molécule organique de structure complexe). De plus, une diminution de la phytotoxicité a été obtenue puisque les valeurs de l'Index de Germination (GI) des graines de Cresson ont augmenté de 46,2% à 88,7% après 8 h de photocatalyse et à 92,8% après 7 jours supplémentaires de traitement biologique.

Nomenclature

AOPs: Advanced Oxydation Processes

AS: Activated sludge

BOD: Biological Oxygen Demand

BOD_5: Biological Oxygen Demand during 5 days

COD: Chemical Oxygen Demand

GI: Germination Index

HRT: Hydraulic retention time

MES: Suspended matter

NDIR: Non-dispersive Infra-Red detector

PI:	Permanganate Index
RG-12:	Reactive Green 12
rpm:	Round per minute
TOC:	Total Organic Carbon
UV-C:	Ultra Violet-C
WWTP:	Waste Water Treatment Plant

Abstract

The combination of a photocatalytic process (as pretreatment step) and a biological treatment of wastewaters can improve the process and achieve satisfactory efficiency. In this context, Reactive Green 12 (RG-12) solutions were treated by photocatalysis with TiO_2 impregnated on UV-C activated polyester as photocatalyst in UV batch system. Photocatalysis as pretreatment (during 4 and 8 h of irradiation) was combined with 7 days of aerobic biological treatment using activated sludge. As first assays, respiratory tests revealed that the removal of RG-12 was improved by 5.44% and 11.68% for photocatalysed solutions that were irradiated for 4 and 8 h, respectively. However, 34.50% and 19.0% of dye solution was discolorated after 7 days of biological treatment for the pre-treated solutions during 4 and 8 h of UV light exposure, respectively. A significant decrease in Chemical Oxygen Demand (COD) was noticed after photocatalysis/biodegradation process. In addition, a decrease in the phytotoxicity was obtained, since the Germination Index (GI) values of Cress seeds increased from 46.2% to 88.7% after 8 h of photocatalysis and then to 92.8% after further 7 days of biological treatment.

Keywords: Activated sludge, Biological treatment, Photocatalytic degradation, Reactive Green 12.

V.1. Introduction

The need for treatment of wastewaters is becoming imperative and indispensable for human life from day to another, because of the crucial role played in the purification and toxicity reduction of consumable water and/or the respect of international norms of aqueous effluents before discharging into the environment (WHO, 2012). A large numbers of synthetics chemical products such as textile dyes are biologically resistant to the available conventional treatment technologies (Gonçalves et al., 2000; Rajeshwar and Ibanez, 1997; Lucas et al., 2007; Chefetz et aI., 2008). This led the researchers to develop new specific and efficient pre-treatment processes in water treatment fields in the last decades (Cooper, 1993; Abidin et al., 2016). For

this reason, a wide variety of Advanced Oxidation Processes (AOPs) have been developed (Bertelli et al., 2006; Enitez et al., 2000; Ormad et al., 2001; Essam et al., 2007; Zeghioud et al., 2017), including heterogeneous photocatalysis which could be applied in several projects. This process is based on the illumination of the semiconductor surface by photons to produce extremely reactive non-specific radicals (Reactive Oxygen Species) which activate a chain of different chemical reactions (Zeghioud et al., 2016). In spite of the many advantages of this method, there are only few plants based on this technology worldwide because of the uneconomic side when it is scaled-up due to 1) the low yield of the illumination system, 2) the high consumption of electrical energy and 3) the solid-liquid separation for particle-recovery in the case of slurry system (Krishnan et al., 2017).

Nevertheless, the combination of a photocatalytic process (as pre- or post-treatment step) and biological treatment have allowed to shorten the global time of the wastewater treatment (compared to the treatment with conventional activated sludge systems only), to reduce the Capital Expenditure (Capex) and the Operating Expenses (Opex) of industrial-scale plants (compared to photocatalytic treatment alone) (Kommineni et al., 2000; Castro et al., 2014; Jafari et al., 2012). Satisfying results toward the treatment of aqueous effluents charged with biorecalcitrant compounds were reported in several studies (Ghoreishi and Haghighi, 2003; Bahnemann, 2004; Harrelkas et al., 2008). The results showed a significant reduction in the hazard and unknown toxicity characters of the by-products towards microorganisms (biologically compatible). Harrelkas et al. (2008) reported the combined process photocatalysis-biological treatment for the degradation of textile dyes (Acid Orange 10, Acid Orange 12, Reactive Black 5, Reactive Orange, Reactive Blue K2LR, …).The authors found that photocatalysis contribute in the decolorization by more than 90% and in the mineralization by more than 50% within 2 h of treatment; in addition, the combination of the two processes was capable to produce non-toxic end-products toward methanogenic bacteria. Jafari et al. (2012) studied the degradation of Reactive Black 5 by biological and photocatalytic processes separately and then by their combination. It was observed that in the biological treatment alone, *Candida tropicalis* JKS2 alone was inefficient to destroy the aromatic rings. Photocatalysis alone showed to be effective in the breaking of both azo bonds and aromatic rings. However, the combined configuration was more effective in aromatic rings remediation.

The degradation of wastewaters obtained from textile plant by applying coupled photocatalysis and biological system was also carried out by Ahmadi et al. (2015). The obtained results revealed that the maximum of Chemical Oxygen Demand (COD) removal and decolorization efficiencies were 79 and 87%, respectively at 20 h of HRT (hydraulic retention times). Similar

results were reported by Parra et al. (2002) in the degradation of isoproturon by photocatalytic-biological flow system using supported TiO_2 and fixed bacteria. 100% of the initial concentration of isoproturon and 95% of COD were removed. The coupled biological-photocatalytic process for the treatment of an effluent produced in a nitrocellulose industry was investigated by Barreto-Rodrigues et al. (2009). The authors compared photocatalysis, biological treatment, coupled photocatalytic-biological sequence and coupled biological-photocatalytic sequence. The last sequence was found to be the most efficient, reducing color, total phenol, Total Organic Carbon (TOC) and toxicity (inhibition of *Escherichia coli* growth) by 94.2%, 92.6%, 4.9% and 62%, respectively. However, the application of the photochemical process as pre-treatment was desired in most cases and then the more toxic by-products generated from the original molecules are destroyed in the subsequent processing step (González et al., 2010; Amat et al., 2003).

The present study aimed at investigating the performance of the combination of photocatalysis with supported catalyst (as pretreatment step) and aerobic biological treatment with activated sludge (AS) for the degradation of Reactive Green 12, an industrial textile reactive azo-dye. The main goal was to demonstrate the role of the biological treatment in improving the degradation process.

V.2. Experimental

V.2.1. Materials

Reactive Green 12 (RG-12) dye (MW =1837 g/mol) came from the textile manufacture of Constantine (Algeria). Sulfuric Acid (96%, Carlo ErbaReagenti), Sodium Oxalate (>99.5%, Sigma Aldrich), Potassium Permanganate (99%, Prolabo), D-(+)-Glucose (≥ 99.5%, SIGMA life science) were used as received without further purification. The aqueous solutions were prepared using ultra-pure quality water with a resistance of 15.0 MΩ cm. The chemical structure and the physicochemical properties of RG-12 were given in our previous study (Zeghioud et al., 2017).

V.2.2. Catalyst preparation and characterization

The TiO_2 impregnated on UV-C activated polyester was used as photocatalyst in all photocatalysis experiments. The preparation method and the characterization were reported in the work of Zeghioud et al. (2017).

V.2.3. Photocatalytic experiments

The photocatalytic experiments were carried out in Schott Duran glass reactors containing 500 mL of dye solution (10 mg/L) under magnetic stirring (**Figure V.1**). A 9-Watt UV Philips Bulb lamp emitting a UV-vis light (λ=365 nm) with measured intensity of 20 W/m^2 was used as illumination source in the photocatalytic system. The solution was stirred in the dark for 30 min to ensure an adsorption–desorption equilibrium before the start of irradiation. The concentration of dye solution samples (V=4mL) was analyzed using a UV–vis spectrophotometer.

The decolorization efficiency (%) of RG-12 solution can be determined according to **Eq. V.1**.

$$\eta(\%) = \left(1 - \frac{A_t}{A_0}\right) \times 100 \qquad \text{(V.1)}$$

Where A_0 and A_t are the initial intensity and the intensity at a given time t of the absorbance peak of RG-12 at λ_{max} (615 nm).

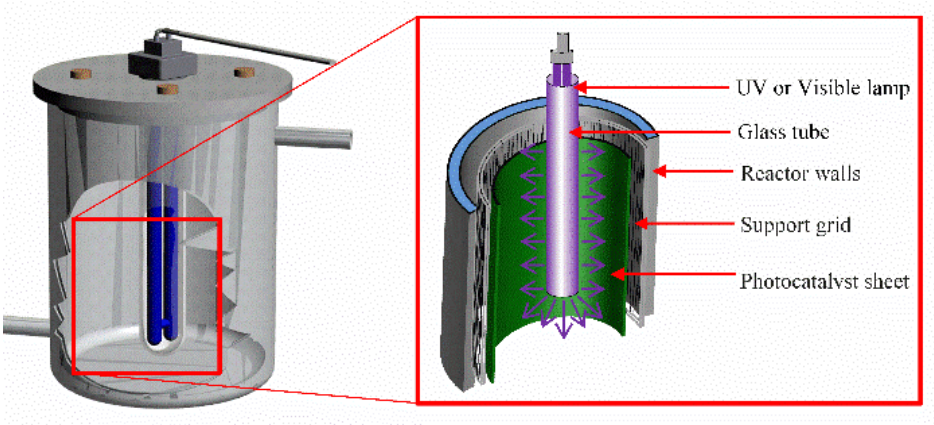

Figure V.1: Photocatalysis experimental setup

V.2.4. Biological treatment

The ability of activated sludge (selected from the WWTP of Rennes city, France) to degrade the different samples of RG-12 was tested by adding 2 mL (23.5 mg/mL) of AS to 100 mL of RG-12 solutions irradiated during different durations (0, 4 and 8 h) in the photocatalytic system (initial concentration: 10 mg/L; catalyst loading: 2.59 g/L; ambient temperature). Experiments were performed in Schott Duran glass Erlenmeyers (250 mL in capacity); the following samples were considered: (a) water with and without adding glucose as carbon source (1 g/L) to investigate the role of the presence of a primary carbon source on the decolorization process, (b) two samples of RG-12 solution without photocatalysis treatment, (c) two samples after 4 h of irradiation and (d) two samples after 8 h of irradiation. In each case one sample contained glucose and the other did not contain glucose. The pH of each sample was adjusted at 6 with

HCl (0.05 mol/L) and/or NaOH (0.05 mol/L) solutions. Experiments were carried out at 25 °C under stirring with Eidolph UNIMAX 2010 System (232 rpm), during 7 days. RG-12 samples were taken daily from the Erlenmeyer's flasks in order to measure the dye removal yield.

V.2.5. Analytical methods

a) UV-vis analysis

The UV-vis spectra of all samples were recorded using a Varian Cary®50 UV-vis spectrophotometer, where the spectra were obtained at a wavelength range of 350–800 nm.

b) Total Organic Carbon (TOC)

TOC was measured by TOC-V_{CPH}/CPG Total Organic Analyzer Schimadzu. The combustion and conversion of organic carbon compounds resulted in obtaining CO_2, which was identified by Non-Dispersive Infra-Red detector (NDIR). Calibration was obtained with potassium hydrogen phthalate standards.

c) Chemical Oxygen Demand (COD)

The measured COD values recorded according to two protocols (heating for 30 min at T=160 °C or heating for 120 min at T=148°C) which respect to the norm ISO 15705:2002(F), using NANOCOLOR EM TUBO DQO 40, KIT P/ 20 Testes - Ref. 985027. The choice of the Tube range (0-40 mg O_2 / L) was made based on the theoretical COD value (19.77 mg O_2/L).

d) Respirometry test

Biological Oxygen Demand (BOD_5) measurement was carried out in Oxitop IS6 (from WTW, Alès, France) system in order to confirm the non-biodegradability of the RG-12 dye. The technique was based on the manometric principle allowing the determination of the BOD_5 according to the standard NF EN 1899-2 relating to the autocontrol. The microorganisms used in this test were activated sludge (AS) supplied from the laboratory bioreactor. The subsequent method was applied to inoculate photocatalyzed samples of RG-12, the blank solution and the control solution.

A volume of AS was centrifuged for 15 min at 4000 rpm. The obtained supernatant was removed and a volume of water was added and followed by centrifugation for 15 min at 4000 rpm. This operation of washing was repeated three times with water and two times with deionized water. Finally, to measure the biomass concentration, the obtained sludge was

suspended in deionized water and a volume of 5 mL was dried at 105 °C during at least 48 h. The concentration of AS (g/mL) was equal to the obtained mass (g) divided by 5 mL. The following mineral medium was used for all experiments; it contained (g/L): 22.5 $MgSO_4 \cdot 7H_2O$; 27.5 $CaCl_2$; 0.15$FeCl_3$; 2.0 NH_4Cl; 6.80 Na_2HPO_4; 2.80 KH_2PO_4.

The BOD_5 value was initially estimated based on the COD value experimentally measured: BOD_5= COD/1.46. The range of expected BOD_5 measurement was then deduced. A similar protocol was applied for the control sample, which consisted of a solution of easily biodegradable compounds, namely glutamic acid (150 mg/L) and glucose (150 mg/L). Before use, NaOH (0.05 mol/L) or HCl (0.05 mol/L) solution was added to achieve neutral pH (7.0 ± 0.2). A similar protocol was also considered for the blank solution, for which the sample was replaced by deionized water to have a negligible BOD_5 value.

e) Determination of the Permanganate Index (PI)

The permanganate Index was used to quantify the organic matter of polluted water when the pollutant concentration was ≤ 10 mg/L.

The laboratory analysis method was the French norm NF T90-050:1989, which complies with the norm ISO 8467:1986. It can be summarized as follows: 25 mL of sample and 5 mL of sulfuric acid (2 mol/L) was introduced into a tube followed by a slight agitation; the system was then placed in a bath at 100°C during 10±2 min. 5 mL of potassium permanganate solution (2 mmol/L) was added at the temperature mentioned above. After 10 min±15 s, 5 mL of sodium oxalate solution (5 mmol/L) was added causing the decolorization of the solution. At this moment, the titration was started by adding the potassium permanganate solution until the appearance of a pink color persisting for 30 seconds. The volume of consumed permanganate corresponded to V1. The same protocol was applied to the distilled water and the obtained volume was called V0. Thereafter, 5 mL of sodium oxalate was introduced in this latter mixture and the system was titrated with potassium permanganate; the new recorded volume was noted as V2. PI was calculated according to **Eq. V.2**.

$$PI\ (mgO_2/L) = \frac{16 \times (V1 - V0)}{V2} \qquad \text{(V.2)}$$

f) Suspended matter

The suspended matter (MES) was obtained by centrifuging a volume V of solution during 30 min at 4000 rpm, the obtained supernatant was eliminated and the pellet was heated at 105 °C

during more than 24 h. The resulted solid was weighed and the mass was noticed as m. The suspended matter is defined by **Eq. V.3**.

$$MES = \frac{m\,(g)}{V(ml)} \tag{V.3}$$

g) Phytotoxicity tests

Seed germination and root length tests were carried out on tap water (as a control sample) and on the three samples at different stages of treatment (0, 4 and 8 h of photocatalysis followed by 7 days of aerobic biological treatment). About 5 mL of each sample was pipetted into a sterilized plastic Petri dish lined with a Whatman filter paper. Ten cress seeds (Alénois Commun from Fourche & Compagnie) were placed on the filter paper and incubated at 25 °C in the dark for 48 h (Emino and Warman, 2004). The operation was replicated ten times (ten plastic Petri dishes) following the same protocol for each sample. The number of germinated seeds was then counted and the length of roots was measured. The responses were evaluated by calculating the Germination Index (GI) according to the formula given by **Eq. V.4** (Zucconi et al., 1981).

$$GI(\%) = \frac{\text{Seed germination (\%)}\times\text{root length of treatment}}{\text{Seed germination (\%)}\times\text{root length of control}} \times 100 \tag{V.4}$$

V.3. Results and discussion

V.3.1. Photocatalysis and biological treatment coupling

In order to prepare the photocatalyzed samples for the biological treatment, a volume of RG-12 solution (10 mg/L) was treated by photocatalysis during 4 and 8 h. From the UV-vis analysis and the calculated decolorization efficiency presented in **Figure V.2**, around 45.4% of the initial pollutant was discolored after 8 h of UV light irradiation, whereas only 27.4% was eliminated within 4 h of irradiation.

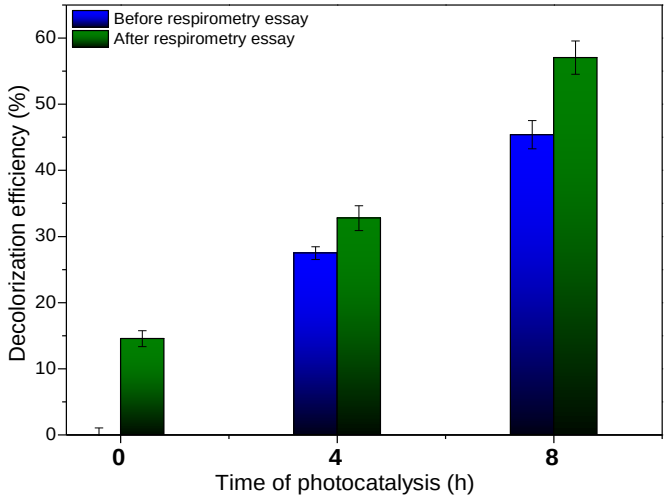

Figure V.2: decolorization efficiency of RG-12 (Dye initial concentration: 10 mg/L; catalyst dosage: 2.59 g/L; natural pH; ambient temperature) before and after respirometric assays of photocatalyzed samples.

After the respirometry test, 5.29% and 11.68% of further RG-12 elimination occurred for irradiated solutions during 4 and 8 h, respectively. However, 14.55% of elimination was recorded for the non-pretreated one. These weak decolorization yields should be related to the high initial dye concentration, if compared to that recently considered by Zeghioud et al. (2017) using the same catalyst with an initial concentration of 2 mg/L. However, to keep significant organic carbon for the subsequent biological treatment, 10 mg/L of azo dye was considered. As shown in **Figure V.3**, the Total Organic Carbon (TOC) evolution during RG-12 decolorization was nearly constant throughout 8 h of photocatalysis. This can be explained by the consumption of Reactive Oxygen Species (ROS) coming from the breaking of the pollutant structure until the full degradation of RG-12 molecules in a first step and the mineralization of the obtained by-products occurring only in a subsequent step, in agreement with the findings reported by Kouloumbos et al. (2003). Therefore, in our experiments only the first step occurred, namely the production of ROS for the breaking the chemical structure.

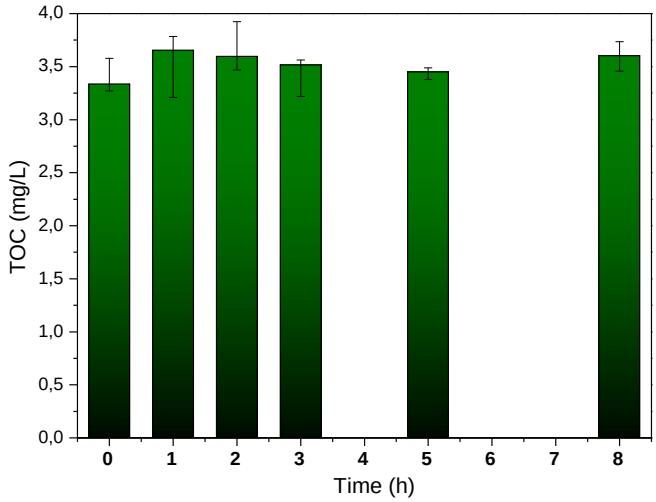

Figure V.3: Total Organic Carbon (TOC) following photocatalytic degradation of RG-12 (Dye initial concentration: 10 mg/L; catalyst dosage: 2.59 g/L; natural pH; ambient temperature)

The Chemical Oxygen Demand (COD) is a measure of the total equivalent mass of dioxygen needed to oxidize chemically the organic and inorganic matter contained in one liter of pollutant solution (Mahmoodi et al., 2006). In **Figure V.4**, an increase of COD after 8 h of photocatalysis was observed irrespective of the protocol considered.

This result could be attributed to the non-efficiency of the oxidant agent used in the test to fragment some molecules with a very complex structure, such as RG-12, and the easiest oxidation of the by-products generated during photocatalysis. This phenomenon has already been observed on industrial effluents (Djelal and Amrane, 2013).

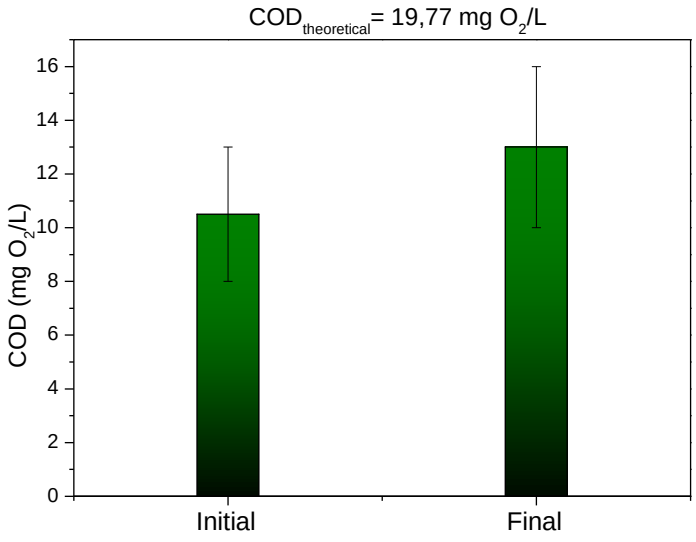

Figure V.4: Chemical Oxygen Demand (COD) of RG-12 (10 mg/L) before and after 8 h of photocatalysis.

Figure V.5 shows a decrease of the pH with the photocatalytic decolorization, from 8.60 to 6.50. This could be explained by the formation of some organic/inorganic acids and/or acidic by-products of degradation and also CO_2 as a product of mineralization. Di Paola et al. (2003) reported in their work on the removal of nitrophenols that the decrease in pH during photocatalytic transformation was due to the formation of HNO_3 as intermediate. Similar result was also reported by Naik et al. (2017) on the photocatalytic degradation of Amaranth dye.

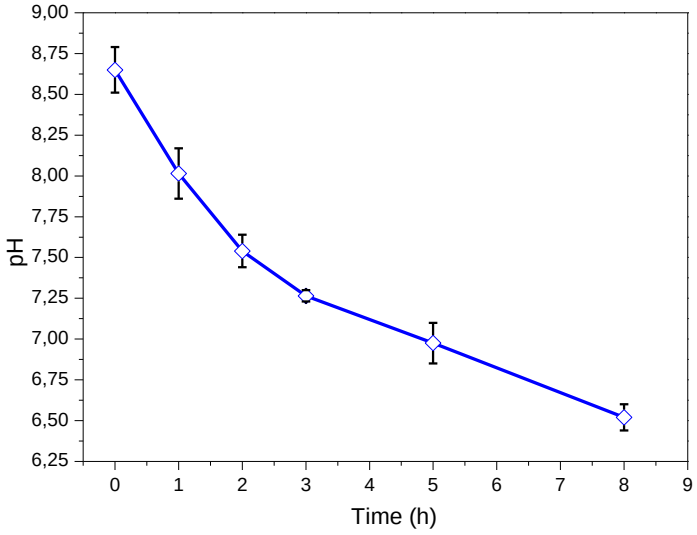

Figure V.5: Evolution of pH during photocatalysis of 10 mg/L of RG-12 solution (Catalyst dosage: 2.59 g/L; ambient temperature)

In order to evaluate photocatalytic by-products biodegradability, the respirometry analysis (BOD) of photocatalyzed RG-12 solution based on the continuous measurement of aerobic respiration of microorganisms was carried out. Oxygen consumption *versus* time for the untreated and the irradiated samples was illustrated in **Figure V.6**. The results clearly showed an increase of the BOD of about 17.02 % and 19.15% for both irradiated samples for 4 and 8 h photocatalysis, respectively. However, no variation was observed for the non-pretreated sample. This can be explained by the presence of by-products generated during photocatalysis easily assimilated by the microorganisms. Similar results were obtained by Vilaseca et al. (2010).

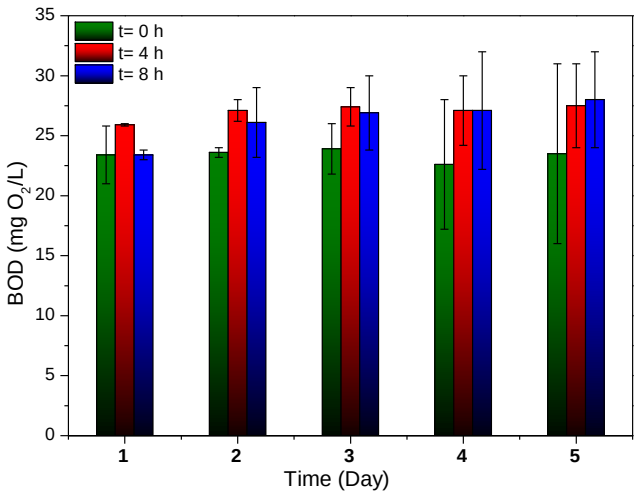

Figure V.6: Respirometric assays of non-pretreated sample and samples irradiated during 4 and 8 h

V.3.2. Effect of glucose on the degradation process

The biological treatment of target compound and photocatalyzed samples was carried out for 7 days of incubation at 25 °C. **Figure V.7** shows a noteworthy degradation of the non-preated dye (10 mg/L of RG-12) from the first day of incubation, since about 32.24 and 35.52% of RG-12 was removed within 24 h in the absence and in the presence of glucose respectively, while weak further disappearance was observed in the next days. Regarding the irradiated solution, a noteworthy degradation was also observed after one day of biological treatment in the case of 4 h pretreatment, from 25.03% initially to 45.35% after one day culture, while the decolorization was significantly lower for the solution irradiated for 8 h, from 55.95% initially to 60.65% after one day, most likely due to the significant decolorization yield recorded during the photocatalytic pretreatment. However, and contrarily to the non-pretreated solution, the decolorization remained significant throughout the biological culture. After 7 days of biological treatment, 45.6% of RG-12 was removed for the non-pretreated solution; similar result was reported by Khellaf et al. (2017). In the other hand, 59.6% and 74.9% of decolorization was achieved for the samples photocatalyzed during 4 and 8 h, respectively. This result can be attributed to the presence of readily biodegradable intermediates resulting from the photocatalytic step (Suryaman et al., 2006) and in this study, we continue with a coupling to increase yields.

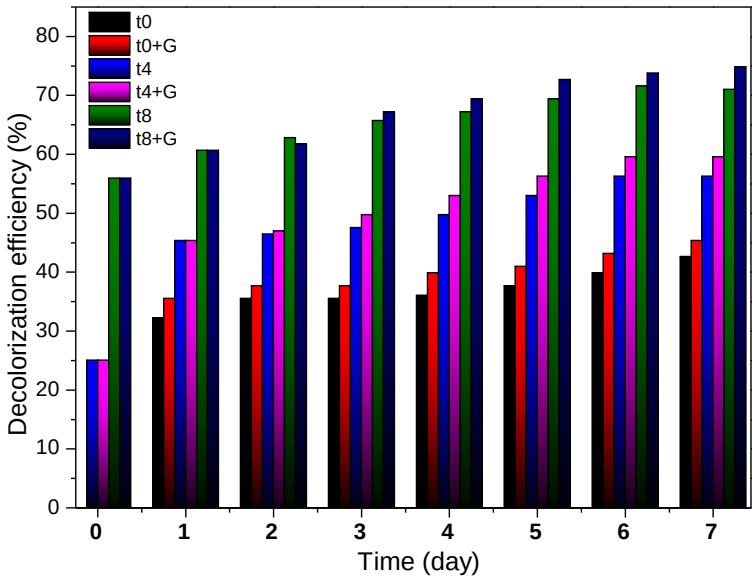

Figure V.7: Decolorization efficiency of RG-12 during biological treatment of photocatalyzed samples with and without glucose (aerobic conditions; T=25 °C).

For all biodegraded samples, a slightly higher microbial activity (around 3%) was observed in the presence of glucose. Similar results were reported in other works on the degradation of dyes using different micro-organisms (Khellaf et al., 2017; Yang et al., 2008).

To understand the effect of the biological treatment, the COD of biologically treated samples was measured and the results are presented in **Figure V.8a**. With the combined treatment, we manage to eliminate a part of the molecule but without reaching the mineralization. As a result, by-products are formed, which explains why COD does not evolve.

Nevertheless, the increase of the TOC of biologically treated samples shown in **Figure V.8b** is explained by the complex structure of the molecule which does not allow to a total oxidation (and mineralization) under the selected operating conditions. By-products which are smaller molecules were then formed in the liquid medium. Moreover, during the biological treatment, the cells are lysed with excretion in the reaction medium, biological material, which increases the TOC.

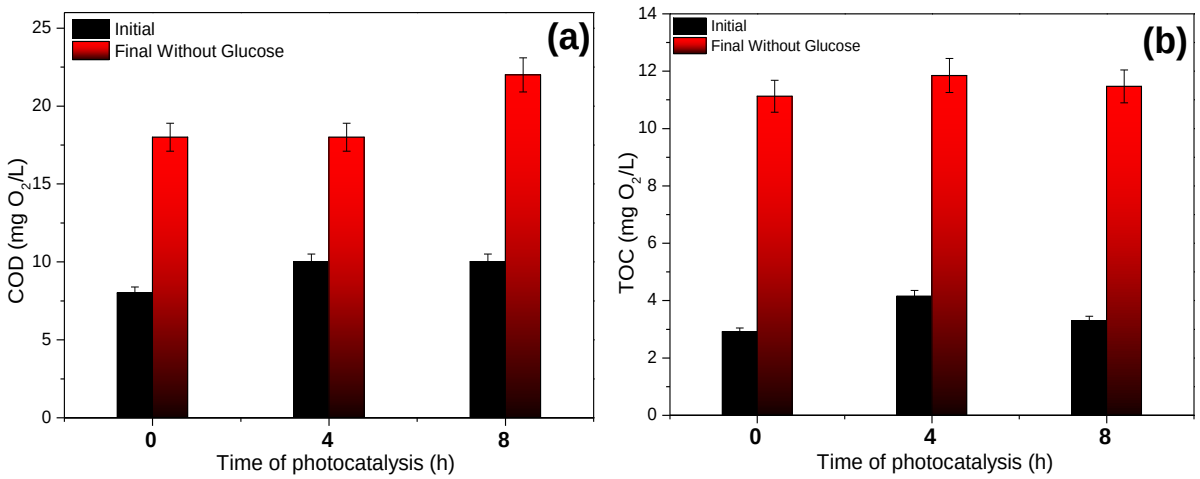

Figure V.8: Values of **(a)**; COD and **(b)**; TOC of RG-12 solutions before and after 7 days of biological treatment with and without glucose of non-pretreated solutions and those irradiated for 4 and 8 h.

Figure V.9 presents biomass growth after 7 days of biological treatment for the non-pretreated dye solution and those irradiated for 4 and 8h. The presence of glucose had a promoting effect, since higher final biomass amounts were observed. This can be related to the microbial biostimulation resulting from glucose addition, in agreement with the findings of Simpanen et al. (2016). However, the decrease in biomass in the case of biological treatment without glucose was probably attributed to lysis of cells because not enough biodegradable organic matter is available during the 7 days of incubation.

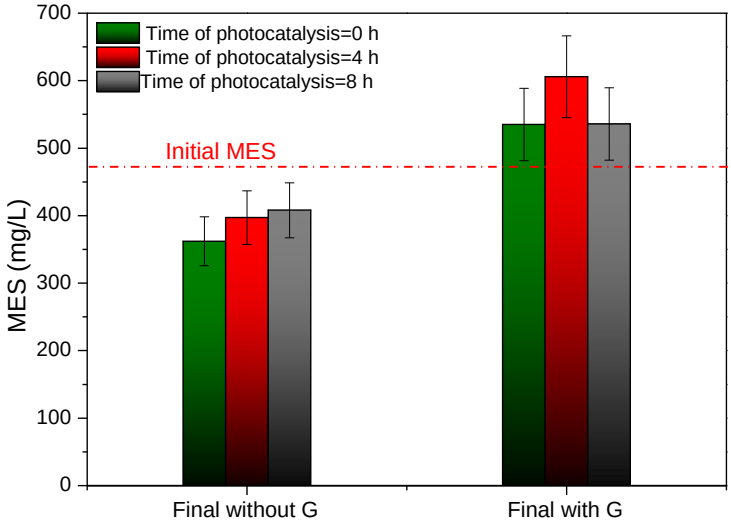

Figure V.9: Biomass growth in RG-12 solution before and after 7 days of biological treatment with and without glucose of non-pretreated dye and irradiated for 4 and 8h. Red dash line indicates the initial biomass concentration.

The Permanganate Index (PI) of photocatalyzed samples before and after biodegradation by the AS was studied in order to evaluate the capacity and the efficiency of AS micro-organisms to reduce water pollution. As shown in **Figure V.10**, PI decreased with increasing the time of the photocatalytic treatment. From these results, it could be concluded that PI is a reliable indicator to quantify the pollution compared to COD measurement with tubes ready for use.

There was a decrease of the pollutant concentration with biological treatment. PI varied from 6.1 to 2.2 mg O_2/L for non-pretreated RG-12 solution (64.0% of PI reduction), from 2.3 to 2.0 mg O_2/L for samples irradiated for 4 h (13.0% of PI reduction) and from 1.7 to 1.5 mg O_2/L for samples irradiated for 8 h (11.8% of PI reduction) (in the case of biological treatment without glucose addition).

For the biologically treated samples in the presence of glucose, it seems that there was an increase in PI which can be due to the residual glucose and the microbial material.

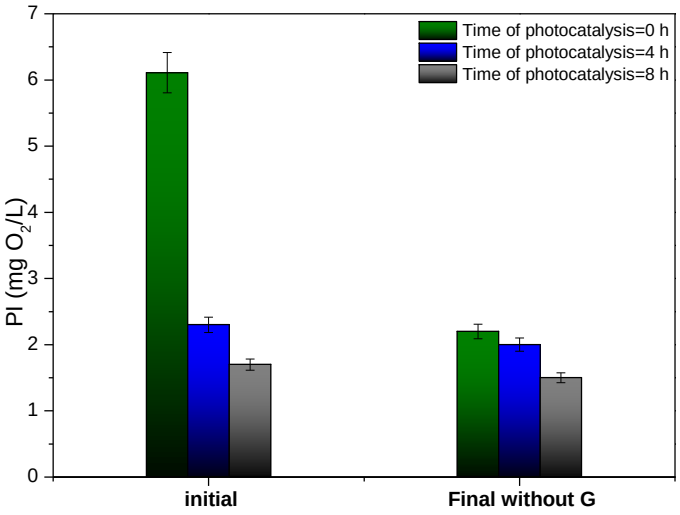

Figure V.10: Permanganate Index (PI) of RG-12 solution before and after biological treatment with and without glucose addition of non-pretreated dye and irradiated for 4 and 8 h

V.3.3. Pytotoxicity tests

The phytotoxicity evaluation of the three samples at different stages of treatment, before photocatalysis and after 8h of photocatalysis, followed by 7 days of aerobic biological treatment, was carried out with the help of a Germination Index test. As shown in Figure V. 11,

the dye (10 mg/L) was characterized by a high phytotoxicity according to Emino and Warman (2004) and Zucconi et al. (1981) classification.

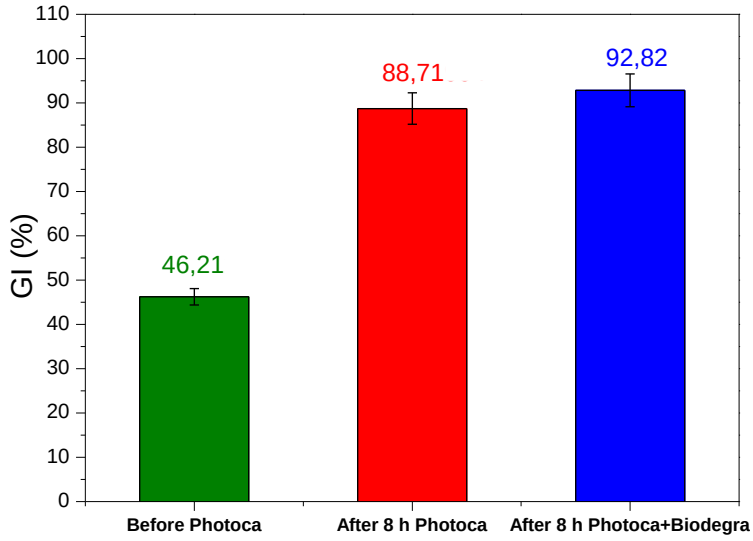

Figure V.11: Germination Index (GI) of RG-12 solutions at different stages of treatment: without pretreatment, after 8h of photocatalysis, and after 8h of photocatalysis followed by 7 days of aerobic biological treatment

The authors propose three categories according to the GI value: 1) high phytotoxicity when GI is below 50%, 2) moderate phytotoxicity when 50% < GI < 80% and 3) absence of phytotoxicity when GI value is above 80% (Emino and Warman, 2004; Zucconi et al., 1985). At the light of the obtained results, the photocatalytic treatment was the main process involved in the reduction of the phytotoxicity of the RG-12 solution, since the GI value increased from 46.2% to 88.7%; the biological treatment (with glucose) also contributed in the enhancement of GI by around 4% additional phytotoxicity reduction.

V.4. Conclusion

The photocatalytic degradation of RG-12 with TiO_2 impregnated on UV-C activated polyester was carried out under UV irradiation. The combination of photocatalysis as pre-treatment and biological treatment with activated sludge was successfully done. The contribution of the biological treatment in RG-12 elimination was found to be the most significant for the lowest time of irradiation (4 h). COD reduction was not observed which could be due to the very complex and resistant structure of the dye to oxidation and the easiest oxidation of the by-products generated during photocatalysis by means of the considered protocol for COD measurement. However, the Permanganate Index (PI) appeared to be a good tool to quantify

the pollution elimination. The presence of glucose as supplementary nutrient for the AS micro-organisms, contributed to the improvement of pollutant decolorization. Photocatalysis played the crucial role in the phytotoxicity reduction of RG-12 solution; nevertheless, the biological treatment also contributed, even if slightly, in the reduction of phytotoxicity measured with the Germination Index (GI). In the coupled process considered for the degradation of RG-12, the biological treatment led to a slight improvement of the global treatment yield.

Acknowledgements

The authors acknowledge the financial help provided by the "Institut Français-Algérie" (Campus France).

References

Abidin C.Z.A., Fahmi, Ong S.A., Mohd Makhtar S.N.N., Rahmat N.R., and Ahmad R., 2016. Decolourization and COD reduction of textile wastewater by ozonation in combination with biological treatment, Inter. J. Automotive Mechan. Eng., 13(1), 3141-3149.

Ahmadi M., Amiri P., Amiri N., 2015. Combination of TiO_2 -photocatalytic process and biological oxidation for the treatment of textile wastewater, Korean J. Chem. Eng., 32(7), 1327-1332.

Amat A.M., Arques A., Beneyto H., García A., Miranda M.A., Seguí S., 2003. Ozonisation coupled with biological degradation for treatment of phenolic pollutants: a mechanistically based study. Chemosphere, 53, 79–86.

Bahnemann D., 2004. Photocatalytic water treatment: solar energy applications. Sol. Energy., 77, 445–459.

Barreto-Rodrigues M., Souza J. V. B., Silva E. S., Silva F.T., Paiva T.C.B., 2009. Combined photocatalytic and fungal processes for the treatment of nitrocellulose industry wastewater, J. Hazard. Mater., 161, 1569–1573.

Bertelli M., Selli E., 2006. Reaction paths and efficiency of photocatalysis on TiO_2 and of H_2O_2 photolysis in the degradation of 2-chlorophenol, J. Hazard. Mater., 138, 46-52.

Castro E., Avellaneda A., Marco P., 2014. Combination of Advanced Oxidation Processes and Biological Treatment for the Removal of Benzidine-Derived Dyes, Environ. Progress Sustain. Energy, 33 (3), 873-885.

Chefetz B., Mualem T., Ben-Ari J., 2008. Sorption and mobility of pharmaceutical compounds in soil irrigated with reclaimed wastewater. Chemosphere, 73(8), 1335–1343.

Cooper P., 1993. Removing colour from dye house wastewater—a critical review of technology available, J. Soc. Dyers Colour., 109, 97–100.

Di Paola A., Augugliaro V., Palmisano L., Pantaleo G., Savinov E., 2003. Heterogeneous photocatalytic degradation of nitrophenols, J. Photochem. Photobiol.A: Chem., 155, 207–214.

Djelal H., Amrane A., 2013. Biodegradation by bioaugmentation of dairy wastewater by fungal consortium on a bioreactor lab-scale and on a pilot-scale, J. Environ. Sci., 25 (9), 1906-1912.

Emino E.R., Warman P.R., 2004. Biological assay for compost quality. Compost Sci. Utilization; 12, 342-348.

Enitez F.J.B, Beltran-Heredia J., Acero J.L., Rubio F.J., 2000. Contribution of free radicals to chlorophenols decomposition by several advanced oxidation processes, Chemosphere, 41, 1271-1277.

Essam T., Amin M.A., El Tayeb O., Mattiasson B., Guieysse B., 2007. Sequential photochemical–biological degradation of chlorophenols, Chemosphere, 66, 2201-2209.

Ghoreishi S.M., Haghighi R., 2003. Chemical catalytic reaction and biological oxidation for treatment of non-biodegradable textile effluent, Chem. Eng. J., 95, 163-169.

Gonçalves I.M.C., Gomes A., Bras R., Ferra M.I.A., Amorim M.T.P., and Porter R. S., 2000. Biological treatment of effluent containing textile dyes, Color. Technol., 116, 393–397.

González L.F., Sarria V., Sánchez O.F., 2010. Degradation of chlorophenols by sequential biological-advanced oxidative process using *Trametes pubescens* and TiO_2/UV. Bioresour. Technol. 101, 3493–3499.

Harrelkas F., Paulo A., Alves M.M., El Khadir L., Zahraa O., Pons M.N., van der Zee F.P., 2008. Photocatalytic and combined anaerobic–photocatalytic treatment of textile dyes, Chemosphere, 72, 1816–1822.

Jafari N., Kasra-Kermanshahi R., Reza Soudi M., Mahvi A.H., Gharav S., 2012. Degradation of a textile reactive azo dye by a combined biological photocatalytic process: *Candida tropicalis* JKS2-TiO_2/UV, Iranian J. Environ. Health Sci. Eng., 9 (33), 1-7.

Khellaf N., Djelal H., Amrane A., Cabrol A., 2017. Biostimulation to improve the dye biodegradation of organic dyes by activated sludge. J. Chem. Health Risks, 7(4), 247-259.

Kommineni S., Zoeckler J., Stocking A., Liang P.S., Flores A., Rodriguez R., Browne T., Roberts P.E.R., Brown A., 2000. Advanced Oxidation Processes. Center for Groundwater Restoration and Protection National Water Research Institute, 3.0.

Kouloumbos V.N., Tsipi D.F., Hiskia A.E., Nikolic D., van Breemen R.B., 2003. Identification of Photocatalytic Degradation Products of Diazinon in TiO_2 Aqueous Suspensions Using

GC/MS/MS and LC/MS with Quadrupole Time-of-Flight Mass Spectrometry, J. Americ. Soc. Mass Spectrom. 14, 803–817.

Krishnan S., Rawindran H., Sinnathambi C.M., Lim J.W., 2017. Comparison of various advanced oxidation processes used in remediation of industrial wastewater laden with recalcitrant pollutants, IOP Conf. Series: Mater. Sci. Eng., 206, 012089.

Lucas M.S., Dias A.A., Sampaio A., Amaral C., Peres J.A., 2007. Degradation of a textile reactive azo dye by a combined chemical-biological process: Fenton, s reagent-yeast. Water Res., 41, 1103- 1109.

Mahmoodi N.M., Arami M., Yousefi-Limaee N., 2006. Photocatalytic degradation of triazinic ring-containing azo dye (Reactive Red 198) by using immobilized TiO_2 photoreactor: Bench scale study. J. Hazard Mater., B133, 113-118.

Naik A.P., Salkar A.V., Majik M.S., Morajkar P.P., 2017. Enhanced photocatalytic degradation of Amaranth dye on mesoporous anatase TiO_2: evidence of C–N, N=N bond cleavage and identification of new intermediates, Photochem. Photobiol. Sci., 16, 1126-1138.

Ormad M.P., Ovelleiro J.L., Kiwi J., 2001. Photocatalytic degradation of concentrated solutions of 2,4-dichlorophenol using low energy light - Identification of intermediates, Appl. Catal. B-Environ., 32, 157-166.

Parra S., Malato S., Pulgarin C., 2002. New integrated photocatalytic-biological flow systemusing supported TiO_2 and fixed bacteria for the mineralization of isoproturon, Appl. Catal. B: Environ., 36, 131–144.

Rajeshwar K., Ibanez J.G., 1997. Environmental Electrochemistry-Fundamentals and Applications in Pollution Abatement, Academic Press Inc.

Simpanen S., Dahl M., Gerlach M., Mikkonen A., Malk V., Mikola J., Romantschuk M., 2016. Biostimulation proved to be the most efficient method in the comparison of *in situ* soil remediation treatments after a simulated oil spill accident, Environ. Sci. Pollut. Res., 23, 25024-25038.

Suryaman D., Hasegawa K., Kagaya S., 2006. Combined biological and photocatalytic treatment for the mineralization of phenol in water. Chemosphere, 65, 2502-2506.

Vilaseca M., Gutierrez M-C., Lopez-Grimau V., Lopez-Mesas M., Crespi M., 2010. Biological Treatment of a Textile Effluent After Electrochemical Oxidation of Reactive Dyes, Water Environ. Res., 82(2), 176–182.

WHO. 2012. Global water supply and sanitation assessment. Report, WHO/UNICEF Joint Monitoring Programme for Water Supply and Sanitation, World Health Organization and United Nations Children Fund,.

Yang Q., Tao L., Yang M., Zhang H., 2008. Effects of glucose on the decolorization of Reactive Black 5 by yeast isolates. J. Environ. Sci. 20(1), 105-108.

Zeghioud H., Khellaf N., Amrane A., Djelal H., Elfalleh W., Assadi A.A., Rtimi S., 2017. Photocatalytic performance of TiO_2 impregnated polyester for the degradation of Reactive Green 12: Implications of the surface pretreatment and the microstructure, J. Photochem. Photobiol. A: Chem., 346, 493–501.

Zeghioud H., Khellaf N., Djelal H., Amrane A., Bouhelassa M., 2016. Photocatalytic Reactors Dedicated to the Degradation of Hazardous Organic Pollutants: Kinetics, Mechanistic Aspects and Design-A Review, Chem. Eng. Comm., 203, 1415–1431.

Zucconi F., Monaco A., Forte M., 1985. Phytotoxins during the stabilization of organic matter. In: Gasser JKR (Ed), Composting of agricultural and other Wastes, Elsevier, London, 73-85.

Zucconi F., Pera A., Forte M., De Bertoldi M., 1981. Evaluation of toxicity of immature compost, BioCycle, 22, 54-57.

CONCLUSION GENERALE

Cette thèse, inscrite dans le cadre du traitement de l'eau chargée en polluants de l'industrie textile algérienne, avait pour objectif la dégradation de colorants par un procédé combinant la photocatalyse et la biodégradation. Les colorants sélectionnés à cet effet sont le Reactive Green (RG 12), l'Ecarlate Solophényl BNLE (ES) et le Marine Cibanone (MC) qui sont des composés biorécalcitrants difficilement éliminés dans les stations d'épuration. Le procédé de photocatalyse hétérogène en mode batch a été élaboré avec divers catalyseurs synthétiques supportés ; le traitement biologique consistait en une dégradation des polluants avec les boues activées. Le couplage des deux procédés a finalement été la partie déterminante du présent projet.

Dans la partie théorique, nous nous sommes focalisés sur une première synthèse bibliographique consacrée aux méthodes de traitements physico-chimiques et biologiques de polluants organiques. Il s'agit notamment des procédés d'oxydation avancée et du traitement par les boues ativées. Divers travaux sur ces deux procédés ont été passés en revue. La deuxième synthèse bibliographique concernait le procédé de photocatalyse dans l'eau et dans l'air avec une mise au point du mécanisme et de l'effet de différents paramètres opératoires sur le phénomène en question. Une bonne partie de cette synthèse était consacrée à l'étude des réacteurs destinés à la mise en œuvre de la photocatalyse.

Les premiers résultats expérimentaux ont mis la lumière sur la préparation, caractérisation et activité photocatalytique du TiO_2 imprégné sur polyester et activé par plasma-FR et Photons UV-C. Le TiO_2 imprégné sur du polyester activé par des photons UV-C s'est révélé actif sous lumière UV et visible avec une activité photocatalytique conservée pour plus de cinq cycles d'utilisation successifs. Les essais relatifs à la photodégradation du colorant RG 12 ont montré l'impact de différents paramètres opératoires sur l'efficacité de décoloration du polluant. Les conditions optimales déterminées ont permis d'aboutir à une décoloration totale de la solution de RG 12 au bout de 120 min d'irradiation UV. L'étude de l'effet du peroxyde d'hydrogène (H_2O_2) sur la vitesse de dégradation a révélé que pour un rapport $[H_2O_2]_0/[\ RG\ 12]_0$ variant entre 20 et 30, la cinétique de dégradation est améliorée pour laquelle le modèle de Langmuir-Hinshelwood a été trouvé le plus représentatif.

La deuxième partie du travail experimental a été consacré à la compréhension du processus photocatalytique en se basant sur le comportement du catalyseur et du polluant et en tentant

d'expliquer certains mécanismes réactionnels. La préparation et la mise en œuvre de plusieurs catalyseurs avec différents semiconducteur a prouvé que l'activité photocatalytique variait avec le type de lumière (UV ou Visible). Le TiO_2 imprégné sur papier cellulosique a présenté une bonne activité photocatalytique sous lumière UV alors que sous lumière visible, aucune activité n'a été enregistrée. Le TiO_2 dopé avec du cuivre (Cu) imprégné sur du textile a présenté seulement une activité catalytique sous irradiation UV. Le TiO_2 imprégné sur du polyester activé par des photons UV-C a montré une très bonne activité aussi bien sous lumière UV que visible. Le degré de dispersion du semiconducteur sur le support durant la préparation du catalyseur (TiO_2 imprégné sur polyester traité par des photons UV-C) semblait jouer un rôle primordial dans l'activité photocatalytique ; une activité élevée a été notée pour la configuration la moins dispersée possible. L'efficacité de dégradation des différents polluants (RG 12, ES et MC) avec ce même catalyseur était fonction de la structure moléculaire du polluant. En effet, avec le colorant RG 12, on a enregistré une bonne adsorption et dégradation et avec le colorant ES une très bonne dégradation juste au début du traitement. Le MC par contre a montré une excellente décoloration pour les faibles concentrations et un problème de solubilité pour des solutions un peu plus concentrées.

Concernant le degré de minéralisation, certains essais ont pu démontrer que la minéralisation du colorant RG 12 est inversement proportionnelle à la concentration initiale. Deux étapes dans le processus de dégradation ont été mises au point : a) la fragmentation de la molécule en sous-produits avec clivage jusqu'à décoloration totale dans un premier temps, b) les radicaux générés durant l'activation du catalyseur sont consommés pour minéraliser les sous-produits en CO_2 et H_2O dans un deuxième temps. Pour des concentrations relativement élevées en polluant, les sous-produits de dégradation peuvent entrer en compétition avec la molécule mère sur les sites actifs disponibles sur le catalyseur.

Pour des mélanges binaires de RG 12 et ES (en gardant la même quantité totale de polluants), un effet compétitif vis-à-vis des sites actifs a été remarqué. La prise en compte et le rôle des espèces oxydantes réactives a montré la dépendance de radicaux responsables de la dégradation avec le type de lumière d'activation du catalyseur. Les radicaux superoxydes ($O_2^{\bullet-}$) se sont montrés responsables de la dégradation de RG 12 sous lumière UV (aussi bien pour TiO_2 imprégné sur cellulose que sur polyester). Les radicaux hydroxyles ($^{\bullet}OH$) ont joué un rôle primordial dans la dégradation du polluant sous lumière visible pendant que les radicaux superoxydes ($O_2^{\bullet-}$) devennaient inhibiteurs.

La dernière partie du travail expérimental a été réservée à la biodégradation du polluant RG 12 et le couplage de la photocatalyse comme pré-traitement avec la biodégradation par les boues

activées. Le traitement biologique de RG 12 a montré un effet significatif dès le premier jour où 35% de sa concentration initiale a été éliminée. Sur des solutions photocatalysées durant 4 et 8 h, 34% et 19% ont été décolorées, respectivement. La combinaison du traitement photocatalytique pendant 4 et 8 h et du traitement biologique pendant 7 jours a conduit à une décoloration de 59,6% et 74,9%, respectivement. Une réduction significative de la matière organique a également été enregistée. Le glucose, présent comme nutriment dans le traitement biologique, a joué un rôle promoteur dans le processus de dégradation biologique et ce pour des solutions photocatalysées pendant 8 h. les solutions de RG 12 ayant manifesté une grande phytotoxicité (tests avec les graines de Cresson), le traitement photocatalytique a contribué à l'élimination de cette phytotoxicité. Par ailleurs, le traitement supplémentaire de dégradation avec les boues activées a contribué à une amélioration de cette toxicité.

Ce travail pourrait être complété en testant des mélanges ternaires des trois colorants et en étudiant la décoloration et la minéralisation. Aussi il est interessant d'essayer le traitement photocatalytique sous la lumiere solaire.

On pourrait également envisager l'étude de l'effet d'autres oxydants qui amélioreraient l'opération de dégradation et aussi penser à examiner l'effet de la présence de polluants minéraux sur le procédé. Par ailleurs, l'utilisation d'autres souches microbiennes isolées d'effluents textiles pourraient améliorer le procédé de biodégradation et conduire à une minéralisation des polluants présents à des concentrations élevées.

ANNEXE 6

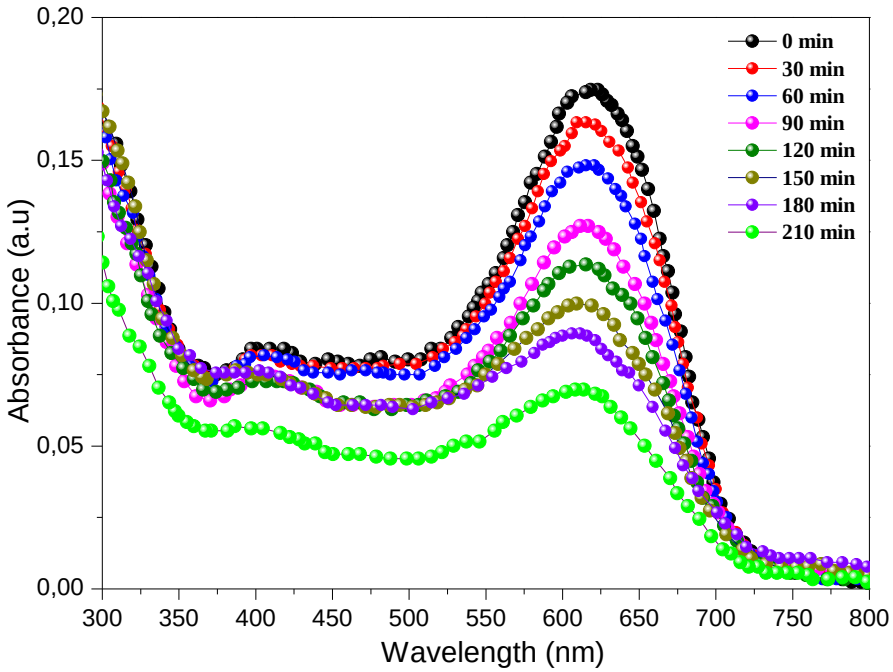

Annexe A: UV–VIS absorption spectra of RG-12 during photocatalytic treatment (RG-12 initial concentration: 10 mg/L; catalyst dosage: 5.176 g/L; natural pH~ 6.5).

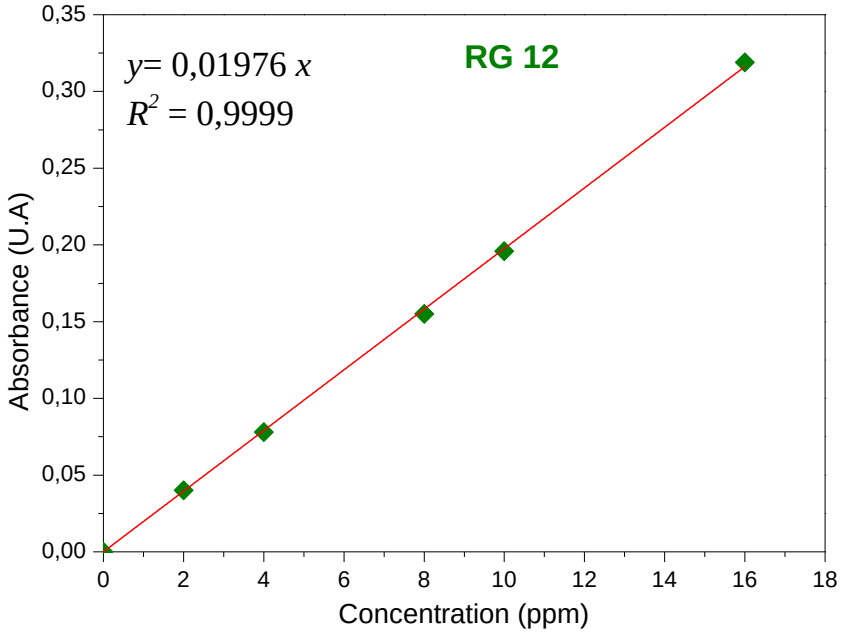

Annexe B: Calibration curve for UV-vis spectroscopy

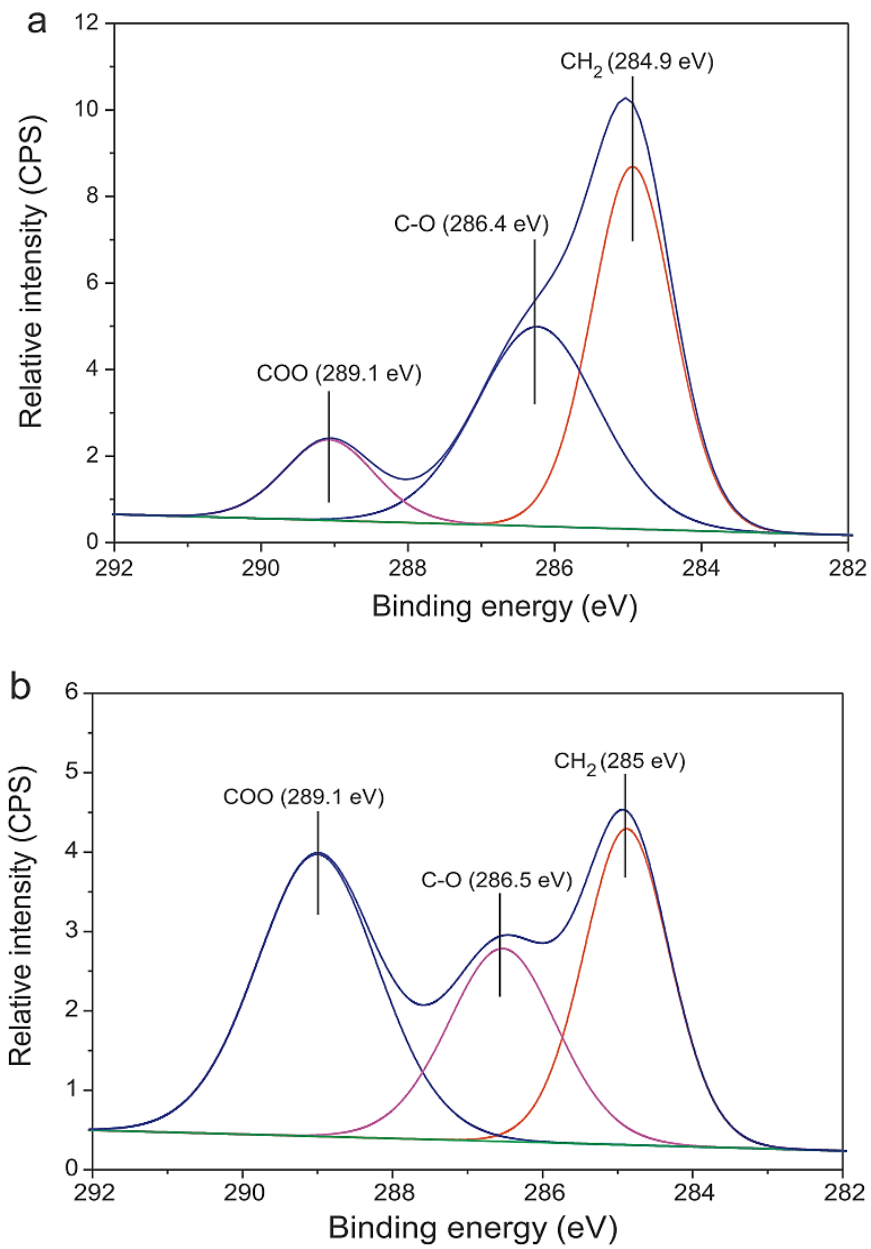

Annexe C: XPS C1s spectra of **(a)** untreated polyester and **(b)** RF-plasma pretreated polyester for 30 min.

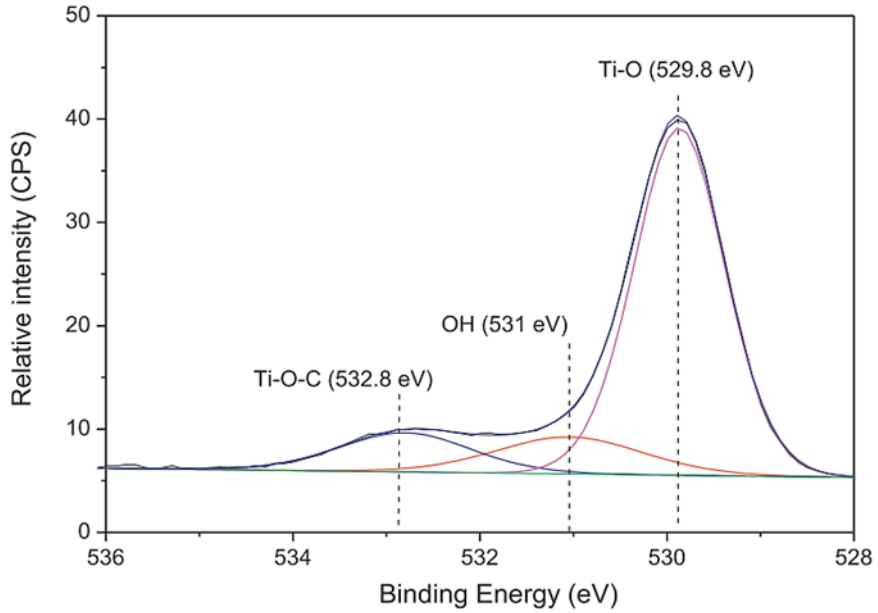

Annexe D: XPS O1s spectra of RF-pretreated polyester loaded TiO2 showing the Ti–O and T–O–C and the OH_{surf} surface groups.

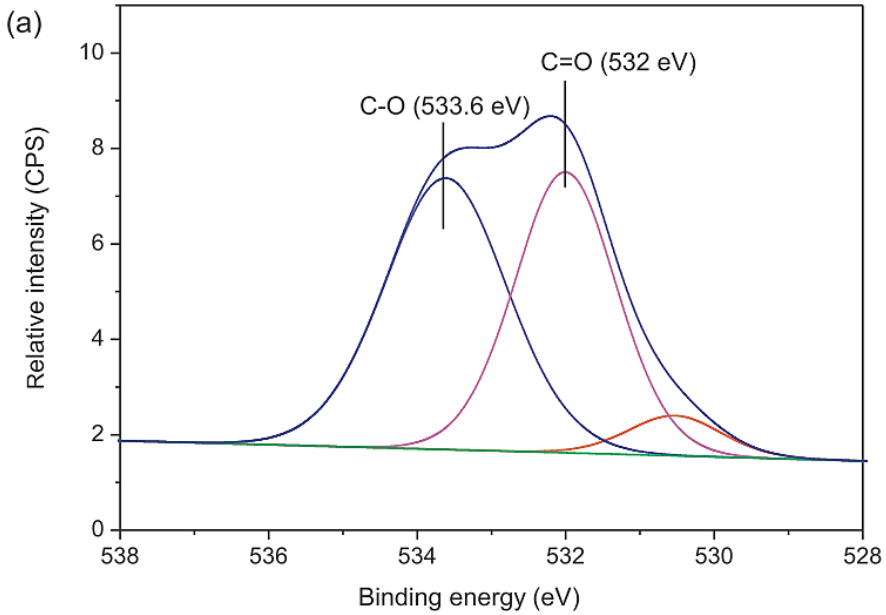

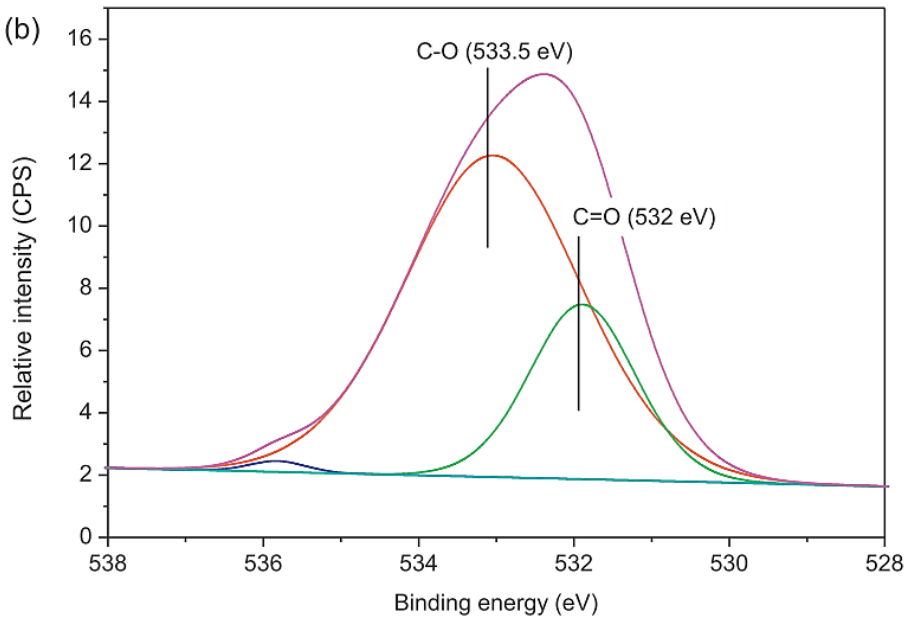

Annexe E: XPS O1s spectra of (a) untreated polyester and (b) RF-plasma pretreated polyester for 120 min.

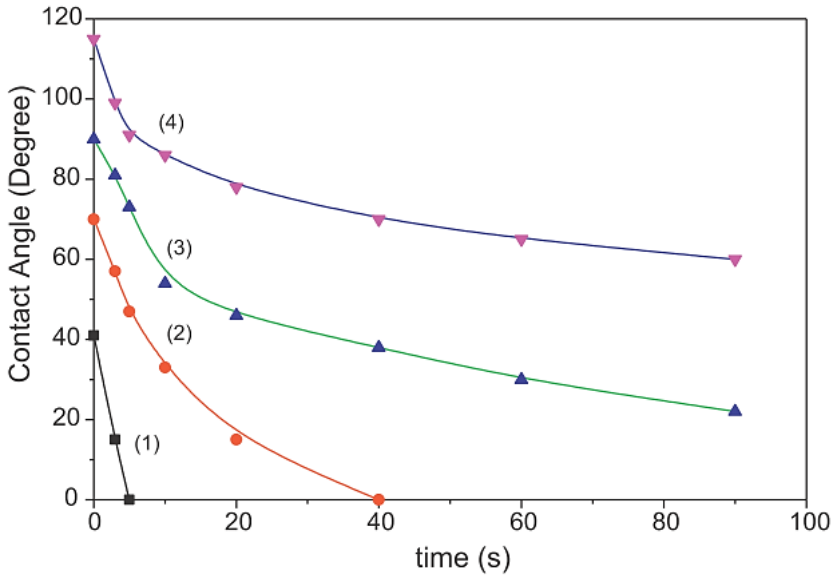

Annexe F: Contact angle as a function of time for (1) polyester samples, (2) RF-plasma pretreated samples for 10 min, (3) RF-plasma pretreated samples for 20 min and (4) RF-plasma pretreated samples for 30 min.